Title
Fun at the leading edge: Biochemical and biomechanical studies of the actin networks that drive cell motility

Author
Hsiao, Jennifer Ying

Publication Date
2014

Peer reviewed|Thesis/dissertation

Fun at the leading edge: Biochemical and biomechanical studies of the actin networks that drive cell motility.

by

Jennifer Ying Hsiao

DISSERTATION

Submitted in partial satisfaction of the requirements for the degree of

DOCTOR OF PHILOSOPHY

in

Biophysics

in the

GRADUATE DIVISION

of the

UNIVERSITY OF CALIFORNIA, SAN FRANCISCO

Acknowledgements & Dedication

My graduate school journey was quite challenging, for both scientific and personal reasons. I could not have made it through without substantial support from the special people at UCSF and in my life.

First, I would like to thank Rebecca Brown and Phoebe Grigg, who made every logistical detail a breeze, and always greeted me with a smile. Dyche was instrumental in creating the idea for my first project. I also would not have been able to deal with my family issues had he not been so generous and supportive during that time. I am grateful to my thesis committee members, Wallace Marshall, Orion Weiner, and at the end, Dave Agard, who have always been supportive of my career choices, and have even thought completely out of the box in order to help me graduate sooner.

From the Mullins lab, I have to thank Orkun Akin for teaching me and passing on his bead motility system to me. I had wonderful and scientifically invigorating conversations with my labmates, Brittany Belin and Natalie Petek, as well as Margot Quinlan, Lillian Fritz-Laylin, Scott Hansen, Peter Bieling, and Brian Margolin. I want to thank our newest graduate student, Johnny Rodriguez, for taking up the tropomyosin torch. I am especially grateful to Chris Rivera, who was always there to support me, and to talk to about math, computational biology and metaphors.

My rotation mentor, Lauren Goins, also turned out to be my mentor and collaborator throughout graduate school. When my initial project failed, she encouraged me to work on tropomyosin biochemistry, which turned out to be a great success in no small way due to her knowledge and guidance. I will never forget our loud laughing, the

“no-fun” zone, and what a great team we were, whether it was doing science or DJ-ing a Woods Hole party.

My collaborations with Elena Ingerman and Dan Lu were special experiences. They are both dear friends who needed some help with their papers. As much as I may have helped them, they really did me the favor. Being able to help them gave me the confidence to continue with science when I was going through a difficult time. I will always be inspired by the care they both take with their science, and the help they were always willing to give to labmates.

I am so lucky to have found my semi-adopted family: Kimi Takagi, Paul Takagi, and Jason Takagi. They welcomed me into their home, and their kindness and love is unparalleled.

I would also not be here without the friendship of my kung fu peeps: Luis Lundgren, Ahmad Moghadam, Ricardo Fainsilber, Ale Bezdikian, and all my other teachers, training partners and students. I would especially like to thank my training partner, Sifu Christina Windholz, for sharing life with me, keeping me on my toes (or stomping on them), and always making me smile.

Lastly, I would like to dedicate my thesis to Sifu Alan Nakamoto. His logical yet positive attitude towards life definitely helped me to maintain perspective throughout this journey. His love and care has sustained me, and I could not be more grateful.

Abstract

Tropomyosin, which binds along the length of actin filaments, has long been considered the master regulator over the binding of other proteins to actin. In particular, non-muscle tropomyosin is considered the key to the transition between the lamellipod and the lamellum in motile cells by inhibiting Arp2/3 complex nucleation and cofilin disassembly. This *in vitro* study of a *D. melangaster* tropomyosin isoform, TM1A, which localizes to the lamellum of S2 cells, shows that Arp2/3 and cofilin both affect the binding of TM1A. Labeled TM1A binds preferentially near the pointed end of actin filaments, and Arp2/3 blocks TM1A from binding to branched networks. Surprisingly, cofilin promotes the binding of TM1A to a branched actin network. Our data provides an exciting look at how actin, tropomyosin, cofilin and Arp2/3 complex together can self-organize to create two structurally and dynamically different actin networks at the leading edge. We also explore the actin-binding characteristics of another non-muscle tropomyosin isoform, TM1J, and show that its binding is dependent on TM1A. Capping protein also contributes to the exclusion of tropomyosin from a branched network. Attempts at measuring the mechanical properties of a branched network ultimately failed, but are presented for potential future inspiration. Finally, the results of two collaborations are presented.

Table of Contents

List of Figures

Chapter 1

Title

Arp2/3 complex blocks, while cofilin promotes, the binding of non-muscle tropomyosin to branched networks: understanding the composition of lamellipodial actin networks.

Abstract

Tropomyosin, which binds along the length of actin filaments, has long been considered the master regulator over the binding of other proteins to actin. In particular, non-muscle tropomyosin is considered the key to the transition between the lamellipod and the lamellum in motile cells by inhibiting Arp2/3 complex nucleation and cofilin disassembly. This *in vitro* study of a *D. melangaster* tropomyosin isoform, TM1A, which localizes to the lamellum of S2 cells, shows that Arp2/3 and cofilin both affect the binding of TM1A. Labeled TM1A binds preferentially near the pointed end of actin filaments, and Arp2/3 blocks TM1A from binding to branched networks. Surprisingly, cofilin promotes the binding of TM1A to a branched actin network. Our data provides an exciting look at how actin, tropomyosin, cofilin and Arp2/3 complex together can self-organize to create two structurally and dynamically different actin networks at the leading edge.

Introduction

In motile cells, there are two actin-based networks at the leading edge that drive motility: the lamellipod and the lamellum. The lamellipod is characterized as an actin-dense region, where branched filaments are nucleated by Arp2/3 complex close to the cell membrane and disassembled by cofilin/ADF 1-2μm away from the membrane

(Iwasa and Mullins, 2007). The lamellipod is thus highly dynamic (Ponti et. al. 2004) and is responsible for reorienting the cell in response to a rapidly changing environment. In contrast, the lamellum is characterized as a less actin-dense region immediately following the lamellipod, where the filaments are linear and stabilized by tropomyosin. Motility is achieved when the activity of myosin on these linear filaments pushes the cell forward (Ponti et. al., 2004).

Thus far, it has been assumed that tropomyosin dominates actin dynamics at the leading edge (Gunning et. al., 2008). *In vivo* data has shown that the lamellum alone is capable of sustained motility in a tropomyosin-dependent manner (Gupton et. al. 2005). This study injected tropomyosin into motile cells and the lamellipod subsequently disappeared. Another study found that the lamellipod has negligible amounts of tropomyosin, while the lamellum is rich in tropomyosin (DesMarais et. al., 2002). Knocking down tropomyosin in *Drosophila* S2 cells resulted in the expansion of the lamellipod at the expense of the lamellum (Iwasa and Mullins, 2007). A combination of *in vivo* and *in vitro* data has shown that various tropomyosin isoforms from other species block Arp2/3 complex from nucleating off of actin filaments (Blanchoin et. al., 2001; DesMarais et. al., 2002; Bugyi et. al., 2010). Certain isoforms can either enhance or inhibit cofilin/ADF disassembly activity (Bernstein and Bambrug, 1982; Kuhn and Bamburg, 2008). Thus, tropomyosin has all the characteristics of a protein capable of binding to a branched network, the lamellipod, and turning it into a stable set of linear filaments, the lamellum.

Tropomyosin is a coiled-coil alpha helix dimer that polymerizes head-to-tail and binds along the length of actin filaments. In *D. melangaster*, there are two tropomyosin genes and 15 isoforms that result from alternative splicing (Goins and Mullins). In general it is difficult to study the role of individual tropomyosin isoforms in mammalian cells because they can express 10 or more at any one time (Gunning et. al., 2008). Many of these isoforms have overlapping localizations and redundant roles. We chose to do *in vitro* assays on a *D. melangaster* tropomyosin isoform, TM1A, because *Drosophila* have relatively few non-muscle isoforms, 3 so far. These isoforms have been characterized extensively *in vivo* by Goins et. al., and have distinct roles in S2 cells. Specifically, TM1A has been shown to be the dominant tropomyosin isoform at the lamellum.

Our study shows that the story is not that simple. While TM1A displays some of the known regulatory characteristics of inhibiting Arp2/3 complex nucleation and cofilin disassembly, Arp2/3 and cofilin both affect the binding of TM1A to a branched network.

Results

Tropomyosin requires the activity of cofilin to bind motile actin networks generated by the Arp2/3 complex and capping protein.

In the absence of cofilin, TM1A is excluded from actin networks generated from ActA-coated polystyrene microspheres by the Arp2/3 complex and capping protein (Figure 1A). However, with the addition of increasing concentrations of cofilin, TM1A increasingly binds into the branched network (Figure 1B). This is a robust dependence on cofilin that occurs in every branched network in every reaction (Figure S1B, Movies

S1 & S2). The same dependence is also seen for rabbit skeletal muscle tropomyosin (Figure S1C).

While cofilin promotes TM1A binding to the branched network, TM1A ultimately protects the network from full severing by cofilin (Figure 1B, 1C). In a reaction without TM1A present, the actin network is generally severed by 13 ± 5 min post reaction start time. Certainly, by 25min, every network has been severed. However, in a reaction with TM1A, none of the networks are severed, even as far out as 45 min into the reaction. This ability of TM1A to protect the network from cofilin's severing activity has been seen before with other tropomyosin isoforms (Bernstein and Bamburg, 1982; Blanchoin et al., 2001; Ono and Ono, 2002; DesMarais et al., 2002).

The ability of TM1A to protect actin filaments from cofilin severing can also be seen on a single filament level. Actin filaments are attached to the surface of coverslips with phalloidin-biotin and pre-bound with Cy5-TM1A for 10min. Cofilin is then flowed into the coverslip chamber and imaged with total internal reflection fluorescence (TIRF) microscopy. Regions of actin filaments that are not bound with TM1A are disassembled by 28min, while regions bound with TM1A are fully protected (Figure 2A). Interestingly, when equal concentrations of Cy5-TM1A and cofilin are added to single filaments at the same time, cofilin blocks TM1A from binding to filaments (Figure S2A). Thus, the ability of cofilin to promote TM1A binding to a branched network is not due to direct recruitment of TM1A by cofilin bound to actin filaments.

Simiilar to other tropomyosin isoforms, TM1A can inhibit Arp2/3 nucleation, but not as potently as rabbit skeletal muscle tropomyosin, as seen in a pyrene actin

polymerization assay (Figure 2B). If we consider that each TM1A can bind 6 actin monomers in a filament, and the concentration of actin used was 4μM, then the saturating concentration of TM1A in these assays is 0.667μM. It is not until we truly surpass the saturating concentration (2μM) that we see significant Arp2/3 inhibition. In fact, when we pre-bind single actin filaments in TIRF with Cy5-TM1A, and then add Arp2/3 complex, we see new actin branches form off of mother filaments bound with TM1A (Figure 2C). Thus, TM1A only weakly inhibits Arp2/3 branching.

TM1A binds near the pointed end, and binding is blocked by the Arp2/3 complex.

After determining some of the activities common to most tropomyosins, we were still left with the question of how TM1A is excluded from a branched network in the absence of cofilin. One possibility is that either capping protein or Arp2/3 binding blocks TM1A from binding onto a filament. This would imply that the initial binding site of TM1A is biased towards either the barbed or the pointed end.

We indeed observe a preference for the pointed end through single filament TIRF microscopy of actin polymerization at low concentrations of TM1A (Figure 3A-B). In these experiments, we can identify the pointed end because it grows much more slowly, and it bleaches earlier than the fast-growing barbed end. At 200nM TM1A, the pointed end preference is the strongest. Curiously, once TM1A binds to the pointed end, it never fully polymerizes along the rest of the filament. On average, TM1A remains bound to within 1μm of the pointed end. At 300nM TM1A, the preference for the pointed end is still strong. It remains bound to within 2.5μm of the pointed end (Movie S3). At 400nM

TM1A, initial binding sites of TM1A are still biased towards the pointed end, but less strongly than at lower concentrations. After the initial binding, TM1A polymerizes along the remaining length of the filament.

Using these concentrations of TM1A where there is a preference for binding to the pointed end, we wanted to examine whether Arp2/3 branching would affect how TM1A binds to actin. Using single filament TIRF, we find that the only part of the actin branched network that is bound by TM1A is the free pointed end of the original mother filament (Figure 3C). All pointed ends that are bound by Arp2/3 are incapable of binding TM1A at these concentrations. This is true even when we lower the Arp2/3 concentration (Figure S3B), which indicates that elongating the length of the branches does not help TM1A bind. In addition, when we look at unbranched filaments and increase the number of free pointed ends (ends not bound by Arp2/3 complex) by increasing the actin concentration, the number of TM1A binding events increases (Figure S3A). This confirms that the binding of TM1A is truly dependent on the number of free pointed ends.

Binding of TM1A is affected by the ATP state of filamentous actin.

After discovering this pointed end binding preference, we wanted to characterize TM1A binding to actin in more detail. TM1A binds to actin cooperatively, much like other tropomyosins (Figure 4A; Yang et. al., 1979; Dabrowska et. al., 1983; Pittenger and Helfman, 1992). From our steady state TIRF binding assays, we measure a Kd of 45nM,

and a Hill coefficient of 5.7. This closely matches our values measured from actin cosedimentation (Figure S4A).

Since the binding of TM1A is biased towards the pointed end, it is possible that TM1A can sense the ATP state of the actin filament. To examine whether TM1A is affected by the ATP state of the actin, we created ADP-actin filaments and measured the binding of TM1A at different concentrations. The binding rate of TM1A to ADP-actin is much more concentration dependent than TM1A binding to ATP-actin (Figure 4B). The preference for the pointed end was also much weaker when looking at binding to ADP-actin (Figure 4C-D). This confirmed that TM1A binds differentially based on the ATP state of actin.

To see if TM1A prefers to bind to the ADP-Pi state, we used a phosphate mimic, BeF_3, to lock the filaments into an ADP-Pi-like state. In this reaction, ATP is still present, so the growing filaments still have an ATP cap, followed by some ADP-Pi-actin subunits, a small but existing population of ADP-actin, and then a large population of ADP-BeF_3-actin subunits (Figure S4C). Interestingly, all the binding events shift to being within 2.5μm of the barbed end (Figure 4F). Many of these binding events were transient, which is in contrast to the stable binding events we see with actin filaments grown in just ATP (Figure 4E). At low enough concentrations (200nM or below), there are no binding events to these ADP-BeF_3-actin filaments. We can conclude TM1A does not bind well to ADP-BeF_3-actin, but it is unclear how well TM1A binds to ADP-Pi-actin and ATP-actin. Given that all the binding events are near the barbed end, it is possible that: i. TM1A is

binding to the small population of ADP-actin present, and/or ii. TM1A has a higher binding affinity to ADP-Pi-actin than to ADP- BeF_3-actin.

Discussion

The prevailing model for actin-based cell motility is that there are two distinct actin networks at the leading edge of the cell: the lamellipod and lamellum (Ponti et. al., 2004). These two networks are generated at or near the cell membrane, and may even overlap in the 1-2μm proximal to the membrane. It is unclear whether the actin filaments for these two networks are generated by the same actin nucleators. One model is that the two networks are nucleated separately: the lamellipod by Arp2/3 and its associated NPFs, and the lamellum by linear actin nucleators such as formins. Another model is that the two networks are nucleated by the same nucleator, Arp2/3 and its NPFs, but then the lamellipod is transformed into the lamellum by cofilin/ADF disassembly and tropomyosin stabilization (Lim et. al., 2010). In either model, it has been posited that tropomyosin's ability to block cofilin severing activity and Arp2/3 branching activity is what establishes the transition from the lamellipod to the lamellum (DesMarais et. al., 2002; Gupton et. al., 2005). This assumption implies that tropomyosin binding to actin is not affected by other actin-binding proteins, and that once bound, tropomyosin governs the effect of the other proteins. What we have shown here is that the opposite can also be true: these other actin-binding proteins can affect tropomyosin binding, and thus tropomyosin's effect on the lamellipod to lamellum transition.

We have shown that TM1A does not inhibit Arp2/3 branching nearly as strongly as rabbit skeletal muscle TM. Conversely, Arp2/3 seems to block TM1A from binding to

actin filaments. In the bead assay, and in the absence of cofilin, TM1A is actually excluded from a branched network. This is a phenomenon that had not been seen before in similar experiments with ActA-coated polystyrene beads and labeled tropomyosin (Bugyi et. al., 2010).

From our single filament TIRF assays, the exclusion from branched networks is likely due to TM1A's bias towards initial binding (loading) near the pointed end of actin filaments. Pointed end binding by tropomyosin has been seen before. In the study by Broschat et. al. (1989), tropomyosin was bound to actin filaments and thus inhibited pointed end depolymerization in pyrene assays, but this study did not determine the initial sites of tropomyosin binding. Almenar-Queralt et. al. (1999) found tropomodulin and tropomyosin staining at pointed ends in the middle of the sarcomere, but again this did not show initial binding sites. The strongest *in vivo* evidence to date of pointed end loading is from a study by Michele et. al. (1999) where time-resolved indirect immuno-fluorescence of tropomyosin loading onto the pointed end of sarcomeric actin was observed. However, it is unclear whether this pointed end loading is influenced by any of the endogenous pointed end capping proteins. Our study is the first time that we have witnessed pointed end loading directly *in vitro*, and as a function of just the protein itself.

We have shown directly that Arp2/3 blocks TM1A from binding to the pointed end, and thus to most of the filaments in a branched network (Figure 5A). TM1A binding only to free pointed ends (i.e. pointed ends not bound by Arp2/3 complex) is consistent with our ActA-bead data where we see TM1A is only bound to the network furthest from the polystyrene bead (a region we call the shell). The shell contains free pointed ends

that are the original mother actin filaments. The shell could also include free pointed ends that result from filaments breaking under the stress of the symmetry breaking event of the shell at the beginning of these reactions (Akin and Mullins, 2008; Dayel et. al., 2009).

From Kuhn and Bamburg, 2008, different tropomyosin isoforms can either inhibit cofilin debranching or enhance cofilin debranching. While TM1A does inhibit cofilin disassembly, a novel interaction seems to be that cofilin enhances TM1A's ability to bind to actin filaments. Our model suggests that this is due to cofilin's severing activity, which creates more free pointed ends for TM1A to bind to (Figure 5B). The enhancement of TM1A binding is not due to direct recruitment by actin-bound cofilin since equal molar cofilin blocks TM1A from binding. This mutually exclusive binding by cofilin and TM1A is consistent with other tropomyosin isoforms (Ono and Ono, 2002).

Cofilin is known to bind and lock actin filaments into an under-twisted state (McGough, 1997), while tropomyosin is known to bind actin filaments that are in their natural state (Gunning et. al. 2008). This probably explains their mutually exclusive binding. Despite the mutually exclusive binding, it is interesting that both cofilin and TM1A binding are sensitive to the ATP state of actin filaments. Cofilin is known to bind to regions of ADP-actin subunits 40 times more strongly than to ATP-actin or ATP-Pi-actin subunits (Blanchoin and Pollard, 1999). It has been posited that this feature of cofilin binding is what determines the 1-2μm width of the lamellipod (Iwasa and Mullins 2007). It is also known that when tropomyosin is knocked down *in vivo* the lamellipod width expands (Iwasa and Mullins, 2007). Taken together, it is possible that the ADP-

actin sensitivity of both proteins, as well as cofilin's ability to enhance TM1A's binding, contributes to how wide the lamellipod is and how sharp the transition is between the lamellipod and lamellum.

While TM1A's sensitivity to the ATP-actin state of filaments can help explain the pointed end binding preference, it does not seem to explain the whole picture. A simulation of the growth of actin filaments with a measured rate of ATP hydrolysis (Blanchoin and Pollard, 2002), and the rate of phosphate release (Carlier, 1987) shows that at the filament lengths that we saw TM1A binding (>5um), more than 95% of the filament is in an ADP-actin state (Figure S4B). This indicates that the tendency for TM1A to bind to the pointed end is more than just ATP-state dependent. TM1A could also be sensing a mechanical/structural difference of the free pointed end.

In conclusion, our data provides an exciting look at how actin, tropomyosin, cofilin and Arp2/3 complex together can self-organize to create two structurally and dynamically different actin networks at the leading edge of a cell. We are confident that some of the interactions we see between tropomyosin and the other proteins are isoform specific. Thus, more *in vitro* and *in vivo* work needs to be done to confirm how common these types of interactions are among the different non-muscle tropomyosin isoforms.

References

Akin O., R.D. Mullins. 2008. Capping protein increases the rate of actin-based motility by promoting filament nucleation by the Arp2/3 complex. *Cell*. 133:841-851.

Almenar-Queralt, A., Lee, A., Conley, C.A., Ribas de Pouplana, L. and Fowler, V.M. (1999). Identification of a novel tropomodulin isoform, skeletal tropomodulin, that caps actin filament pointed ends in fast skeletal muscle. J. Biol. Chem. 274, 28466–28475.

Antonny B., Chabre M. 1992. Characterization of the aluminum and beryllium fluoride species which activate transducin: analysis of the binding and dissociation kinetics. Journal of Biological Chemistry. 267: 6710-6718.

Bernstein BW, Bamburg JR (1982) Tropomyosin binding to F-actin protects the F-actin from disassembly by brain actin-depolymerizing factor (ADF). Cell Motil 2: 1-8.

Blanchoin, L., and Pollard, T.D. (1999). Mechanism of interaction of Acanthamoeba actophorin (ADF/Cofilin) with actin filaments. J. Biol. Chem. 274: 15538–15546.

Blanchoin L., Pollard T.D. 2002. Hydrolysis of ATP by polymerized actin depends on the bound divalent cation but not profilin. Biochemistry. 41: 597-602.

Blanchoin L., Pollard T.D., Hitchcock-DeGregori S.E. 2001. Inhibition of the Arp2/3 complex-nucleated actin polymerization and branch formation by tropomyosin. Curr Biol 11: 1300-1304.

Broschat K.O., Weber A., Burgess D.R. 1989. Tropomyosin stabilizes the pointed end of actin filaments by slowing depolymerization. Biochemistry 28: 8501-8506.

Bugyi B., Didry D., Carlier M.F. 2010. How tropomyosin regulates lamellipodial actin-based motility: a combined biochemical and reconstituted motility approach. EMBO Journal. 29: 14-26.

Carlier, M.F. 1987. Measurement of Pi dissociation from actin filaments following ATP hydrolysis using a linked enzyme assay. Biochemical and Biophysical Research Communications. 143: 1069-1075.

Carlier, M.F., V. Laurent, J. Santolini, R. Melki, D. Didry, G.X. Xia, Y. Hong, N.H. Chua, D. Pantaloni. 1997. Actin depolymerizing factor (ADF/cofilin) enhances the rate of filament turnover: implication in actin-based motility. *J. Cell Biol*. 136:1307-1322.

Cooper, J.A., S.B. Walker, and T.D. Pollard. 1983. Pyrene actin: documentation of the validity of a sensitive assay for actin polymerization. *J. Muscle Res. Cell Motil.* 4:

253-262.

Suarez C., Roland J., Boujemaa-Paterski R., Kang H., McCullough B.R., Reymann A., Gue´rin C., Martiel J., De La Cruz E.M., and Blanchoin L. 2001. Cofilin Tunes the Nucleotide State of Actin Filaments and Severs at Bare and Decorated Segment Boundaries. Current Biology 21, 862–868.

Dabrowska R., Nowak E., Drabikowski W. 1983. Some functional properties of nonpolymerizable and polymerizable tropomyosin. Journal of Muscle Research and Cell Motility. 4: 143-161.

Dayel M.J., Akin O., Landeryou M., Risca V., Mogilner A., Mullins R.D. 2009. In silico reconstitution of actin-based symmetry breaking and motility. PLoS Biol 7(9): e1000201.

Dayel M.J., E.A. Holleran, and R.D. Mullins. 2001. Arp2/3 complex requires hydrolyzable ATP for nucleation of new actin filaments. *Proc. Natl. Acad. Sci. U.S.A*. 98:14871-14876.

DesMarais V., Ilia Ichetovkin, John Condeelis and Sarah E. Hitchcock-DeGregori. Spatial regulation of actin dynamics: a tropomyosin- free, actin-rich compartment at the leading edge. Journal of Cell Science 2002; 115, 4649-4660.

Goins, L.M. and Mullins, R.D. Tropomyosin isoforms cooperate with Myosin II and Diaphanous to influence cell cycle progression. Manuscript in preparation.

Gunning P., O'Neill G., Hardeman E. 2008. Tropomyosin-based regulation of the actin cytoskeleton in time and space. Physiol Rev. 88: 1-35.

Gunning P.W., Schevzov G., Kee A.J., Hardeman E.C. 2005. Tropomyosin isoforms: divining rods for actin cytoskeleton function.

Gupton, S.L., K.L. Anderson, T.P. Kole, R.S. Fischer, A. Ponti, S.E. Hitchcock-DeGregori, G. Danuser, V.M. Fowler, D. Wirtz, D. Hanein, and C.M. Waterman-Storer. 2005. Cell migration without a lamellipodium: translation of actin dynamics into cell movement mediated by tropomyosin. *J. Cell Biol*. 168:619-631.

Iwasa, J.H. and R.D. Mullins. 2007. Spatial and temporal relationships between actin-filament nucleation, capping, and disassembly. Curr. Biol. 17:395-406.

Kawska, A., K. Carvalho, J. Manzi, R. Boujemaa-Paterski, L. Blanchoin, J.L. Martiel, and C. Sykes. How actin network dynamics control the onset of actin-based motility. 2012. *Proc. Natl. Acad. Sci. U. S. A*. 109:14440-14445.

Kuhn T.B., Bamburg J.R. "Tropomyosin and ADF/cofilin as collaborators and competitors." 2008.

Lim J.I., Sabouri-Ghomi M., Machacek M., Waterman C.M., Danuser G. 2010. Protrusion and actin assembly are coupled to the organization of lamellar contractile structures. Exp Cell Res. 316: 2027-2041.

Littlefield, R., Almenar-Queralt, A. and Fowler, V.M. (2001). Actin dynamics at pointed ends regulates thin filament length in striated muscle. Nat. Cell Biol. 3, 544–551.

McGough, A. 1998. F-actin-binding proteins. Current Opinion in Structural Biology. 8: 166-176.

McGough, A., B. Pope, W. Chiu, and A. Weeds. 1997. Cofilin changes the twist of F-actin: implications for actin filament dynamics and cellular function. J. Cell Biol. 138: 771–781.

Michele D.E., Albayya F.P., and Metzger J.M. 1999. Thin filament protein dynamics in fully differentiated adult cardiac myocytes: toward a model of sarcomere maintenance. J. Cell Biol. 145, 1483-1495.

Mullins, R.D., J.A. Heuser, and T.D. Pollard. 1998. The interaction of Arp2/3 complex with actin: nucleation, high affinity pointed end capping, and formation of branching networks of filaments. *Proc. Natl. Acad. Sci. U. S. A.* 95:6181-6186.

Ono S, Ono K (2002) Tropomyosin inhibits ADF/cofilin-dependent actin filament dynamics. J Cell Biol 156: 1065–1076.

Palmgren, S., P.J. Ojala, M.A. Wear, J.A. Cooper, and P. Lappalainen. 2001. Interactions with PIP2, ADP-actin monomers, and capping protein regulate the activity and localization of yeast twinfilin. *J. Cell Biol.* 155: 251-260.

Pittenger M.F., Helfman D.M. 1992. In vitro and in vivo characterization of four fibroblast tropomyosins produced in bacteria: TM-2, TM-3, TM-5a, and TM-5b are co-localized in interphase fibroblasts. Journal of Cell Biology. 118: 841-858.

Pollard TD (1986) Rate constants for the reactions of ATP- and ADP-actin with the ends of actin filaments. Journal of Cell Biology. 103: 2747–2754.

Ponti A., Machacek M., Gupton SL., Waterman-Storer CM., Danuser G. Two distinct actin networks drive the protrusion of migrating cells. *Science* 2004; 305(5691).

Reichstein E., Korn E.D. 1979. *Acanthamoeba* profilin. A protein of low molecular weight from *Acanthamoeba castellanii* that inhibits actin

nucleation. J. Biol. Chem. 254, 6174-6179.

Reymann, A.C., C. Suarez, C. Guérin, J.L. Martiel, C.J. Staiger, L. Blanchoin, and R. Boujemaa-Paterski. 2011. Turnover of branched actin filament networks by stochastic fragmentation with ADF/cofilin. *Mol. Biol. Cell*. 22: 2541-2550.

Rogers, S.L., U. Wiedemann, N. Stuurman, and R.D. Vale. 2003. Molecular requirements for actin-based lamella formation in Drosophila S2 cells. *J. Cell Biol.* 162: 1079-1088.

Schaus TE, Taylor EW, Borisy GG (2007) Self-organization of actin filament orientation in the dendritic-nucleation/array-treadmill- ing model. Proc Natl Acad Sci USA 104: 7086-7091.

Singh A., Hitchcock-DeGregori S.E. 2007. Tropomyosin's periods are quasi-equivalent for actin binding but have specific regulatory functions. Biochemistry. 46: 14917-14927.

Smillie, L.B. 1982. Preparation and identification of alpha- and beta-tropomyosins. Methods Enzymol. 85: 234–241.

Spudich J.A., Watt S. 1971. The regulation of rabbit skeletal muscle contraction. I. Biochemical studies of the interaction of the tropomyosin-troponin complex with actin and the proteolytic fragments of myosin. J. Biol. Chem. 15: 4866-71.

Svitkina, T.M. and G.G. Borisy. 1999. Arp2/3 complex and actin depolymerizing factor/cofilin in dendritic organization and treadmilling of actin filament array in lamellipodia. *J. Cell Biol*. 145:1009-1026.

Trinick J., Cooper J., Seymore J., Egelman E.H. 1986. Cryo-electron microscopy and three-dimensional reconstruction of actin filaments. J Microscopy. 141: 349-360.

Vindin H., Gunning P. 2013. Cytoskeletal tropomyosins: choreographers of actin filament function diversity. J Muscle Res Cell Motil. 34: 261-274.

Yang Y., Korn E.D., Eisenberg E. 1979. Cooperative binding of tropomyosin to muscle and *Acanthamoeba* actin. Journal of Biological Chemistry. 254: 7137-7140.

Materials and Methods

Design of labeled tropomyosin.

We took great care in designing our labeled tropomyosin so that the label would be least disruptive to the protein's structure and function. The two regions of the protein that we avoided placing a cysteine for labeling were: i. the coiled-coil dimerization interface, and ii. the actin binding regions of the protein (Figure S1A; Singh and Hitchcock-DeGregori, 2007). To identify the actin binding regions, we searched for the motif: K/R, X, X, X, N ,X, E, X, X, X, E/D, K/R, A/Y, X, D/E, X, A, X, N, A/S. For TM1A, we replaced the endogenous cysteine with an alanine, C32A. By following the two principles above, we then chose a serine to replace with a cysteine, S82C.

Since TM1A is acetylated *in vivo* (Goins and Mullins), we also attached an acetylation mimic to the N terminus of the protein: AS-TM1A.

Protein Purification & Labeling

Rabbit Skeletal Muscle Actin

Actin was purified from rabbit acetone powder by the method of Supich and Watt (1971). Briefly, rabbit muscle acetone powder (Pel-Freeze) was resuspended in G buffer (0.5 mM TCEP, 0.1 mM $CaCl_2$, 0.2mM ATP, 2mM Tris pH 8.0) and let to stir on ice for 30min. The acetone powder was pelleted by centrifugation at 30k rcf for 30 min. The supernatant was filtered through cheesecloth. The actin was polymerized by adding KCl and MgCl2 to 50mM and 2mM, respectively. Polymerization occurred at RT for 15min, and continued on ice for 15 min. KCl was added to 0.8M, and allowed to stir at 4°C for

15 min to dissociate tropomyosin. Actin was pelleted in a Ti45 rotor for 2hrs at 142k rcf. The pellet was resuspended in G buffer and dounced before dialysis into G buffer for 2-3 days. Actin was gel filtered and stored in G buffer at 4°C.

Actin Labeling

Rabbit skeletal muscle actin was labeled on Cys-374 with pyrene-iodoacetamide (Invitrogen), as described (Cooper et al., 1983). Briefly, gel-filtered Rabbit Skeletal Muscle actin was diluted to around 1mg/ml (27μM) and polymerized by addition of KMEI (50 mM KCl, 1 mM $MgCl_2$, 1 mM EGTA, 10 mM imidazole pH 7.0). Polymerized actin was dialyzed against L-KMEI (100 mM KCl, 2 mM $MgCl_2$, 25 mM imidazole pH 7.5, 0.3 mM ATP). Actin was transferred to a small beaker and 4-7 moles of pyrene-iodoacetamide (Invitrogen) per mole of actin, were added while stirring. The reaction was covered with foil and allowed to proceed overnight, with gentle stirring. The reaction was quenched with 10mM DTT and precipitated dye was removed by low speed centrifugation at 4k rcf. Labeled actin filaments were pelleted by centrifugation for 2 hours at 142k rcf in a Type 45 Ti Rotor (Beckman-Coulter). Filamentous labeled actin was depolymerized by dialyzing into Buffer A (2mM Tris HCl, pH 8.0, 0.2mM ATP, 0.1mM $CaCl_2$, 0.5mM TCEP, 0.04% azide) and gel filtered on an S75 column (GE Healthcare). Labeled actin was stored at 4°C in the dark.

Actin was labeled with Alexa-488 maleimide (Invitrogen) while in the de-polymerized state. Briefly, G-Actin was dialyzed overnight into L-Buffer A (5 mM Tris pH 8.0, 0.2 mM ATP, 0.1 mM $CaCl_2$). 5 molar excess of Alexa-488 maleimide was added to

the actin. The reaction proceeded on ice for 15 minutes and was quenched with 10mM DTT. Actin was polymerized by addition of 1X KMEI (50 mM KCl, 1 mM $MgCl_2$, 1 mM EGTA, 10 mM imidazole pH 7.0). Filamentous, labeled actin was collected by centrifugation, and both resuspended in and dialyzed against Buffer A to depolymerize. Labeled actin was gel filtered on an S75 column (GE Healthcare).

AS-TM1A

The AS-TM1A C32A/S82C construct, in a pET20b vector, was expressed in BL21 *E. coli* cells. Bacterial pellets were resuspended in a 3X volume of lysis buffer (50 mM Tris pH 7.5, 10 mM EDTA, 2 mM DTT, 200mM NaCl, 1 mM PMSF, 5 mg/L DNAse1, 10 mg/L RNAseA) and lysed by passage through a microfluidizer and cleared by centrifugation. The supernatant, in a 50 ml conical tube, was placed in a boiling water bath (95°C) for 7 min (or until the supernatant precipitates), then placed in RT water for 7 min, then on ice for 30 min. The precipitate was pelleted by centrifugation at 150k rcf, 4°C for 45 min, and the supernatant recovered. Precipitate the tropomyosin by adding 1N HCl until the pH is below the PI (4.69). The precipitate was pelleted by centrifugation at 20k rcf, 4°C for 20 min. The pellet was resuspended in 20mM Tris-HCl pH 7.5, 0.5mM TCEP, and KOH added until the pH returned to 7.5. A 20-40% ammonium sulfate cut was taken from the resuspended pellet, and centrifuged at 130k rcf for 20 min at 4°C. The pellet was resuspended in and dialyzed into 10mM imidazole pH 7, 100mM KCl, 0.5mM TCEP. The purified protein was flash frozen and stored at -80°C.

Rabbit Skeletal TM

Rabbit skeletal tropomyosin was purified from rabbit acetone powder by the method of Smillie (1982). Briefly, rabbit muscle acetone powder (Pel-Freeze) was resuspended in extraction buffer (25mM Tris pH 8.0, 1M KCl, 0.1 mM $CaCl_2$, 0.2mM ATP, 0.5 mM DTT) and let to stir at RT for 16hrs. The acetone powder was filtered out with cheesecloth, and the filtrate cleared by centrifugation at 20k rcf for 10 min at 4°C. Precipitate the tropomyosin by adding 1N HCl until the pH is below the PI (4.69). The precipitate was pelleted by centrifugation at 20k rcf, 4°C for 10 min. The pellet was resuspended in 1M KCl, 0.5mM DTT, and the pH adjusted to 7.4 by addition of 1N KOH. The solution was clarified by centrifugation at 20k rcf, 4°C for 10 min. A 25-35% ammonium sulfate cut was taken from the supernatant, and centrifuged at 20k rcf for 10 min at 4°C. The pellet was resuspended in and dialyzed into 25mM imidazole pH 7.4, 100mM KCl, 2mM $MgCl_2$, 1mM EGTA, 1mM β-ME. The purified protein was flash frozen and stored at -80°C.

TM Labeling

The *D. melangaster* tropomyosin isoform was labeled on an engineered cysteine (AS-TM1A C32A/S82C). The rabbit tropomyosin was labeled on the native cysteines (alpha TM: C190, beta TM: C36). Each isoform was first pre-reduced in 5mM TCEP, 10mM Imidazole pH 7.0, 100mM KCl for 10min. The protein was then buffer exchanged into 10mM Imidazole pH 7.0, 100mM KCl with a pre-equilibrated PD-10. AlexaFluor 488, Cy3-MonoMaleimide, or Cy5-MonoMaleimide (all Sigma) was added to 4 times above

the molar concentration of protein, and allowed to incubate on ice for 30min. Any aggregate label was removed by centrifugation at 230k rcf, 4°C for 20min. Free label was removed by buffer exchanging into 10mM imidazole pH 7, 100mM KCl, 0.5mM TCEP. The labeled protein was flash frozen and stored at -80°C.

Capping Protein

Recombinant mouse capping protein CPα1β2 was purified as described (Palmgren et al., 2001). Briefly, the protein construct, in a pET3d vector, was expressed in BL21 *E. coli* cells. Bacterial pellets were resuspended in a 3X volume of lysis buffer (50mM Tris pH 8.0, 1mM EDTA, 1mM DTT, 1mM PMSF) and lysed by passage through a microfluidizer and cleared by centrifugation. A 50-70% ammonium sulfate cut was taken from the cleared lysate and centrifuged at 32k rcf for 20 min at 4°C. The pellet was resuspended in 20mL of HA dialysis buffer (1mM NaH_2PO_4 pH 7.0, 1mM DTT) and dialyzed overnight into the same buffer with at least three changes. The dialysate was loaded onto an HA column (GE Healthcare) with 10mM NaH_2PO_4 pH 7.0, and then eluted with a gradient from 10-250mM NaH_2PO_4. Peak fractions were pooled and dialyzed against QA dialysis buffer (10mM Tris pH 8.0, 10mM KCl, 0.5mM EDTA, 0.5mM TCEP). The sample was loaded onto a MonoQ column (GE Healthcare) and eluted with a 10-400mM KCl gradient. Selected fractions were dialyzed into SA dialysis buffer (10mM MES pH 5.8, 0.5mM EDTA, 1mM DTT). The sample was loaded onto a MonoS column (GE Healthcare) and eluted with a 0-350mM NaCl gradient. Selected fractions were dialyzed into storage buffer (10mM Tris pH 8.0, 40mM KCl, 0.5mM

TCEP, 50% glycerol), flash frozen, and stored at -80°C.

Ancanthamoeba *castellani* Arp2/3 Complex

Arp2/3 was prepared from *Acanthamoeba* castellini by the method of Dayel et. al. (2001). Briefly, 15L of *Ancanthamoeba castellani* were grown up, harvested and washed into 10mM Tris, pH 8.0 at 4°C, 100mM NaCl. The cells were ruptured by release from a Parr bomb equilibrated wtih nitrogen at 400 p.s.i. Lysate was cleared with centrifugation first at a low speed, 15 min, 4k rcf at 4°C; then at a higher speed, 2 hrs, 113k rcf at 4°C. After centrifugation, the top layer of lipids was removed by gentle aspiration, and the pellet discarded. The lysate was loaded onto a DEAE column, and the flow through collected. The flow through was then loaded onto an NWASP WWCA-Sepharose column, washed with 10mM Tris pH 8.0, 50mM NaCl, 0.1mM $CaCl_2$, 0.2mM ATP, 1mM DTT, 15 ug/mL Benzamidine. The protein complex was eluted with 10mM Tris pH 8.0, 400mM $MgCl_2$, 1mM DTT, and dialyzed into MonoS low buffer (10mM Tris pH 8.0, 0.5mM TCEP, 0.5mM $MgCl_2$, 0.1mM ATP). The sample was loaded onto a MonoS column (GE Healthcare) and eluted with a 0-500mM NaCl gradient. Selected fractions were gel filtered using a Superdex 200 column (GE Healthcare) into 20mM HEPES pH 7.0, 0.5mM TCEP, 25mM KCl, 0.2mM $MgCl_2$, 0.1mM ATP. Glycerol was added to 10% and the purified protein flash frozen and stored at -80°C.

ActA$^{30\text{-}612}$-KCK-6XHis

ActA$^{30\text{-}612}$-KCK-6XHis was purified as described (Akin and Mullins, 2008). Briefly, the construct, cloned in a pET 17b vector, was expressed in BL21 *E. coli* cells. Bacterial pellets were resuspended in 4-5X volume of lysis buffer (100mM NaH_2PO_4 pH 8.0, 10mM Tris base, 6M Guanidium HCl, 10mM 2-mercaptoethanol, 1mM PMSF) and lysed by nutating overnight at room temperature. Clarified lysate was batch bound to Ni-NTA resin (1-2mL of resin per liter of culture) for 30 min. The resin was washed with wash buffer (100mM NaH_2PO_4 pH 7.8, 10mM Tris base, 10mM Imidazole, 6M Guanidium HCl, 10mM 2-mercaptoethanol), and eluted with elution buffer (100mM NaH_2PO_4 pH 7.5, 10mM Tris base, 250mM Imidazole, 6M Guanidium HCl, 10mM 2-mercaptoethanol). The eluate was dialyzed into Buffer QA (10mM Bistrispropane pH 7.0, 1mM EDTA, 0.5mM TCEP), loaded onto a MonoQ column (GE Healthcare) and eluted with a 100-300mM KCl gradient. Selected fractions were dialyzed into storage buffer (10mM HEPES pH 7.0, 50mM KCl, 1mM TCEP), flash frozen, and stored at -80°C.

Profilin 1

Recombinant human Profilin1 was purified, as described (Reichstein and Korn, 1979), with the following modifications. The Profilin1, in vector pET16B, was expressed in *E. coli* BL21 pLysS. Bacterial cell pellets were resuspended in lysis buffer (10 mM Tris pH 8.0, 1 mM EDTA, 2 mM DTT, 1 mM PMSF) and lysed using an Emulsiflex. Ammonium sulfate was added to the clarified lysate to a concentration of 35%. After

centrifugation, an additional 26% ammonium sulfate to a final concentration of 61% was added to the supernatant. After centrifugation, the pellet was resuspended in lysis buffer and dialyzed overnight against more lysis buffer. Protein was applied to a DEAE column and the flow through and wash fractions were collected. These fractions were dialyzed against HA Buffer (5mM K_2HPO_4 pH 7.5, 1mM DTT) and applied to a hydroxyapatite column. Flow through and wash fractions were pooled, and gel filtered (10mM Tris pH 7.5, 50mM NaCl, 0.5mM TCEP) using a Superdex 200 column connected to an ÄKTA Purifier system. Glycerol was added to 20% final concentration to the peak fractions. Protein was flash frozen in liquid nitrogen and stored at -80°C.

hCofilin 1

Recombinant human Cofilin1 was purified as described (Carlier et al., 1997), with the following modifications. The construct, cloned into a pET16b vector, was expressed in BL21 Rosetta cells (Novagen). *E. coli* lysate was dialyzed into DEAE buffer (10 mM Tris pH 7.8, 50 mM NaCl, 0.2 mM EDTA, 2 mM DTT, 1 mM PMSF). The flow through and wash from the DEAE column was dialyzed into (10 mM PIPES pH 6.5, 15 mM NaCl, 2 mM DTT, 0.2 mM EDTA), and loaded onto a MonoS 5/50 GL column connected to an ÄKTA Purifier system (GE Healthcare). Protein was gel filtered using a Superdex 200 column into 10 mM Tris pH 7.5, 50 mM NaCl, 0.5 mM TCEP; glycerol was added to 20% to peak fractions and protein was flash frozen and stored at -80°C.

Microscopy

Glass Chamber Treatment & Assembly

The same glass treatment and chamber assembly was used for both Bead Motility assays and Single Filament TIRF assays. To minimize non-specific protein absorption, glass slides were washed in ethanol and KOH. Glass coverslips were first washed in ethanol and KOH, and then fully cleaned with plasma glow discharge. The coverslips were then treated with a 2.5% solution of APTES (3-Aminopropyltriethoxysilane from Sigma) in 5% water, 95% ethanol pH 4.5 (with acetic acid). After rinsing in ethanol and water, the coverslips were treated with 10% NHS-PEG(5000)-Biotin and 90% NHS-PEG(5000) in DMF. Microscopy chambers were prepared with double-stick tape between the slide and coverslip.

Bead Motility Assay

Carboxylated, polystyrene, 5μm diameter beads (Bangs Labs) were coated with ActA$^{30\text{-}612}$-KCK-6XHis using EDC-SulfoNHS chemistry, as described (Akin and Mullins, 2008). Coated beads were stored in 1mg/mL BSA, 2mM Tris pH 8.0 and used at 1:120 dilution in motility assays.

For motility assays without recycling agents (cofilin and profilin), we mixed the ActA-coated beads with 7.4μM 3% Alexa488 labeled actin, 210nM capping protein, 125nM Arp2/3, and varying amounts of labeled TM1A. All assays were carried out in 0.2% methyl cellulose (400 cP), 2.5mg/mL BSA, 1mM $MgCl_2$, 1mM EGTA, 20mM HEPES pH 7.0, 50mM KOH [pH 7.0 with 15mM TCEP HCl], and 250μM ATP. For

motility assays with recycling agents, we included the indicated concentration of hCofilin1, and added an equal concentration of hProfilin1.

All images were acquired at room temperature on a software-controlled (MicroManager) Nikon Eclipse TE2000-E inverted epifluorescence microscope equipped with an EM CCD camera (Andor iXon), and a Nikon 60X water immersion objective. After flowing in 10μL of the motility mix, glass chambers were sealed with VALAP (molten mixture of Vaseline, lanolin, and paraffin at 1:1:1 mass ratio), and imaged immediately. Images were taken at 60 second intervals.

Single Filament TIRF

All images were acquired at room temperature on a software-controlled (NIS Elements 4.1) Nikon Ti-E inverted TIRF microscope equipped with an EM CCD camera (Andor DU897), and a Nikon 100X oil immersion objective. Each chamber was initially incubated for 1 min with blocking solution (10mM Imidazole, pH 7.0, 50mM KCl, 1mM $MgCl_2$, 1mM EGTA, 1mg/mL BSA, 1% Pluronic acid, 250 μg/mL κ-casein).
The chamber was then rinsed with 1X KMEI/BSA (10mM Imidazole, pH 7.0, 50mM KCl, 1mM $MgCl_2$, 1mM EGTA, 1mg/mL BSA). For assays where the filaments were not attached to the coverslip, the protein mix (labeled actin, tropomyosin, Arp2/3, hcofilin1 in 0.2% methyl cellulose (400cP), 1mg/mL BSA, 1mM $MgCl_2$, 1mM EGTA, 50mM KCl, 200μM ATP, 20mM glucose, 250μg/mL glucose oxidase, 50μg/mL catalase, 20mM βME, and 10mM Imidazole, pH 7.0) was flowed in, then the chamber sealed with VALAP (molten mixture of Vaseline, lanolin, and paraffin at 1:1:1 mass ratio), and

imaged immediately. For assays where the filaments were attached, before flowing in the protein mix, the chamber was treated with 1μM Streptavidin, rinsed with 1X KMEI/BSA, then 1μM biotin-phalloidin, and rinsed with 1X KMEI/BSA. For assays with BeF_3, 1mM $BeCl_2$ and 5mM KF were added to the protein mix before starting the reaction. Images were taken at 10 second intervals.

TIRF binding assay

To determine the binding affinity of TM1A for actin using single filament TIRF, 20% 200nM A488-actin with varying amounts of Cy5-TM1A (5-160nM) were sealed in glass chambers with VALAP and allowed to incubate in the dark at room temperature for 3.5 hrs to reach steady state. 2-color images of 20 random fields were taken for each concentration of TM1A.

TIRF with Cofilin

To examine TM1A's ability to protect actin filaments from cofilin severing, the chambers were first incubated with 1μM streptavidin and 1μM biotin-phalloidin so the actin filaments would be attached to the coverslip. A single filament TIRF reaction with 20% 600nM A488-actin and 600nM Cy5-TM1A was flowed into the glass chamber and allowed to incubate in the dark for 10min. At 10min, a second reaction containing no actin, 150nM hCofilin1, and 500nM Cy5-TM1A was flowed into the chamber, displacing the first reaction. The chamber was then sealed with VALAP and imaged immediately at 10 second intervals.

ADP-Actin

ADP-actin was polymerized the night before in KMEI (50 mM KCl, 1 mM $MgCl_2$, 1 mM EGTA, 10 mM imidazole pH 7.0) and ADP-Buffer A (2mM Tris HCl, pH 8.0, 0.2mM ADP, 0.1mM $CaCl_2$, 0.5mM TCEP, 0.04% azide). To mark the pointed end, 10% 5μM A488-actin was polymerized for 5min at RT, then actin was added to 20% 5μM A488-actin. The actin was allowed to polymerize overnight on ice. As a control, the opposite labeling was also made: 20% 5μM A488-actin was polymerized for 5min at RT, then actin was added to 10% 5μM A488-actin. On the day of imaging, the labeled actin was diluted to 1μM, and final reactions included 20nM pre-polymerized actin.

Pyrene Assay

Actin polymerization was measured by monitoring an increase in fluorescence (λ_{ex} = 365nm, λ_{em} = 407nm) of 5%-pyrene-iodoacetamide labeled actin that was purified from *Acanthamoeba castellanii*. We mixed Arp2/3, Arp2/3 activator ($ActA^{30-612}$-KCK-6XHis) in KMEI (50mM KCl, 1mM $MgCl_2$, 1mM EGTA, 10mM imidazole pH 7.0). Actin polymerization reactions contained 4μM actin (5% pyrene-labeled), all other components were as specified in figure legends. All reaction components, except for actin were mixed in a single tube. Separately, actin was pre-incubated with ME (50μM $MgCl_2$, 20μM EGTA) for 2 minutes, to facilitate the exchange of Ca^{2+} ions for Mg^{2+} ions. Reactions were initiated by addition of actin to the other components.

Cosedimentation binding assay

AS-TM1A C32A/S82C (TM1A) was first diluted to 6.4μM in KMEI and Buffer A. Any aggregates were removed from the TM1A by centrifugation at 4°C, 227k rcf for 20min. The TM1A was then diluted serially by 1/2X into KMEI and Buffer A. RSK G-actin was then added to a final concentration of 4μM in KMEI and Buffer A to start the reaction. Since TM1A can polymerize and sediment on its own, at each concentration of TM1A, a control reaction was made that did not include actin. Once the reaction was started, a load gel sample was taken immediately, while the binding reactions were allowed to incubate at RT for 2hrs. The reactions were centrifuged at 20°C, 190k rcf for 30min. Gel samples of the supernatant and the pellet were made. All gel samples were made with 250μg/mL BSA as a loading control. Gel samples were run on a NuPAGE 4-12% Bis-Tris gel, stained with Sypro-Red stain (Life Technologies), and imaged on a GE Healthcare Typhoon imager. A titration of actin concentrations was used as a standard. A simple fit of the data was done to determine the Kd and Hill coefficient.

Actin ATP State Growth Simulation

A visual simulation of the ATP state of individual actin subunits in a growing actin filament was developed in MATLAB. These were the conditions and values used:

- Actin monomer size = 6 nm (Trinick et. al., 1986)
- ATP hydrolysis rate = 0.3 1/sec (Blanchoin and Pollard, 2002)
- Pi release rate = 0.0062 1/sec (Carlier, 1987)
- BeF_3 Kon rate = $4*10^{-3}$ 1/(μM * sec) (Antonny and Chabre, 1992)

- ATP-actin growth rate = 11.6 1/(μM * sec) (Pollard, 1986)
- Actin concentration = 0.5 μM
- Time step = 1 sec

Each simulated filament was frozen once it reached a particular length so that the distribution of the different ATP states of the actin subunits could be observed.

Image Analysis

Motility Assay Image Analysis

All image analysis was accomplished with MATLAB code written by the authors. The lengths of the motile actin comet tails were determined by hand-drawn line scans through the middle of the long axis of the tail in each image, using MATLAB code written in-house.

Single Filament TIRF Image Analysis

TM1A binding distances along single actin filaments was determined by hand-drawn line scans in ImageJ. The hand-drawn kymographs were made in MATLAB where for each filament, a separate line-scan was hand-drawn for every frame. This was necessary because the filaments were not attached to the coverslip.

Analysis for TIRF binding assay

Each 2-color image was analyzed with MATLAB code written by the authors to determine the sum of the length of the filaments. A simple ratio was taken between the

length of the actin filaments, and 1/6 * the length of the TM1A filaments. A simple fit of the data was done to determine the Kd and Hill coefficient.

Acknowledgements

The authors would like to thank Orkun Akin for generously giving us his ActA and capping protein constructs, and for teaching JYH how to do bead motility assays. We would like to thank Peter Bieling for giving us his hCofilin1 and hProfilin1 constructs. We are grateful to Elena Ingerman for lending us her NWASP WWCA-Sepharose column, and helping JYH with the Arp2/3 prep, as well as teaching JYH how to do single filament TIRF assays. We are also grateful to Chris Rivera, who provided many intellectually stimulating conversations. We would like to thank Kurt Thorn and DeLaine Larsen from the UCSF Nikon Imaging Center, who helped us use and maintain the TIRF scope used in these assays.

Contributions

JYH did the cloning, protein purifications, assays, analysis, modeling, figure making and writing. LMG made the WT AS-TM1A construct from which the AS-TM1A C32A/S82C construct was made. LMG also optimized the TM1A purification protocol, and gave useful scientific guidance throughout the project. RDM gave useful scientific guidance throughout the project and contributed to the writing of this paper.

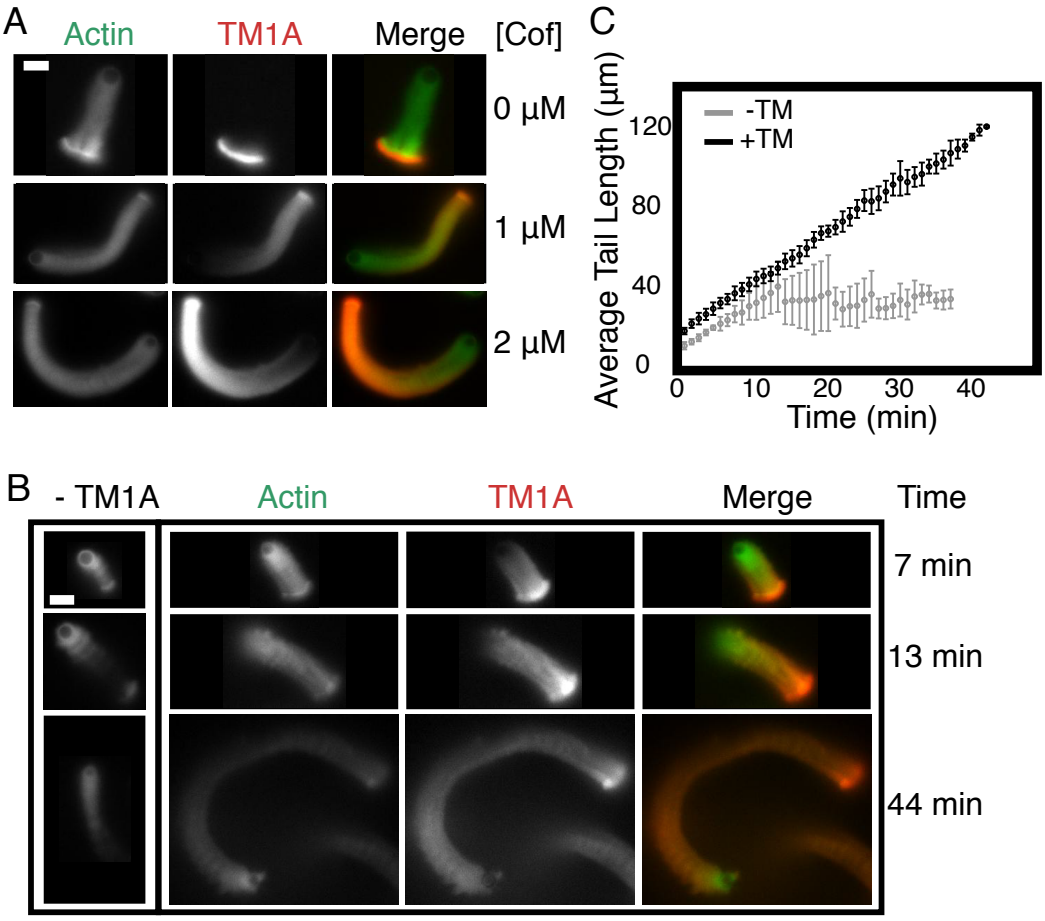

Figure 1. Cofilin promotes the binding of tropomyosin to motile actin networks generated by the Arp2/3 complex and capping protein. (A) Actin networks generated from ActA-coated polystyrene microspheres by the Arp2/3 complex and capping protein exclude tropomyosin in the absence of Cofilin. Cofilin renders dendritic actin networks competent to bind tropomyosin. Left: fluorescence of Alexa488-labeled actin. Middle: Cy3-labeled Drosophila non-muscle tropomyosin isoform, TM1A. Right: merge of actin and TM1A fluorescence. Each row has the indicated concentration of added Cofilin. Scale bar: 10μm. (B) Effect of tropomyosin on depolymerizing activity of cofilin. Left Box: Motile actin networks generated by the Arp2/3 complex in the presence of capping protein and Cofilin. Right Box: Addition of TM1A. Left: Alexa488-labeled actin. Middle: Cy3-labeled TM1A. Right: Merge. Scale bar: 10μm. (C) Graph of actin network length versus time in the presence and absence of Tm1A. Temperature: 24C. Buffer: [components]. Reagents: 3% 7.4 μM A488-actin, 125nM Arp2/3 complex, 210nM Capping Protein, 1μM Cy3-Tm1A.

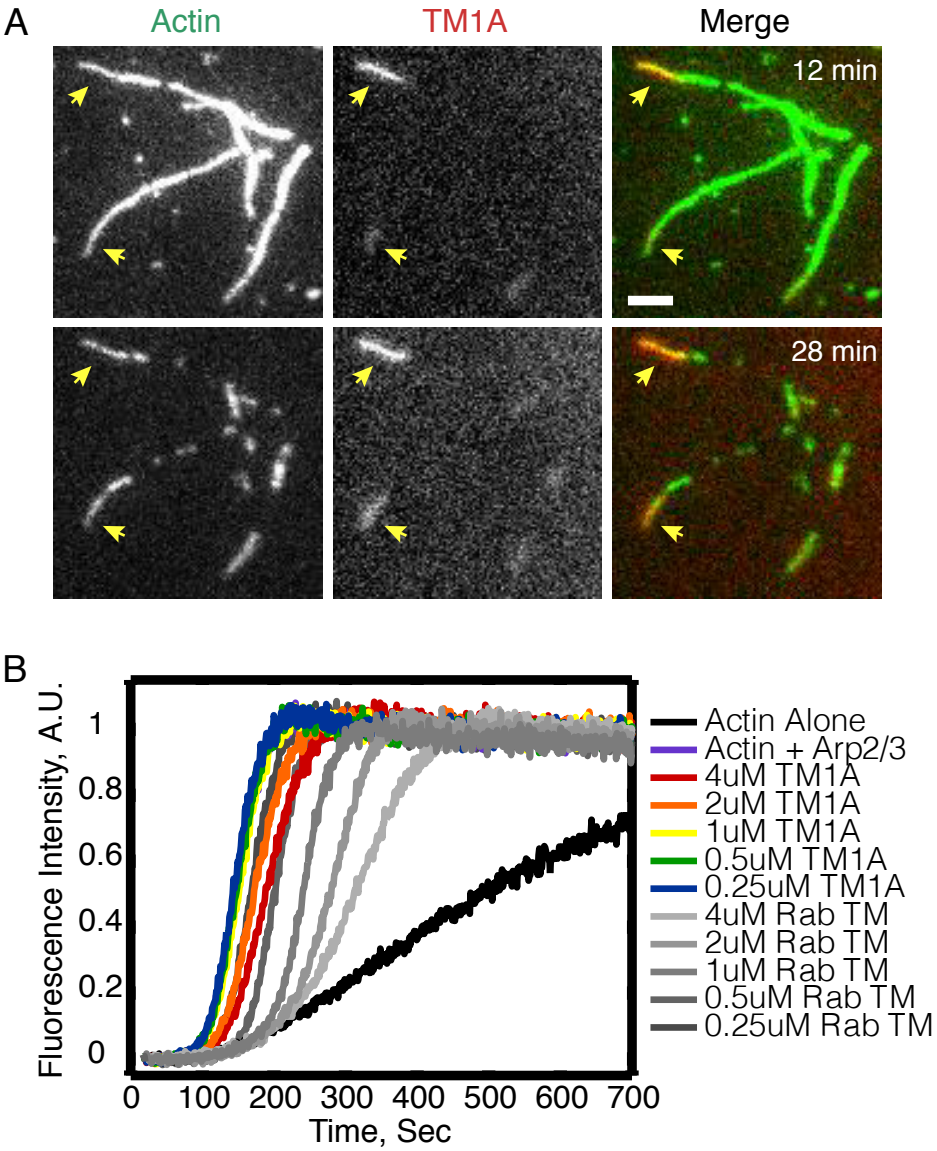
A
Actin
TM1A
Merge
12 min
28 min
B
Fluorescence Intensity, A.U.
1
0.8
0.6
0.4
0.2
0
0
100
200
300
400
500
600
700
Time, Sec
Actin Alone
Actin + Arp2/3
4uM TM1A
2uM TM1A
1uM TM1A
0.5uM TM1A
0.25uM TM1A
4uM Rab TM
2uM Rab TM
1uM Rab TM
0.5uM Rab TM
0.25uM Rab TM
C
Actin
TM1A

Figure 2. TM1A protects actin filaments from cofilin severing, and weakly inihibits Arp2/3 nucleation off the sides of actin filaments. (A) Single filament TIRF. Actin filaments pre-bound by TM1A (indicated by arrows) are protected from cofilin's severing activity. Left: fluorescence of Alexa488-labeled actin. Middle: Cy5-labeled Drosophila non-muscle tropomyosin isoform, TM1A. Right: merge of actin and TM1A fluorescence. Prebinding conditions: 20% A488 600nM RSK muscle actin, 600nM TM1A-Cy5. Severing conditions flowed into chamber 10min after the start of the reaction: 150nM Cofilin, 500nM TM1A-Cy5. Scale bar: 3μm. (B) Tm1A binding to actin filaments has weak effect on nucleation by the Arp2/3 complex. Time-resolved pyrene fluorescence of polymerizing actin filaments nucleated by the Arp2/3 complex in the absence and presence of Tm1A and RSK muscle tropomyosin. (C) TIRF microscopy of actin filaments nucleated from the sides of pre-existing, Tm1A-coated, mother filaments. Large scale bar: 5μm. Small scale bar: 1μm.

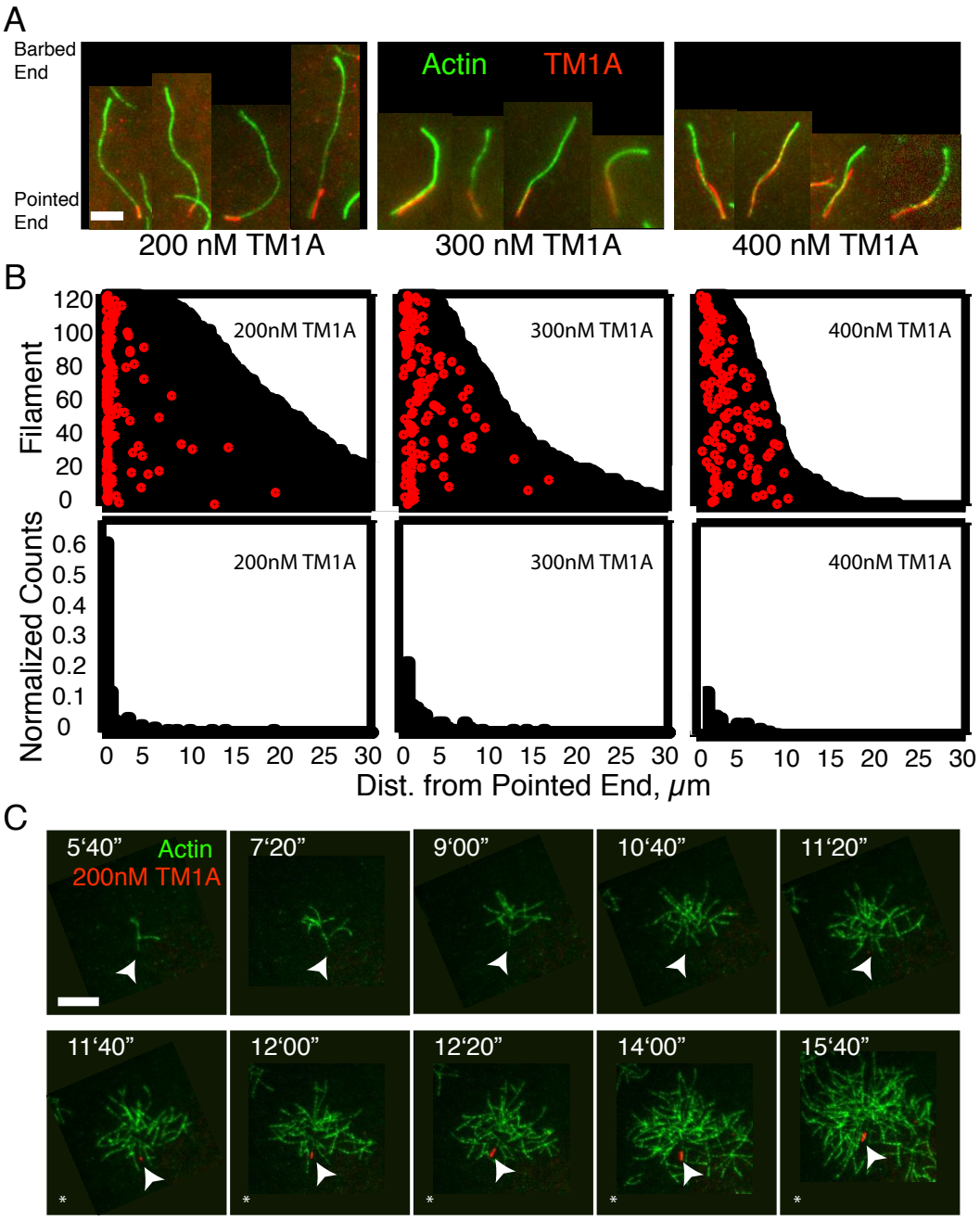
A
Barbed End
Pointed End
Actin
TM1A
200 nM TM1A
300 nM TM1A
400 nM TM1A
B
Filament
Normalized Counts
200nM TM1A
300nM TM1A
400nM TM1A
Dist. from Pointed End, μm
C
5‘40”
Actin
200nM TM1A
7‘20”
9‘00”
10‘40”
11‘20”
11‘40”
12‘00”
12‘20”
14‘00”
15‘40”

Figure 3. TM1A binds from the pointed end, and binding is blocked by the Arp2/3 complex. (A) Single filament TIRF. Cy5-Tm1A binding to actin filaments at different concentrations of Cy3-TM1A. Cy5-TM1A in red, 600nM A488-actin in green. (B) Visual representation of each binding event of Cy3-TM1A to actin filaments, as shown in A. Each filament's length is in black, and the distance from the pointed end of each binding event is plotted in red. (C) Normalized histograms of TM1A binding events as a function of the distance from the pointed end of actin filaments. 200nM: 126 binding events, 300nM: 121 binding events, 400nM: 115 binding events. (D) Frames from time-lapse movie of Cy5-Tm1A binding to Arp2/3 branched actin filaments. 5% 0.6μM A488-actin, 4nM Arp2/3, 40nM ActA, 200nM Cy5-TM1A. An arrow indicates the pointed end of the original mother filament in each frame. Stars indicate frames where TM1A is bound. Scale bar: 10μm.

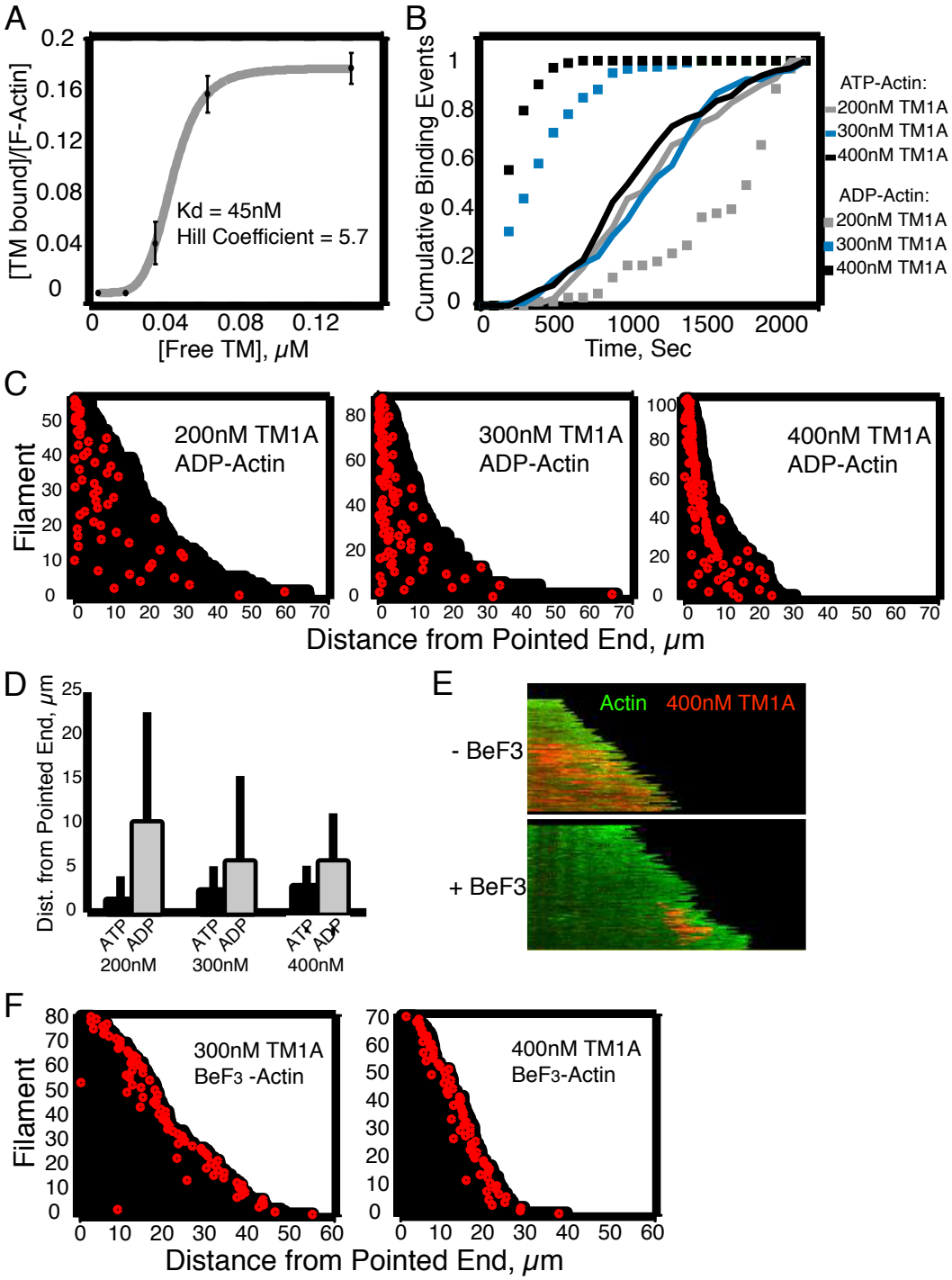
A
[TM bound]/[F-Actin]
0.2
0.16
0.12
0.08
0.04
0
Kd = 45nM
Hill Coefficient = 5.7
0
0.04
0.08
0.12
[Free TM], μM
B
Cumulative Binding Events
1
0.8
0.6
0.4
0.2
0
0
500
1000
1500
2000
Time, Sec
ATP-Actin:
200nM TM1A
300nM TM1A
400nM TM1A
ADP-Actin:
200nM TM1A
300nM TM1A
400nM TM1A
C
Filament
200nM TM1A
ADP-Actin
300nM TM1A
ADP-Actin
400nM TM1A
ADP-Actin
Distance from Pointed End, μm
D
Dist. from Pointed End, μm
25
20
15
10
5
0
ATP
ADP
200nM
300nM
400nM
E
Actin
400nM TM1A
- BeF3
+ BeF3
F
Filament
300nM TM1A
BeF3 -Actin
400nM TM1A
BeF3-Actin
Distance from Pointed End, μm

Figure 4. Binding of TM1A to filamentous actin is highly cooperative, and is affected by the ATP state within the filament. (A) Binding affinity of tropomyosin isoform TM1A with actin filaments using single filament TIRF. (B) Cumulative counts of TM1A binding events over time. ATP actin; 200nM TM1A: 110 events, 300nM TM1A: 105 events, 400nM TM1A: 97 events. ADP actin; 200nM TM1A: 61 events, 300nM TM1A: 119 events, 400nM TM1A: 103 events. (C) Visual representation of each binding event of Cy3-TM1A to ADP-actin filaments. Each filament's length is plotted in black, and the distance from the pointed end of each binding event is plotted in red. (D) Average TM1A binding distance from the pointed end for ATP-actin and ADP-actin. (E) Binding of TM1A to BeFl3 bound actin filaments is transient. Representative hand-drawn kymographs of A488-actin and Cy5-TM1A, with and without BeF3. (F) Visual representation of each binding event of Cy3-TM1A to BeF3-actin filaments.

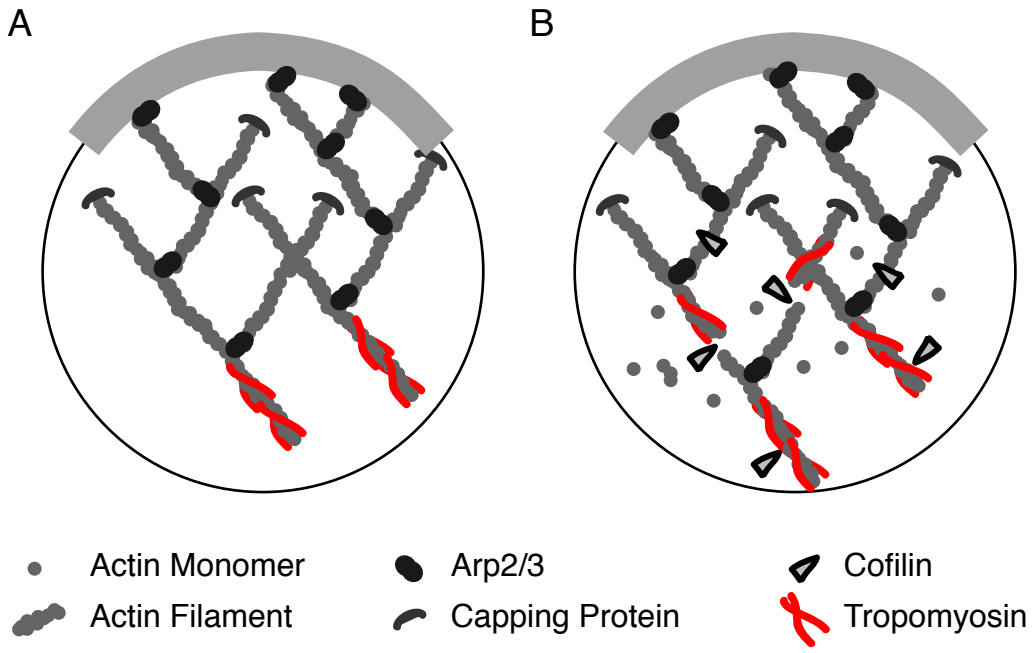

Figure 5. Model: Cooperation of the severing activity of cofilin and tropomyosin binding help establish the border between the lamellipod and lamellum. (A) Tropomyosin binding is blocked by Arp2/3 branches in the absence of cofilin. (B) In the presence of cofilin, new pointed ends are created, which allows tropomyosin to bind.

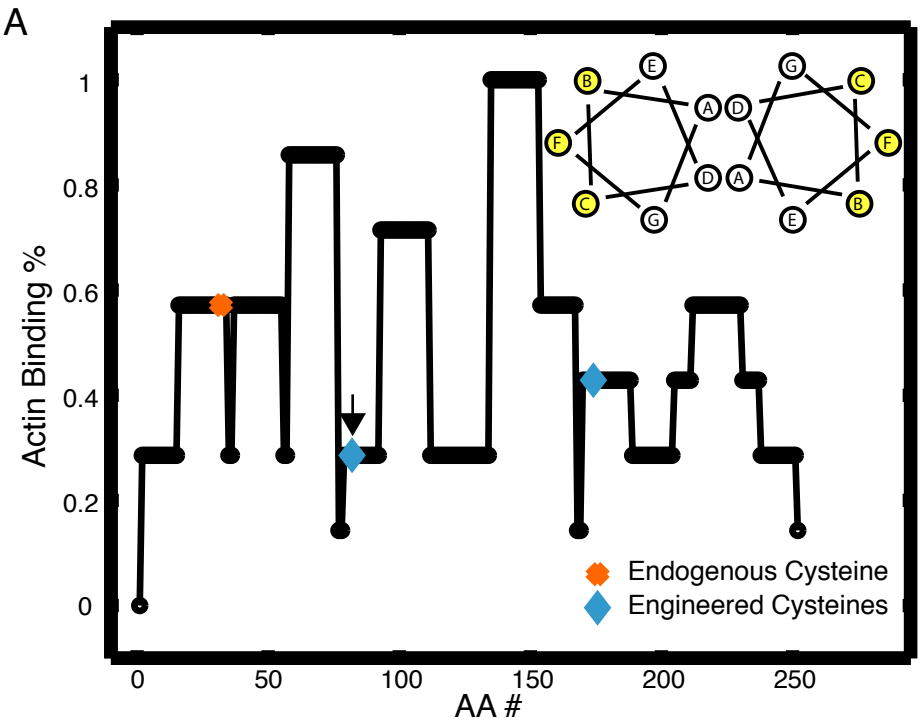
A
Actin Binding %
1
0.8
0.6
0.4
0.2
0
0
50
100
150
200
250
AA #
Endogenous Cysteine
Engineered Cysteines

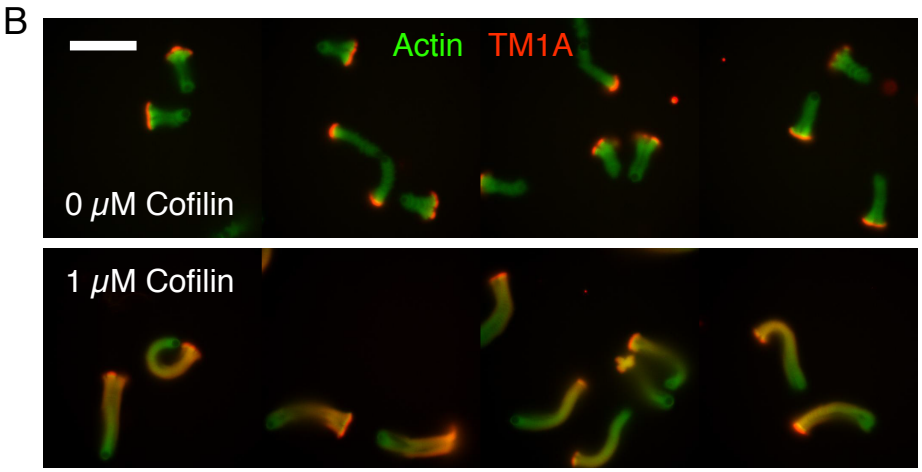
B
Actin
TM1A
0 μM Cofilin
1 μM Cofilin

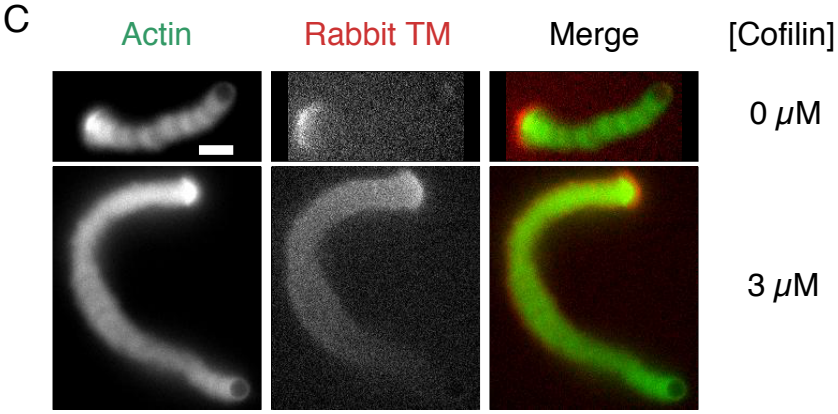
C
Actin
Rabbit TM
Merge
[Cofilin]
0 μM
3 μM

Figure S1. (A) Design of labeled TM1A to minimize the fluorophore's effect on TM1A binding. Plot shows how strong each actin binding region is along the coiled-coil. The endogenous cysteine (orange 'X') was removed, C32A. Blue diamonds indicate possible sites for introducing a cysteine. An engineered cysteine was placed at S82C (arrow) because the position will not disrupt TM1A dimerization, and it is in a region of low actin binding affinity. Inset shows the coiled-coil structure, and yellow highlights amino acid positions that do not disrupt dimerization. (B) Actin networks generated from ActA-coated polystyrene microspheres by the Arp2/3 complex and capping protein exclude tropomyosin in the absence of Cofilin. Cofilin renders dendritic actin networks competent to bind tropomyosin. Four random fields showing that the effect is robust. Green: Alexa488-labeled actin. Red: Cy3-labeled TM1A. Each row has the indicated concentration of Cofilin. Scale bar: 40μm. (C) Rabbit skeletal muscle (RSK) TM also requires the activity of cofilin to bind motile actin networks generated by the Arp2/3 complex and capping protein. Left: fluorescence of Alexa488-labeled actin. Middle: Cy3-labeled RSK TM. Right: merge of actin and RSK TM fluorescence. Scale bar: 10μm.

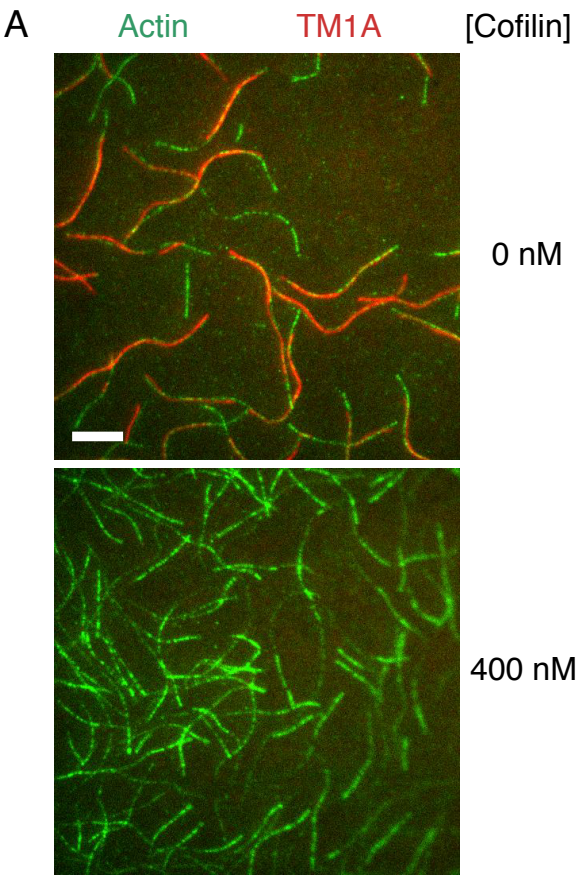

Figure S2. Cofilin and TM1A binding are mutually exclusive. Green: Alexa488-labeled actin. Red: Cy5-labeled TM1A. Top: 5% 1μM A488-actin, 400nM Cy5-TM1A. Bottom: 5% 0.8μM A488-actin, 400nM Cy5-TM1A, 400nM Cofilin.

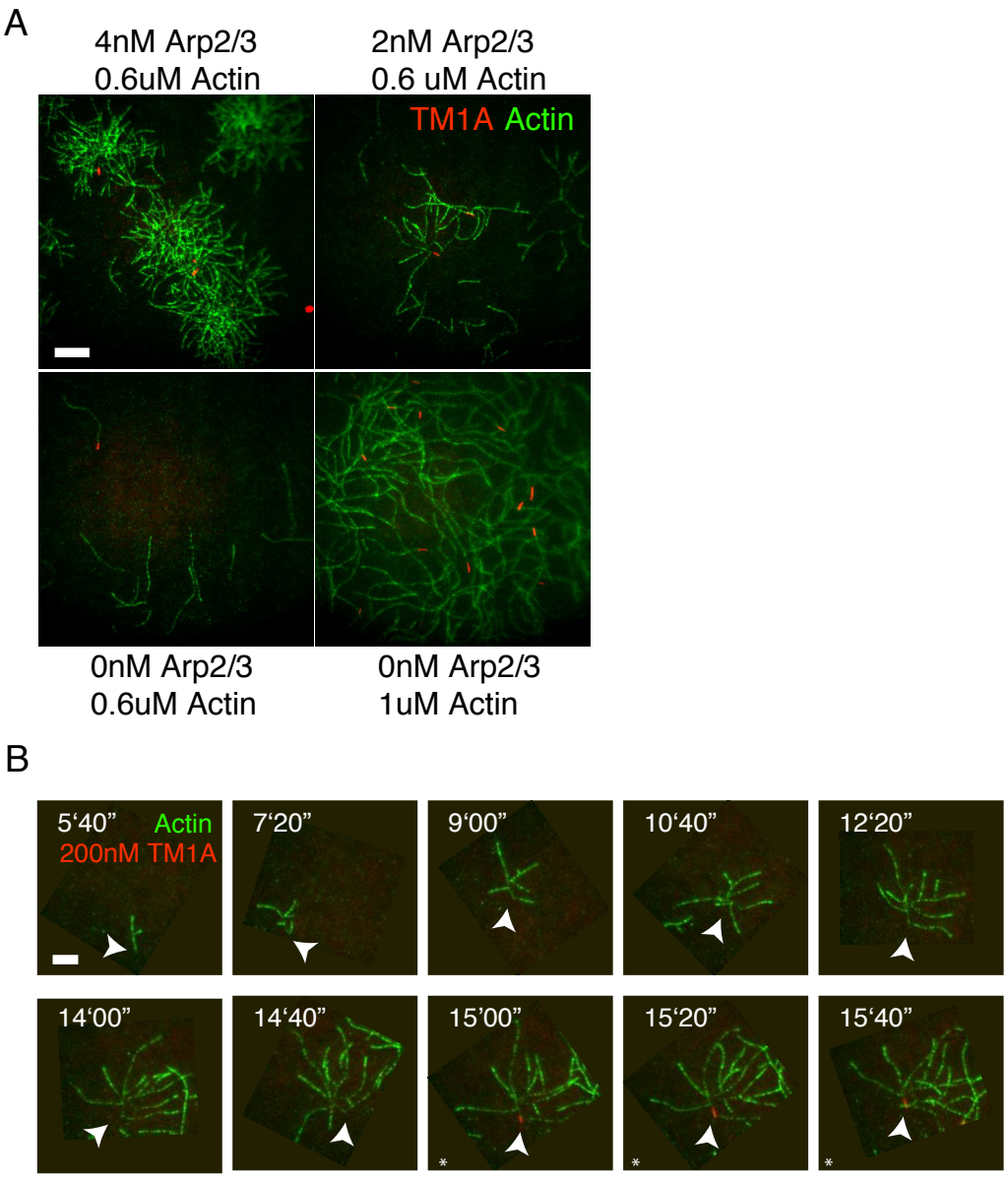

Figure S3. TM1A only binds free pointed ends. (A) Green: Alexa488-labeled actin. Red: 200nM Cy5-labeled TM1A. Top panels: Left: 4nM Arp2/3, 40nM ActA, 0.6μM A488-actin; Right: 2nM Arp2/3, 40nM ActA, 0.6μM A488-actin. Bottom panels: 0nM Arp2/3; Left: 0.6μM A488-actin; Right: 1μM A488-actin. (B) Frames from time-lapse TIRF movie of Cy5-Tm1A binding to Arp2/3 branched actin filaments. 5% 0.6μM A488-actin, 2nM Arp2/3, 200nM Cy5-TM1A. An arrow indicates the pointed end of the original mother filament in each frame. Stars indicate frames where TM1A is bound. Scale bar: 5μm.

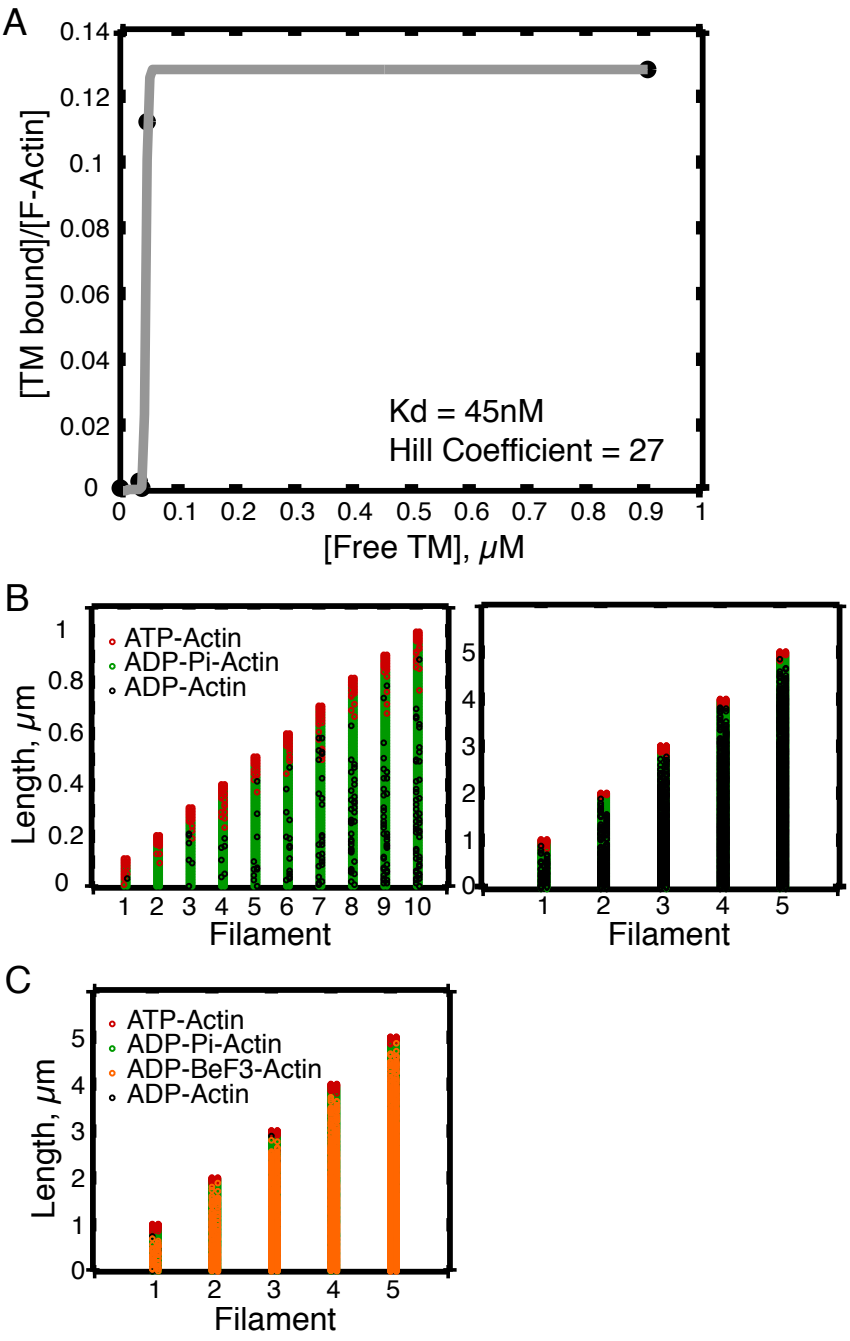

Figure S4. (A) Co-pelleting of TM1A with actin filaments. Kd = 45nM, Hill Coefficient = 27. (B) Simulation of the ATP state of subunits in growing actin filaments. Left: filaments frozen at 0.1μm intervals. Right: filaments frozen at 1μm intervals. (C) Simulation of the ATP state of subunits in growing actin filaments with BeF3. Filaments are frozen at 1μm intervals.

Chapter 2

Title

A nonmuscle tropomyosin isoform, TM1J, can only bind to actin as a co-polymer with another nonmuscle isoform, AS-TM1A or DcTM1A.

Abstract

Recently, three tropomyosin isoforms were identified in *Drosophila* S2 cells. Two of them, TM1A and TM1J, co-localize to the lamellum near the leading edge. We purified and labeled both of these isoforms to investigate their biochemical interactions with branched and un-branched actin filaments. We find that TM1J cannot bind to rabbit skeletal muscle actin without TM1A as a co-binder. We also find that each TM1J dimer can only polymerize surrounded by two TM1A dimers.

Introduction

Tropomyosin is a coiled-coil dimer that polymerizes head-to-tail along the major groove of actin filaments. Non-muscle tropomyosin has been shown to play an important role in many cellular processes including cell shape, cell adhesion, cell motility, vesicle transport, endocytosis and exocytosis, Golgi function, cytokinesis, and membrane function. However, because many different isoforms from each tropomyosin gene are generated, it is difficult to understand the role of any one isoform. For example, mammals have four tropomyosin genes, which together generate over 40 distinct tropomyosin isoforms. In addition, any one cell type can express over 10 different isoforms. (Gunning et. al., 2008)

To try to simplify the study of different tropomyosin isoforms, Goins and Mullins decided to use *D. melangaster* S2 cells as a model system because they were believed

to express only one non-muscle tropomyosin isoform. With RNAi, mass-spectrometry, RT-PCR, and immuno-staining, Goins and Mullins were able to determine that up to four isoforms are expressed in S2 cells: DcTM1A, TM1A, TM1J, and TM2A. DcTM1A is the un-acetylated version of TM1A. It is possible that there are more isoforms present, but they would be expressed at thus-far undetectable levels.

Goins and Mullins overexpressed labeled isoforms in S2 cells and imaged their localizations throughout the cell cycle. It was found that TM1A localized to the lamellum, cell cortex and cytokinetic ring during cell division. TM1J also localized to the lamellum during G1 and G2, but also formed rings around Golgi stacks. After nuclear envelope breakdown, TM1J disassembles from the Golgi, and reassembles onto kinetochores. It then moves into the mid-zone during cytokinesis before returning to the Golgi stacks for the next cell cycle. TM2A only localizes to Golgi stacks. In this study, we investigate the biochemical interactions between TM1A and TM1J on single actin filaments, as well as on a lamellipod-like Arp2/3 branched actin network.

Results

While *Drosophila* cytoplasmic AS-TM1A and DcTM1A can bind to rabbit skeletal muscle actin (RSK actin), AS-TM1J cannot bind to actin. Every attempt to co-pellet AS-TM1J with RSK is negative (Figure 1A). This includes scanning a wide range of buffer conditions: changing KCl and $MgCl_2$. In addition, labeled AS-TM1J does not bind to single actin filaments in TIRF, while labeled AS-TM1A does (Figure 1B). Labeled AS-TM1J also does not bind to actin networks generated from ActA-coated polystyrene

microspheres by the Arp2/3 complex and capping protein, no matter how much extra dark AS-TM1J is added (Figure 1C).

This result seemed odd at first since Goins and Mullins had clearly seen AS-TM1J in the lamellipod *in vivo* along with AS-TM1A, presumably bound to actin filaments. It was exactly this *in vivo* result that led us to try co-binding AS-TM1J with AS-TM1A. Indeed, AS-TM1J can co-bind to actin with AS-TM1A and DcTM1A. This is supported by co-pelleting assays where AS-TM1A and AS-TM1J are added together, and both co-pellet with filamentous actin (Figure1A). We also see labeled AS-TM1J co-bind with labeled AS-TM1A to single actin filaments (Figure 1B). In Figure 1C we see that AS-TM1J can co-bind with AS-TM1A, DcTM1A and to a minor degree, native rabbit skeletal muscle tropomyosin. AS-TM1J, however, does not co-bind with AS-TM2A, another long tropomyosin isoform proven to be present in Drosophila S2 cells (cite LG's paper). However, we do not yet know whether our purified AS-TM2A binds to RSK actin.

With this result that AS-TM1J could co-bind with AS-TM1A, we wanted to understand more about the nature of that co-binding. Specifically, we wanted to know whether AS-TM1J could bind to ends of filaments that are pre-bound with AS-TM1A – in essence, does AS-TM1J just need a primer to bind onto filaments (AAAA-JJJJ)? Or does AS-TM1J need to bind in an alternating fashion (A-J-AA-J-AAAA-J), so that every AS-TM1J dimer is always surrounded by two AS-TM1A dimers? Two-color co-binding of AS-TM1J with AS-TM1A in single filament TIRF shows that AS-TM1J cannot bind by itself onto the ends of actin filaments pre-bound with AS-TM1A (Figure 2B). In this assay, actin filaments are first incubated in the reaction chamber with Cy3 labeled AS-

TM1A. Then a second reaction mixture containing actin, and Cy5 labeled AS-TM1A or AS-TM1J (or a mix of AS-TM1A-Cy3 and AS-TM1J-Cy5) is flooded in, so that it replaces the first reaction mixture. The result is that while AS-TM1A-Cy5 can bind to the ends of pre-bound AS-TM1A-Cy3, AS-TM1J-Cy5 cannot. However, if in the second reaction mixture AS-TM1A-Cy3 and AS-TM1J-Cy5 are both present, then AS-TM1J-Cy5 can bind.

So it is clear from this data that the model of AAAA-JJJJ binding is not supported. The other possibility is that AS-TM1J and AS-TM1A form a heterodimer. However, since they are different lengths (AS-TM1A is 252 amino acids and spans 6 actin monomers, while AS-TM1J is 285 amino acids and spans 7 actin monomers), it is geometrically challenging to link several heterodimers into a head-to-tail polymer without gaps. Thus it is likely that AS-TM1J and AS-TM1A bind head to tail, in an alternating fashion (A-J-AA-J-AAAA-J).

Discussion

We have shown that TM1J is not competent to bind to actin filaments, but co-binding with TM1A helps TM1J bind. This has been confirmed *in vivo* by Goins (data not shown). When Goins knocks TM1A down in S2 cells, TM1J no longer localizes to the lamellum. In our *in vitro* experiments, TM1J always binds with very low affinity, even in the presence of TM1A. However, TM1J seems to bind more strongly when co-binding with DcTM1A. Surprisingly, both TM1J's low signal and stronger binding to over-expressed DcTM1A is also seen *in vivo* (data not shown).

One implication is that DcTM1A might be the tropomyosin isoform endogenously present in the lamellum, while AS-TM1A might be the isoform present in the cortex. This would be an intriguing way for the cell to control these two actin-tropomyosin populations separately, and thus individually control the actin dynamics at these two locations.

In Iwasa and Mullins (2007), the authors thought they were knocking down the only tropomyosin isoform present in S2 cells: TM1A. This led to the expansion of the lamellipod at the expense of the lamellum. However, Goins revealed that Iwasa and Mullins had in fact knocked down TM1J. Given our results that TM1A is the dominant isoform present in the lamellum, their results could imply that the concentration of TM1A is still quite low in the lamellum, and extra TM1J is needed to maintain a full lamellum.

Given that TM1J alone cannot bind to actin filaments, this leaves us with the intriguing question of how TM1J can bind to the other regions of the cell where TM1A is not present. For instance, how does TM1J bind around golgi stacks? How does TM1J bind to kinetochores? An interesting hypothesis is that TM1J could have a different obligate binding partner at each of its subcellular localizations. For instance, at the golgi, since TM2A is also present, TM2A could be TM1J's binding partner, if TM2A itself can bind to actin filaments. A lot more work needs to be done *in vivo* and *in vitro* in order to determine the answers to this question.

References

Goins, L.M. and Mullins, R.D. Tropomyosin isoforms cooperate with Myosin II and Diaphanous to influence cell cycle progression. Manuscript in preparation.

Gunning P., O'Neill G., Hardeman E. 2008. Tropomyosin-based regulation of the actin cytoskeleton in time and space. Physiol Rev. 88: 1-35.

Iwasa, J.H. and R.D. Mullins. 2007. Spatial and temporal relationships between actin-filament nucleation, capping, and disassembly. Curr. Biol. 17:395-406.

Materials & Methods

Most of the materials and methods for this chapter can be found in the materials and methods section of Chapter 1.

Protein Purification

AS-TM1A & AS-TM1J & DcTM

Separately, each of the AS-TM1A C32A/S82C, AS-TM1J C25A/S, and DcTM constructs, in pET20b vectors, were expressed in BL21 *E. coli* cells. Bacterial pellets were resuspended in a 3X volume of lysis buffer (50 mM Tris pH 7.5, 10 mM EDTA, 2 mM DTT, 200mM NaCl, 1 mM PMSF, 5 mg/L DNAse1, 10 mg/L RNAseA) and lysed by passage through a microfluidizer and cleared by centrifugation. The supernatant, in a 50 ml conical tube, was placed in a boiling water bath (95°C) for 7 min (or until the supernatant precipitates), then placed in RT water for 7 min, then on ice for 30 min. The precipitate was pelleted by centrifugation at 150k rcf, 4°C for 45 min, and the supernatant recovered. Precipitate the tropomyosin by adding 1N HCl until the pH is below the PI (4.69). The precipitate was pelleted by centrifugation at 20k rcf, 4°C for 20 min. The pellet was resuspended in 20mM Tris-HCl pH 7.5, 0.5mM TCEP, and KOH

added until the pH returned to 7.5. A 20-40% ammonium sulfate cut was taken from the resuspended pellet, and centrifuged at 130k rcf for 20 min at 4°C. The pellet was resuspended in and dialyzed into 10mM imidazole pH 7, 100mM KCl, 0.5mM TCEP. The purified protein was flash frozen and stored at -80°C.

Contributions

Lauren Goins purified the DcTM used in these assays.

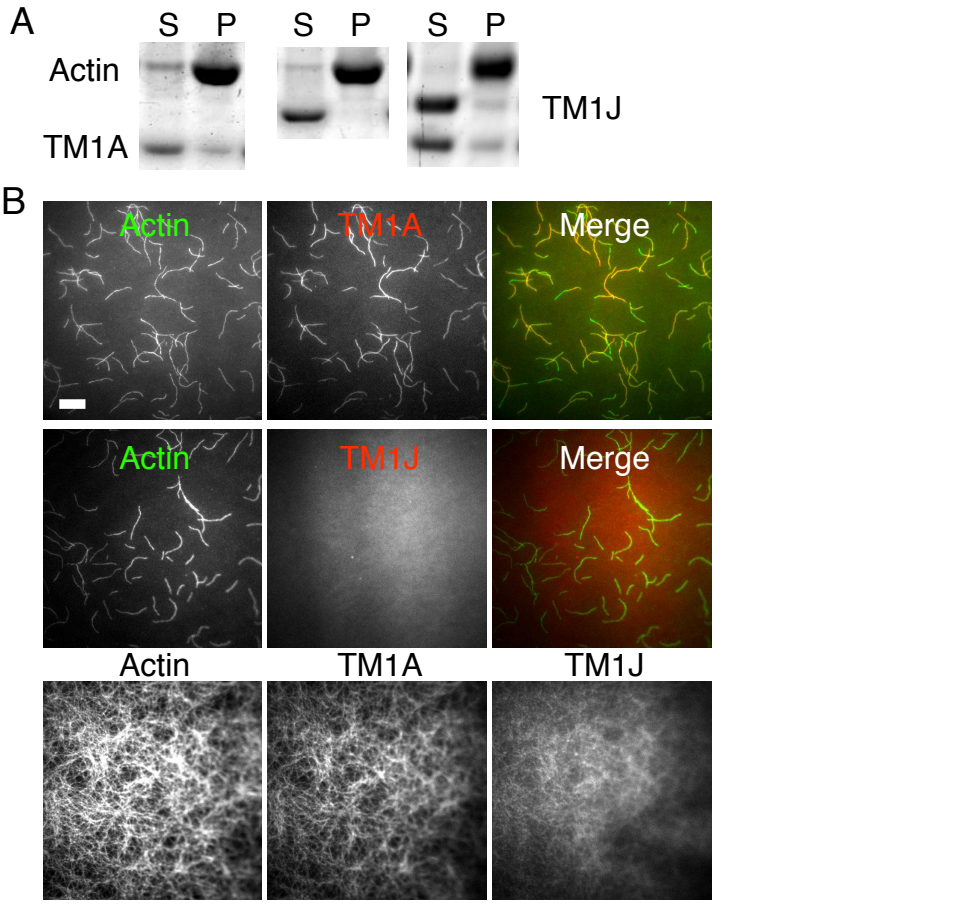
A
S
P
S
P
S
P
Actin
TM1A
TM1J
B
Actin
TM1A
Merge
Actin
TM1J
Merge
Actin
TM1A
TM1J
C
Actin
TM1J
Merge
Dark TM:
TM1J
AS-TM1A
DcTM1A
AS-TM2A
Rabbit TM

Figure 1. TM1J can only bind to actin as a co-polymer with AS-TM1A or DcTM1A. (A) Co-pelleting of tropomyosin isoforms with actin filaments. Left: Actin and AS-TM1A. Middle: Actin and AS-TM1J. Right: Actin, AS-TM1A, and AS-TM1J. Conditions: Temp: 24C. Buffer: 50mM KCl, 1mM MgCl2, 1mM EGTA, 10mM Imidazole, pH 7.0. (B) TIRF microscopy of single actin filaments in the presence of fluorescently labeled AS-Tm1A and/or AS-TM1J. Top Row, 6min into reaction: (Left) Actin-A488 (Middle) AS-TM1A-Cy5 (Right) Merge. Middle Row, 8min into reaction: (Left) Actin-A488 (Middle) AS-TM1J-Cy5 (Right) Merge. Bottom Row, 62min into reaction: (Left) Actin-A488 (Middle) AS-TM1A-Cy3 (Right) AS-TM1J-Cy5. Conditions: Temp: 24C. (C) Actin networks generated from ActA-coated polystyrene microspheres by the Arp2/3 complex and capping protein show co-binding of AS-TM1J with other tropomyosin isoforms. Left: fluorescence of Alex488-labeled actin. Middle: Cy3-labeled Drosophila non-muscle tropomyosin isoform, AS-TM1J. Right: merge of actin and AS-TM1J fluorescence. Each reaction has one isoform of dark tropomyosin added. First row: AS-TM1J. Second Row: AS-TM1A. Third Row: DcTM1A. Fourth Row: AS-TM2A. Fifth Row: Native Rabbit Skeletal Muscle Tropomyosin. Conditions; Temperature: 24C. Buffer: [components]. Reagents: 7.4 μM RSK muscle actin, 125nM Arp2/3 complex, 210nM Capping Protein, 1μM AS-TM1J-Cy3, 1μM added dark tropomyosin isoform.

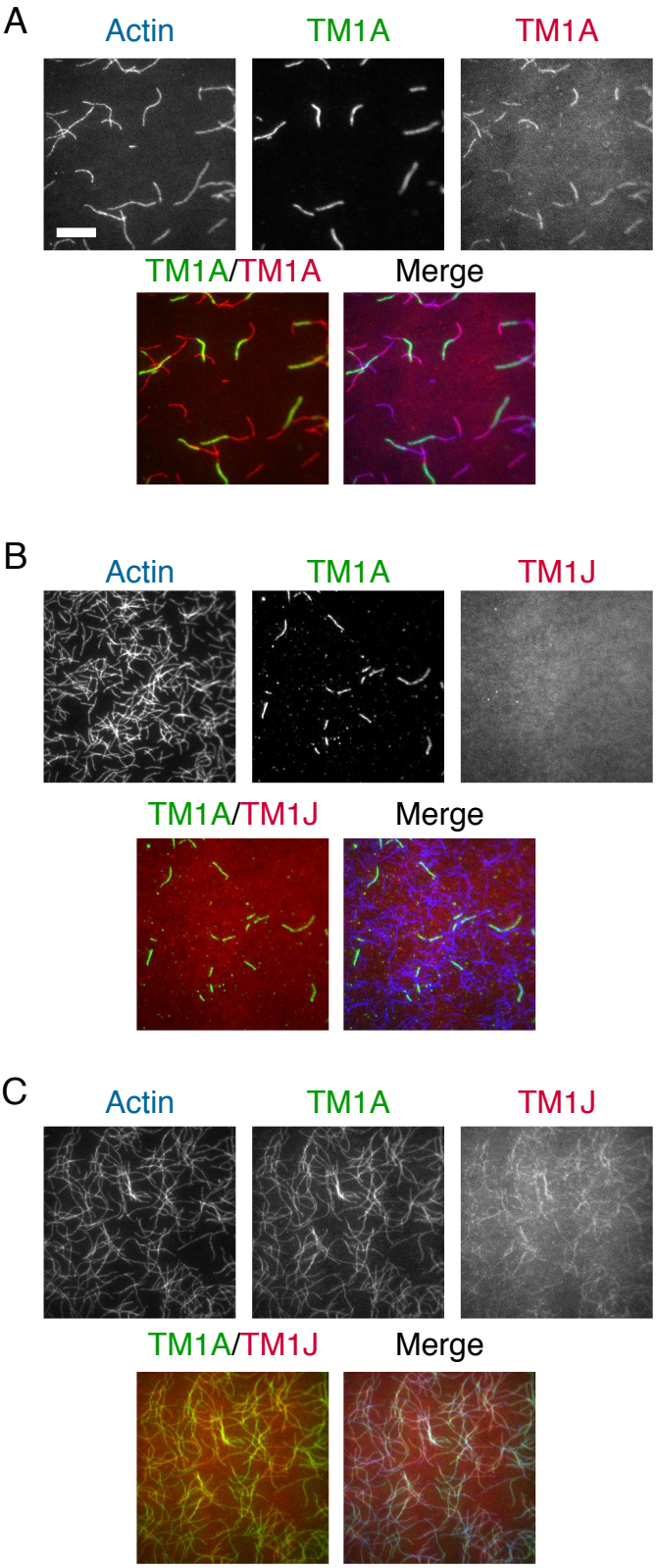
A
Actin
TM1A
TM1A
TM1A/TM1A
Merge
B
Actin
TM1A
TM1J
TM1A/TM1J
Merge
C
Actin
TM1A
TM1J
TM1A/TM1J
Merge

Figure 2. Two-color co-binding of AS-TM1J with AS-TM1A in single filament TIRF shows that AS-TM1J cannot bind by itself onto the ends of actin filaments pre-bound with AS-TM1A. (A) AS-TM1A binding to the ends of AS-TM1A pre-bound filaments. Top-Left: Actin-A488. Top-Middle: AS-TM1A-Cy3, pre-bound. Top-Right: AS-TM1A-Cy5. Bottom-Left: Merge of AS-TM1A-Cy3 pre-bound and AS-TM1A-Cy5. Bottom-Right: Full merge. (B) AS-TM1J binding to the ends of AS-TM1A pre-bound filaments. Top-Left: Actin-A488. Top-Middle: AS-TM1A-Cy3, pre-bound. Top-Right: AS-TM1J-Cy5. Bottom-Left: Merge of AS-TM1A-Cy3 pre-bound and AS-TM1J-Cy5. Bottom-Right: Full merge. (C) AS-TM1J and AS-TM1A co-binding to the ends of AS-TM1A pre-bound filaments. Top-Left: Actin-A488. Top-Middle: AS-TM1A-Cy3, pre-bound and flowed in. Top-Right: AS-TM1A-Cy5. Bottom-Left: Merge of AS-TM1A-Cy3 pre-bound and flowed in, and AS-TM1A-Cy5. Bottom-Right: Full merge.

Chapter 3

Title

Capping protein contributes to the exclusion of tropomyosin from a branched actin network.

Introduction

In Chapter 1, we showed convincing data that Arp2/3 complex inhibits tropomyosin from binding to branched filaments. While this is true, it is not the entire story. Here we show that even a relatively small concentration capping protein also contributes to the exclusion of TM1A from a branched network.

Results & Discussion

When we build actin networks off of ActA-coated polystyrene microspheres with only Arp2/3 complex, a hazy branched network grows symmetrically off of the bead surface. This network never breaks symmetry. When TM1A is added to this network, in the early time points, TM1A seems to bind mostly to the outer edge of this network (data not shown). However, by 19min into the reaction, TM1A seems to bind to the entire network, up to the surface of the bead (Figure 1A). This is supported by single filament TIRF data not shown: with 1μM TM1A, 1μM actin, and 10nM Arp2/3 complex, 50nM ActA, TM1A bound to the branched filament. In contrast, even when a minimal concentration of capping protein is added (10nM), at 19min, the TM1A is clearly excluded from the branched network. As a reminder, to create robust symmetry breaking and tail growth, we usually use 210nM capping protein. This effect is sustained as we add more capping protein (Figure 1A).

Given the data from Chapter 1, it seems that Arp2/3 complex inhibition of TM1A binding is TM1A concentration dependent. In fact, even 400nM TM1A can overcome the Arp2/3 complex inhibition (data not shown). Full exclusion of TM1A from branched networks at any concentration of TM1A only occurs when capping protein is present. This addition to the model actually more robustly explains how TM1A could be excluded from the lamellipod in cells, where the concentration of TM1A could fluctuate over time.

There are some intriguing hypotheses for how capping protein could help inhibit tropomyosin binding. Is TM1A binding dependent on the length of the actin filaments? Capping protein could shorten the branched filaments to a degree that decreases TM1A binding. There could also be a slight conformation change in the twist of the actin filament when the barbed end is bound to capping protein that also prevents TM1A from binding. To fully understand the mechanism of capping protein's effect on TM1A binding, more detailed single filament assays need to be done.

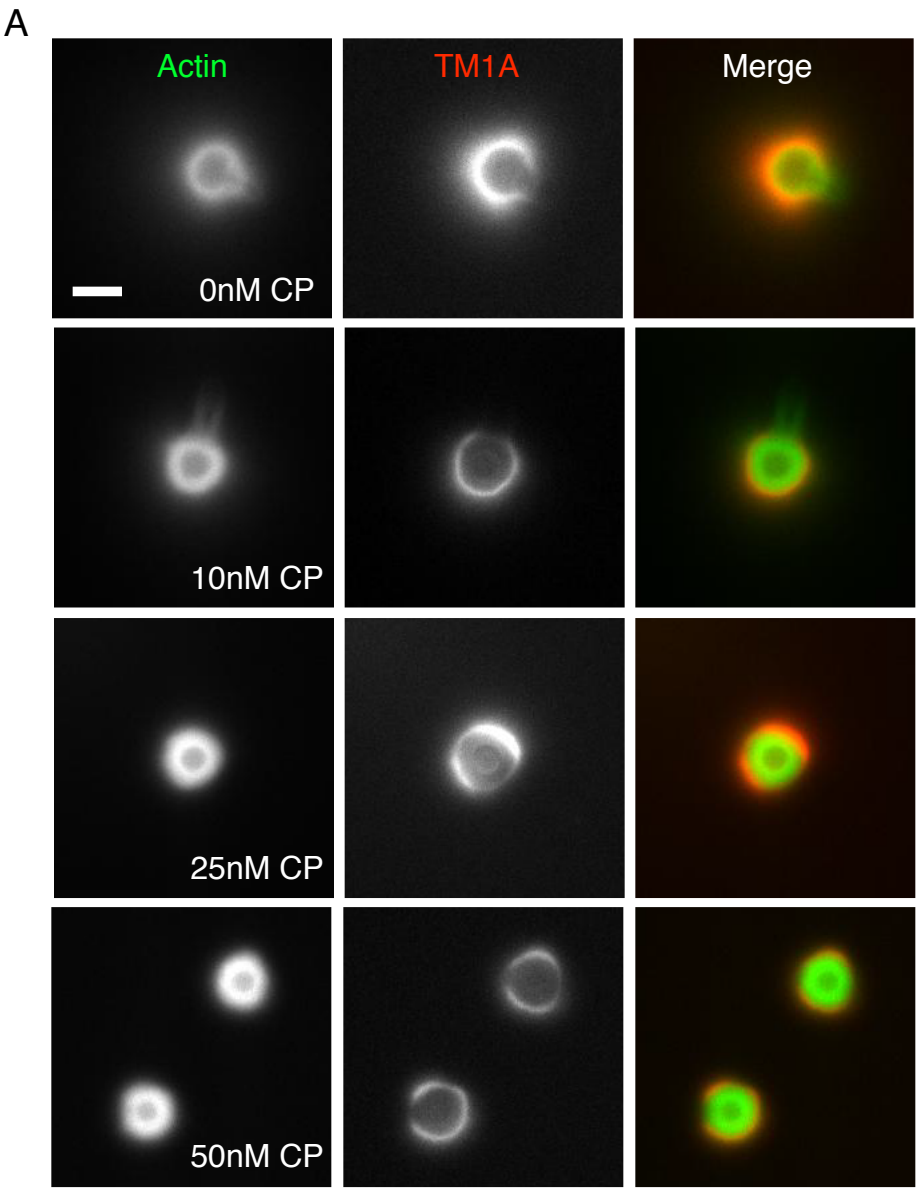

Figure 1. The addition of capping protein to the bead motility assay excludes TM1A from the branched actin network. (A) Actin networks generated from ActA-coated polystyrene microspheres by the Arp2/3 complex and capping protein show that TM1A is only excluded from the branched network when capping protein is present. Left: fluorescence of Alex488-labeled actin. Middle: Cy3-labeled Drosophila non-muscle tropomyosin isoform, AS-TM1A. Each row has the indicated amount of capping protein, and images are taken at 19min. Right: merge of actin and AS-TM1A fluorescence. Proteins: 7.4μM rabbit skeletal muscle actin, 125nM Arp2/3, 1μM Cy3-AS-TM1A.

Chapter 4

Title

Viscoelastic moduli are robust features of an *in vitro* actin network that drives motility

Personal Note

I defended this project for my orals exam, and focused solely on it for four years. I spent a lot of the time trying to validate the use of quantum dots as a mechanical probe particle. I developed particle tracking code in MATLAB, and validated the tracking code by creating my own simulated image data. Experimentally, I tried to validate the method by measuring quantum dots in acrylamide, as well as comparing quantum-dot measurements of polymerized actin to rheometry data of the same actin. The quantum-dot measurements of isotropic actin filaments turned out to work well. However, in the end, using the quantum-dots in the bead motility tails did not work out. I believe this is because the network might have been too stiff to measure accurately, and thus the measurements were dominated by the gross movements of the tail. The last experiment that killed the entire project showed that the measured stiffness scaled with the length of the tails. Thus, I was not making the correct measurement, and none of the data below is believable. I include this paper draft that I wrote in 2010 to summarize some of the main ideas and directions of this project.

Abstract

Eukaryotic cells construct many different structures from actin that are fundamental to diverse cellular processes, including cell motility. These structures exhibit differing mechanical properties that are determined by a variety of actin binding proteins. It is of fundamental interest how these underlying biochemical interactions

between actin and its various binding partners influence a dynamic and anisotropic actin network's mechanical properties. We used a physiologically relevant reconstituted system for generating anisotropic, Arp2/3 branched actin networks of the type that drive cell motility. To measure the viscoelastic properties of this network, we developed a novel microrheology method that incorporates the use of quantum-dots connected to the network. Our results indicate that the viscoelastic moduli of the actin network are robust qualities indifferent to fluctuations in capping protein and Arp2/3 concentrations. These methods further our understanding of how the cell changes its biochemical makeup to create actin networks with different mechanical properties.

Introduction

Eukaryotic cells construct many different structures from a single polymer, actin. These structures are fundamental to diverse cellular processes, including cell motility, adhesion, division, intracellular trafficking, and cytoplasmic streaming. Such structures are formed with a variety of actin binding proteins and they exhibit different mechanical properties, as determined by the viscoelastic moduli. It is unclear what the mechanical properties of a biologically relevant network are in response to fluctuations in actin binding protein concentrations. This is because there has not been a biomimetic *in vitro* system for studying actin network mechanics. A truly biomimetic actin network is dynamic (polymerizing and depolymerizing) and anisotropic. Here we present a new *in vitro* method for passively measuring the viscoelastic moduli of a dynamic and anisotropic actin network of the type that drives cell motility. We use this method to probe how a cell changes and utilizes its biochemical makeup to create actin networks

with different mechanical properties. Such an understanding may prove useful to bioengineers interested in altering a motile cell's mechanical properties for medicinal or basic science purposes.

The new method involves combining an existing *in vitro* reconstituted system for generating anisotropic, Arp2/3 branched actin networks with microrheology using quantum dots as the mechanical probe particle. This system gives us full control over protein concentrations, including the addition of actin binding proteins. The quantum dots are physically linked to the network and thus provide a high optical contrast mechanical probe particle that can be tracked with an epi-fluorescence microscope. The rest of the introduction explains each part of the system in more detail.

The inspiration for the reconstituted system came from the actin-based motility of the intracellular pathogen *Listeria monocytogenes*. This pathogen coats one end of itself with a nucleation promoting factor, ActA, that activates Arp2/3 network branching. The comet tail of branched actin that forms off the ends of *Listeria* has been shown to be structurally similar to the one that drives the eukaryotic lamellapod forward, and thus this is a model *in vitro* system for studying lamellapodial actin network biomechanics. The assay includes all the purified components required for continually building and recycling a polarized and anisotropic Arp2/3 branched network on the surface of a bead (actin, ActA on the bead, Arp2/3, capping protein, cofilin, and profilin). The Arp2/3 complex nucleates actin filaments off existing filaments at a 70^{o} angle, creating a meshwork (Figure 1A). Free filament ends are prevented from further elongation by capping protein, and the network is degraded at the back end by the severing protein,

cofilin. The spatial and temporal distribution of polymerization and degradation depends on the concentration of the components. At physiological concentrations, the network has a stable growing front with gel-like mechanical properties and an unstable back end with unknown mechanical properties. This provides a constantly changing network, allowing me to probe how the viscoelastic moduli change spatially and temporally due to changes in the network architecture. Additionally, I altered the biochemical environment by adding actin crosslinkers at various concentrations to the network.

I measured the local mechanical properties of this *in vitro* network with a new form of microrheology involving the use of quantum dots instead of the regularly used glass beads. In general, microrheology measures the mechanical properties of a material by measuring the thermal fluctuations of a probe particle embedded in the material. By determining the mean squared displacement of these probe particles over many time intervals, one can calculate the elastic and viscous moduli of the material over a range of frequencies. These viscoelastic moduli are calculated using the generalized Stokes-Einstein equation below, where ω is the frequency, G'(ω) the elastic or storage modulus, G"(ω) the viscous or loss modulus, $F\{\langle \Delta r^2(\tau)_{\tau=1/\omega} \rangle\}$ the Fourier transform of the mean-squared displacement (the experimentally measured quantity), and a the radius of the probe particle. These moduli tell us how the material will respond to strains of varying frequency and intensity.

$$G'(\omega) + iG''(\omega) = \frac{2k_B T}{3\pi a i\omega F\{\langle \Delta r^2(\tau) \rangle_{\tau=1/\omega}\}}$$

Previous *in vitro* microrheology measurements of actin networks have used

beads as the mechanical probe particle. These measurements have provided useful insights, but they are limited by the fact that they were done with a static isotropic network. With the system I described above, I will be using a physiologically relevant model system.

Previous methods are also limited by the large size of the bead (0.5-1μm) relative to the width of the branched actin network *in vivo* (0.5-1.5μm). This prevents local measurements of mechanical properties that could distinguish between the front of a network and the back. I will measure the thermal fluctuations of this evolving network by attaching quantum dots directly to the actin network, and measuring their movements at nanometer spatial resolution under a microscope. Quantum dots (10-50 nm) are an order of magnitude smaller than beads previously used, and are much brighter and more stable than organic fluorophores.

Results

Quantum-dot microrheology accurately measures viscoelastic moduli.

In vitro actin networks grown on bead surfaces provide a controlled way to study mechanical properties in a network with biologically relevant geometries. We designed a novel method that incorporates quantum-dots into this network as mechanical probes to measure the viscoelastic moduli using the principles of microrheology. To determine whether this method could accurately measure the viscoelastic moduli, G'(w) and G"(w), we made some control measurements. To prevent drift in our microscope images, an Ezrin actin binding domain was used to secure the actin network to the glass surface. Ezrin binding did not significantly change G'(w) nor G"(w) anywhere above the glass

surface, as seen in Figure 1A. Increasing the phalloidin-quantum-dot concentration also did not affect G'(w) nor G"(w) until the concentration was so high that the quantum-dots could not be optically distinguished (starting around 2nM), as seen in Figure1B. These controls show that quantum-dot microrheology is a feasible and accurate method for measuring actin network mechanical properties.

Viscoelastic moduli are independent of Arp2/3 and capping protein concentrations.

To determine the effect of Arp2/3 and capping protein on the networks' viscoelastic moduli, we altered their concentrations. Decreasing Arp2/3 concentration by 2x did not significantly change G'(w) nor G"(w), data not shown. Increasing capping protein concentration by 2x also did not significantly change G'(w) nor G"(w), Figure 2B. Thus the viscoelasticity of the actin network seems to be a robust feature of the system, resistant to fluctuations in component concentrations.

Discussion

Viscoelastic moduli are constant over changes in capping protein concentrations.

We found that changes in capping protein concentrations do not affect the viscoelastic moduli over a large range of frequencies. In experiments done with the same *in vitro* actin motility system, but without the quantum dots, Akin & Mullins (2008) found that increasing capping protein concentration increased the velocity of the beads and decreased the density of the actin in the network. These observations were confirmed in my system. Combined with my observations of the mechanical properties

of these networks, these results indicate that changing the capping protein concentration changes the network architecture (seen as a change in actin density), but does not change the mechanical properties.

There are two opposing factors when considering the effect of capping protein on the stiffness (elastic modulus) of the network. One is that increasing the concentration shortens the length of the individual filaments in the network (Schafer et. al. 1996). Shorter filaments might give rise to a stiffer network. The second is that from Akin & Mullins (2008) we also know that the density of the network overall is decreased. This sparser network might give rise to a network that is less stiff. My results suggest that these two opposing factors may balance each other out to maintain specific mechanical properties. These specific viscoelastic moduli allow a motile cell such as a neutrophil to be stiff enough to move through small openings in an extra-cellular matrix. Simultaneously, the cell's actin cytoskeleton is viscous enough to be able to flow around solid barriers.

Acknowledgements

I would like to thank the Healy and Kumar labs at Berkeley, and the Barron lab at Stanford, for allowing me to use their rheometers.

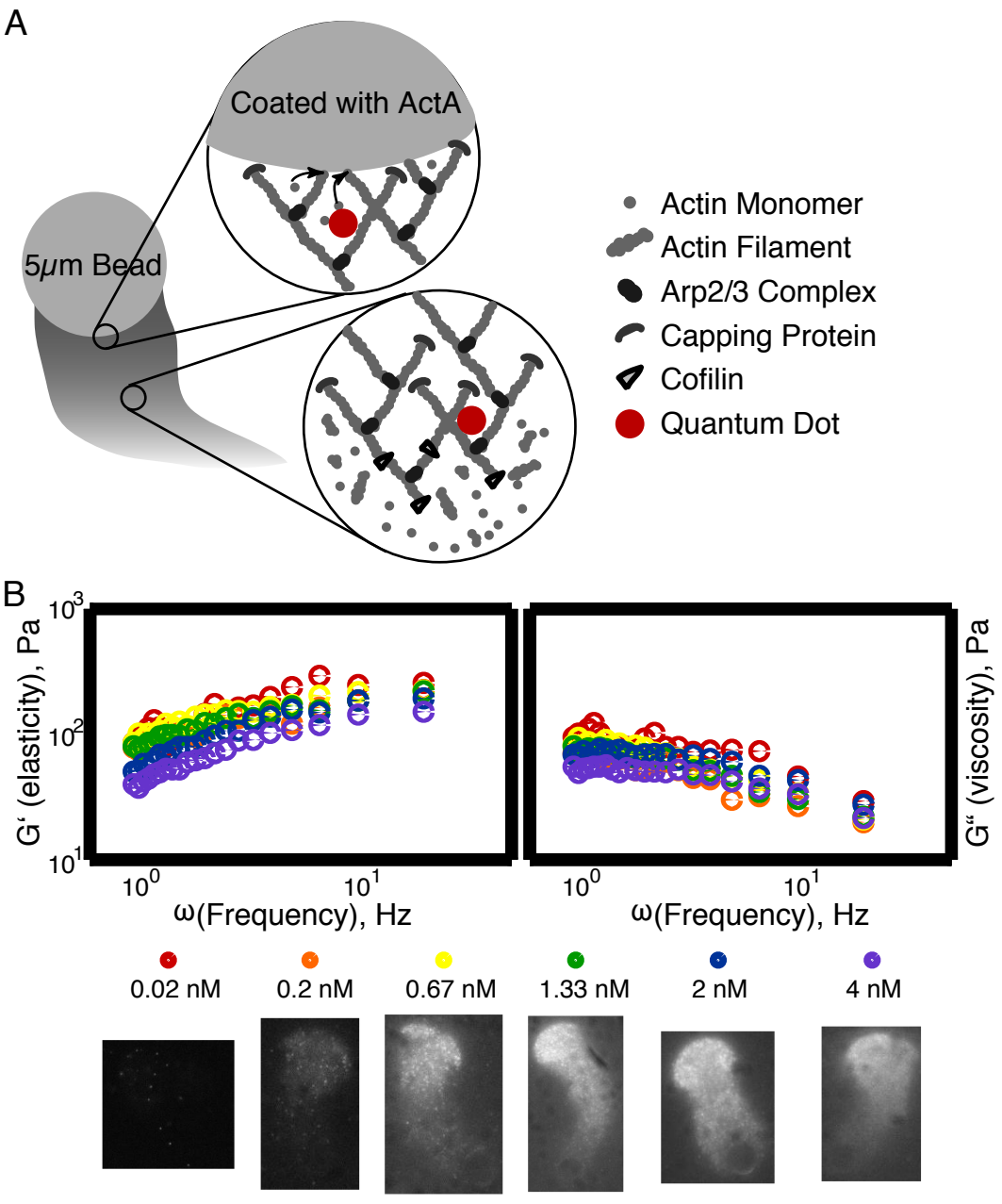

Figure 1. (A) Bead motility quantum-dot mechanics assay setup. (B) Quantum-dot concentration scan. Only above 2nM did the viscoelastic moduli change due to the density of the quantum-dots.

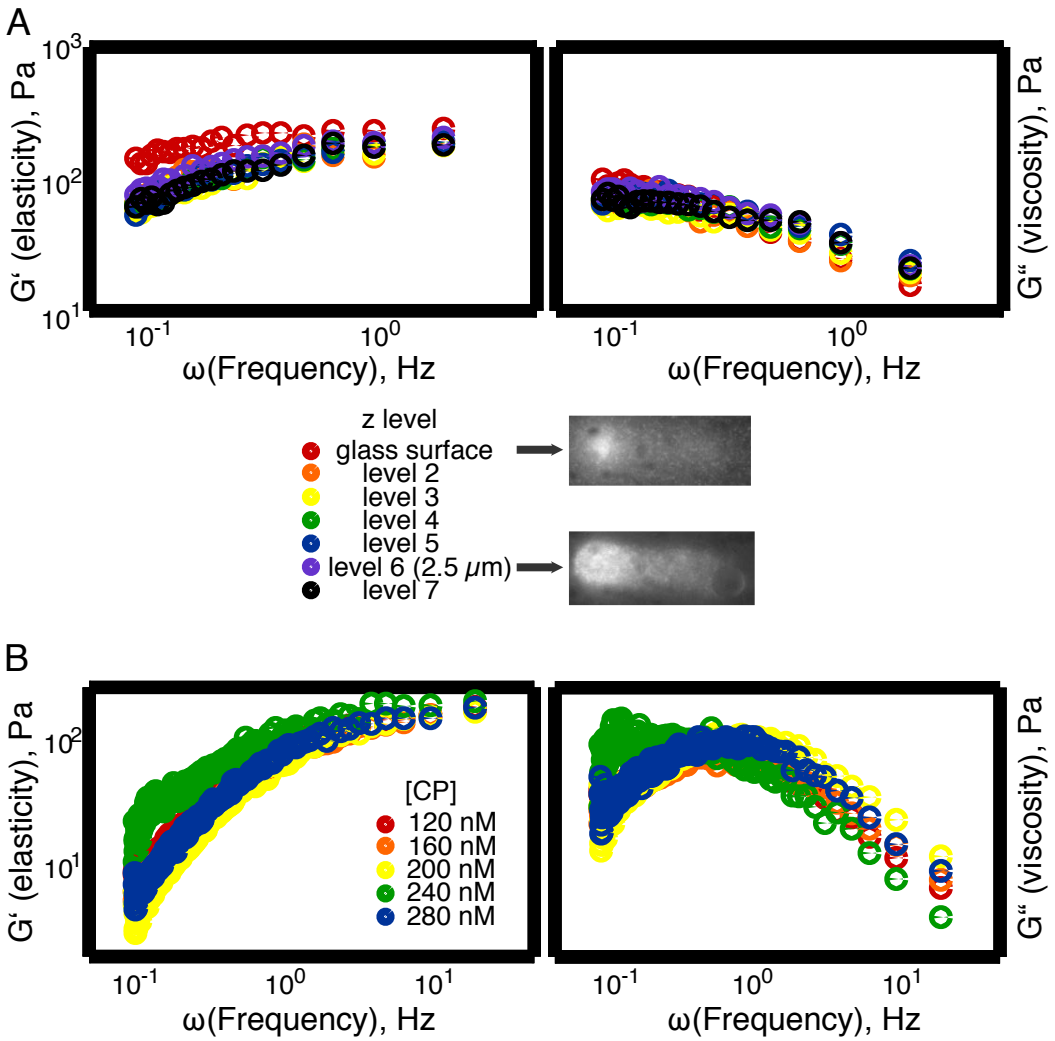

Figure 2. (A) Z scan through a tail bound to the glass surface by the Ezrin actin binding domain. Only the quantum dots on the glass surface showed a difference in stiffness (G'(w)). Microrheology measurements are always done 2.5 um above the glass surface, well above where the Ezrin could have an effect on the viscoelasticity. (B) Capping protein concentration scan. A 2-fold increase in capping protein concentration did not change the viscoelastic moduli within error.

Chapter 5

Published Paper

Arp2/3 complex ATP hydrolysis promotes lamellipodial actin network disassembly but is dispensable for assembly.

Ingerman E., Hsiao J.Y., Mullins R.D. 2013. Arp2/3 complex ATP hydrolysis promotes lamellipodial actin network disassembly but is dispensable for assembly. J Cell Biology. 200: 619-633.

Personal Note about my collaboration with Elena Ingerman

Elena Ingerman, a postdoc and dear friend in the Mullins lab, had done an impressive amount of work both *in vivo* and *in vitro* to show that ATP hydrolysis mutants of the Arp2 and/or Arp3 subunits of the Arp2/3 complex led to the expansion of the lamellipod. The hypothesis was that these ATP hydrolysis mutants were resistant to actin filament disassembly activity by proteins such as cofilin/ADF. The reviewers asked for this hypothesis to be confirmed using the bead motility assay.

I was more than happy to help with that request. Together, with her purified Arp2/3 complex WT and mutant proteins, and my bead motility system, we were indeed able to confirm the hypothesis. Below is our paper.

Abstract

We examined the role of ATP hydrolysis by the Arp2/3 complex in building the leading edge of a cell. By studying the effects of hydrolysis defects on the behavior of the complex in the lamellipodial actin network of *Drosophila* S2 cells and in a reconstituted, *in vitro*, actin-based motility system. In S2 cells, non-hydrolyzing Arp2 and Arp3 subunits expanded and delayed disassembly of lamellipodial actin networks and the effect of mutant subunits was additive. Arp2 and Arp3 ATP hydrolysis mutants

remained in lamellipodial networks longer and traveled greater distances from the plasma membrane, even in networks still containing wild-type Arp2/3 complex. *In vitro*, wild-type and ATP hydrolysis-mutant Arp2/3 complexes each nucleated actin and built similar dendritic networks. However, networks constructed with Arp2/3 hydrolysis-defective mutants were more resistant to disassembly by cofilin. Our results indicate that ATP hydrolysis on both Arp2 and Arp3 contributes to dissociation of the complex from the actin network but is not strictly necessary for lamellipodial network disassembly.

Introduction

Actin-based cellular motility is critical for cell spreading, tissue formation, and in immune responses. Motility relies on the formation of a three dimensional lamellipodial actin network, composed of actin, capping protein, Arp2/3 complex, and other factors. The Arp2/3 complex nucleates new (daughter) filaments from the sides of preexisting (mother) filaments to generate space-filling dendritic arrays, *in vitro* (Mullins et al., 1998; Blanchoin et al., 2000) and at the leading edge of migrating cells (Svitkina and Borisy, 1999). The architecture and assembly dynamics of this network are governed by the timing of Arp2/3 activation, and the disassembly of this network is critical for the recycling of its components and for sustained network growth (Cramer, 1999).

The Arp2/3 complex comprises seven subunits, two of which, Arp2 and Arp3, are actin related proteins that contain actin-like, ATP-binding pockets. Yet, the role of ATP hydrolysis by the Arp2/3 complex is not well understood. Residues important for the catalytic mechanism of hydrolysis were elucidated by crystal structures of non-

vertebrate actin (Vorobiev et al., 1999). Experiments in budding yeast, using mutant based on this crystal structure, indicate that ATP binding on Arp2 and Arp3 are required for function of the complex in endocytosis and in actin patch dynamics (Martin et al., 2005; Martin et al., 2006).

Although ATP is hydrolyzed on the Arp2 subunit at roughly the same time that the complex produces new filaments (Dayel and Mullins, 2004), hydrolysis on a single ATP-binding subunit (Arp2 or Arp3) does not appear to be required for nucleation (Martin, et al. 2006). However, nucleation by an Arp2/3 complex unable to hydrolyze ATP on both Arp2 and Arp3 has not been shown. While conventional actin binds ATP with nanomolar affinity and hydrolyzes bound nucleotide soon after incorporating into a filament (Blanchoin and Pollard, 2002), Arp2 and Arp3 bind ATP with 1000-fold weaker affinity (Dayel et al., 2001). The Arp2 subunit hydrolyzes bound ATP soon after creating a new filament or capping the pointed end of a preexisting one (Dayel and Mullins, 2004).

Actin nucleation by Arp2/3 is regulated by intracellular signals and requires the participation of a nucleation promoting factor (NPF) such as N-WASP, WAVE, WHAMM, WASH, or JMY (Machesky et al., 1999; Rohatgi et al., 1999; Welch and Mullins, 2002; Campellone et al., 2008; Zuchero et al., 2009; Campellone and Welch, 2010; Duleh et al., 2010). The minimal NPF sequence able to activate Arp2/3 is a three-part motif, called a VCA domain. VCA consists of a Verprolin-homology (or WASP-Homology 2, WH2) domain that binds monomeric actin (Higgs et al., 1999), an Acidic region that binds to Arp2/3 complex (Marchand et al., 2001), and a Central region that binds both

actin and the Arp2/3 complex (Kelly et al., 2006). Nucleation of a new filament requires three factors: (1) binding of the Arp2/3 complex to the side of a pre-formed actin filament (Mullins et al., 1997; Mullins et al., 1998; Machesky et al., 1999); (2) binding of two VCA domains to the Arp2/3 complex (Padrick et al., 2011); and (3) delivery of at least one actin monomer to the complex *via* the WH2 domain (Dayel and Mullins, 2004).

To examine the role of ATP hydrolysis by the Arp2/3 complex, in the context of building a cell's leading edge, we used fluorescence speckle microscopy to follow the dynamics of Arp2/3 complexes containing non-hydrolyzing Arp2 and Arp3 subunits in the lamellipodia of *Drosophila* S2 cells. We also examined the structural properties of dendritic actin networks in an *in vitro* motility system reconstituted using purified components. Loss of ATPase activity on Arp2 and Arp3 have similar effects. Neither mutant inhibits cell spreading or assembly of the lamellipod. Rather, both mutant alleles prolong the association of the Arp2/3 complex with the lamellipodial actin network, promote expansion of the lamellipod, and prevent its disassembly. Likewise, *in vitro*, ATP hydrolysis mutants hinder disassembly of the actin network. Our results indicate that ATP hydrolysis on both Arp2 and Arp3, is not absolutely required for network disassembly, but does facilitate dissociation of the complex from lamellipodial actin networks.

Results

Mutations that abolish ATP hydrolysis in Arp2 and Arp3 have minimal effects on actin filament nucleation by the Arp2/3 complex.

To study the role of ATP hydrolysis by the Arp2/3 complex, we mutated critical residues in the ATP binding sites of Arp2 and Arp3. In actin, residue Q137 positions a water molecule near the gamma phosphate of the bound ATP, while residue H161 functions as a base catalyst, abstracting a proton from water, and priming it for nucleophilic attack on ATP (Vorobiev et al., 2003). We mutated Arp2 and Arp3 residues analogous to Q137 and H161 of actin (Supplemental Figure S1A) and integrated these mutations into the yeast genome, under control of the endogenous gene promoters. We then purified five variants of the Arp2/3 complex from budding yeast: wild type Arp2/3 complex and four ATP hydrolysis mutants, each containing a single mutation in Arp2 or Arp3 (Arp2Q137A, Arp2H161A, Arp3Q137A, or Arp3H161A).

To confirm loss of ATPase activity in the Arp2/3 mutants, we performed ATP hydrolysis assays, using purified Arp2/3 complex cross-linked to 8-azido-γ-^{32}P-ATP. We stimulated hydrolysis of the radiolabeled ATP covalently cross-linked to the Arp2 and Arp3 subunits by adding actin and the purified VCA domain of yeast Arp2/3 activator, Las17. We observed rapid hydrolysis on the Arp2 subunit of the wild type complex, but observed no detectable hydrolysis by Arp2Q137A or Arp2H161A subunits (Figure 1A and data not shown). This result is consistent with that of Martin, et al. (2006), who also found that Arp2H161A was unable to hydrolyze ATP. We could not accurately quantify ATP hydrolysis by Arp3 mutants due to poor cross-linking of azido-ATP to this subunit.

When integrated into yeast under the native promoter, we found that, as previously described (Martin et al., 2006), *arp2H161A* exhibited growth defects on formamide and on 0.9 M NaCl, both stress-inducing conditions (Supplemental Figure

S1B). In contrast, yeast strains *arp2Q137A* and *arp3Q137A* exhibited normal growth under all conditions. This suggests that the H161A mutant complex may have additional defects unrelated to ATP hydrolysis, while the Q137A mutation likely does not. Thus, in our analysis of Arp2/3 ATPase activity, we focused on the Q137A mutation. We performed experiments in parallel, on wild type (WT), Arp2 and Arp3 Q137A, and Arp2 and Arp3 H161A Arp2/3 complex. We include our results for the Arp2/3 H161A mutants, which are very similar to those obtained for the Q137A mutants, in Supplemental Figures S3 and S4. Surprisingly, despite the lack of phenotype displayed by the *arp2-* and *arp3-Q137A* alleles, even under stressful conditions, the two mutations together were synthetically lethal (Supplemental Figure 1D). This result suggests that, despite our inability to detect it, ATP hydrolysis on the Arp3 subunit is important for the function of the complex. Nucleation activity of the four mutant yeast Arp2/3 complexes (Arp2Q137A, Arp3Q137A, Arp2H161A, Arp3H161A), varied slightly from the activity of wild type yeast Arp2/3, the H161A mutants being slightly more active than wild type and the Q137A mutants being slightly less active (Supplemental Figure S1C).

Purification of Arp2/3 complex from yeast has some limitations: low quantities of purified protein and difficulty in obtaining a double ATP hydrolysis mutant (Arp2Q137A, Arp3Q137A) Arps2/3 complex, due to synthetic lethality. Thus, we used a baculovirus purification protocol, which allowed us to obtain a double ATP hydrolysis mutant human Arp2/3 complex, in addition to the same single mutant complexes that we had obtained previously from yeast. Using pyrenyl-actin assembly assays, we found that all four baculovirus-produced Arp2/3 variants (Arp2Q137A, Arp3Q137A, double mutant, and

wild type) were capable of accelerating actin polymerization in an NPF-dependent manner (Figure 1B), indicating that nucleotide hydrolysis on either Arp2, Arp3, or both subunits is not specifically required for nucleation of actin filaments by the Arp2/3 complex.

Arp2/3 ATP hydrolysis mutants remain attached to the dendritic lamellipodial actin network longer than WT Arp2/3, in the leading edge of Drosophila S2 cells.

To better understand the cellular and physiological role of ATP hydrolysis by the Arp2/3 complex, we examined the effects of ATPase mutants on the morphology of the cell's leading edge. We created Drosophila S2 cell lines stably expressing fluorophor-labeled Arp2 and Arp3. We depleted endogenous Arp2 or Arp3 from the stable cell lines by RNAi, thus replacing endogenous protein with a stably expressed, fluorophore-tagged ATP hydrolysis-dead variant.

We verified the efficiency of our RNAi knockdown procedure using light microscopy and by immuno-blotting cell extracts. Nucleation activity of the Arp2/3 complex, which helps form the dendritic actin network at the cell edge, is required for S2 cell spreading. When Arp2/3 complex subunits are depleted, cells fail to spread normally and exhibit a serrated morphology, rather than a smooth, circular boundary. We used stable S2 cell lines expressing Actin-GFP alone (9), Actin-GFP and Arp2-mCherry (9-1), or Actin-GFP and Arp3-mCherry (9-2). (Stable cell lines listed in Table 1.) Consistent with previous studies, Arp2/3 complex activity was decreased by double stranded RNA (dsRNA) targeting the full coding sequence of either *ARP2* or *ARP3*, as judged by the

fraction (90%) of cells with serrated phenotypes (Figure 2B, 2E, 2H, 2K). We also observed serrated cells when we used dsRNA targeting the 5' and 3' untranslated regions (UTR) of *ARP2* or *ARP3* (Figure 2C, 2I). The serrated phenotype produced by dsRNA targeting the 5' and 3' UTRs of *ARP2* or *ARP3* was rescued by expression of mCherry-labeled Arp2 and Arp3 constructs, respectively (Figure 2F, 2L). We verified Arp2 knockdown by immuno-blotting whole cell Drosophila S2 extracts (Supplemental Figure S1E) with Arp2 antibodies. Antibodies recognizing Drosophila Arp3 were not commercially available.

Confident that our dsRNA targeting the 5' and 3' UTR could deplete endogenous Arp2 and Arp3, while leaving exogenously expressed fluorophore-labeled Arp2 and Arp3 intact, we proceeded to examine the effects of Arp2 and Arp3 ATPase mutants on the behavior of Arp2/3 complex in the lamellipodial actin network. For these experiments, we created stable S2 cell lines expressing Arp2WT-GFP (3), Arp2Q137A-GFP (4), Arp3WT-GFP (6), and Arp3Q137A-GFP (7). (See Table 1.) We depleted endogenous Arp2 or Arp3 from cells, using dsRNA targeting the 5' and 3' UTRs, and replaced the depleted protein with the stably expressed GFP-labeled ATPase variant (Figure 3A). GFP-tagged proteins were expressed at low levels, allowing us to quantify the behaviors of individual Arp2 and Arp3 speckles. For movies of live cells, we used kymograph analysis to reconstruct speckle trajectories (Figure 3B-E, second column). Using speckle trajectories, we recorded distances traveled and speckle lifetimes for Arp2(WT)-GFP, Arp2Q137A-GFP, Arp3(WT)-GFP, and Arp3Q137A-GFP speckles (Supplemental Figure S2, A-D). We observed differences between the behaviors of

speckles containing WT versus hydrolysis-dead variants of Arp2 and Arp3. Arp 2 and Arp3 ATP hydrolysis mutants had longer lifetimes and traveled greater distances than their wild type counterparts (Figure 3F, 3G). For each cell line, we examined 20-50 cells, constructed at least 12 kymographs per cell from sections evenly distributed around the cell's perimeter, and recorded metrics for at least 200 speckles.

To further explore and contrast the behaviors of WT Arp2/3 versus ATPase mutant Arp2/3 *in vivo*, we created stable S2 cell lines which co-express mCherry-labeled WT and GFP-labeled ATP hydrolysis mutant, as follows: (1-3): Arp2(WT)-mCherry, Arp2(WT)-GFP; (1-4): Arp2(WT)-mCherry, Arp2Q137A-GFP; (2-6): Arp3(WT)-mCherry, Arp3(WT)-GFP; (2-7): Arp3(WT)-mCherry, Arp3Q137A-GFP (Table 1, Figure 4A). We quantified the behavior of Arp2/3 speckles, and could clearly distinguish behavior of WT Arp2/3 from that of hydrolysis defective Arp2/3, within the same cell.

For each tracked GFP or mCherry speckle, we recorded its lifetime and distance traveled from the leading edge. Surprisingly, we found that, within single cells, ATP hydrolysis mutant Arp2Q137A-GFP speckles behave in a markedly differently manner than WT Arp2-mCherry speckles (Figure 4B, 4C, 4F). Arp2Q137A-GFP speckles remain attached to the Arp2/3-actin network longer than WT Arp2/3 speckles, as indicated by their increased speckle lifetimes: 33 seconds for the Q137A Arp2 mutant versus 22 seconds for WT Arp2 (Figure 4C, lower graph). Arp2 ATPase mutant speckles also traveled longer distances (1500 nm) than WT speckles (1100 nm) (Figure 4B, lower graph), before disappearing. Remarkably, Arp3 ATPase mutants also had longer lifetimes and traveled greater distances than their WT counterparts (Figure 4D, 4E, 4F).

This result is surprising, given the dearth of previous information about Arp3, but consistent with the synthetic lethality of the Arp2 ATP hydrolysis mutant allele with the Arp3 mutant allele in budding yeast (Supplemental Figure S1D).

The synthetic lethality in yeast and the effect of the Q137A mutation on *ARP3* prompted us to examine the effect of having both ATP hydrolysis defective mutations simultaneously present in S2 cells. We created additional cell lines, this time placing fluorophor tags on both Arp2 and on Arp3: (3-2) Arp2(WT)-GFP, Arp3(WT)-mCherry; (4-13) Arp2Q137A-GFP, Arp3Q137A-mCherry (Table1, Figure 5A). To avoid potential artifacts caused by differential photostability of GFP *versus* mCherry, we also created stable cells lines in which we switched the fluorophors used on Arp2 and Arp3: (1-6) Arp2(WT)-mCherry, Arp3(WT)-GFP; (10-7) Arp2Q137A-mCherry, Arp3Q137A-GFP (Table 1). We used RNAi to simultaneously deplete both endogenous Arp2 and Arp3, and measured speckle lifetimes and distances traveled. RNAi depletes most, but not all, endogenous Arp2 and Arp3 in S2 cells. Thus, in knocking down and replacing both Arp2 and Arp3 with ATPase mutants, we also likely created complexes that contained one mutant and one wild type subunit, along with the desired complexes, which contained two mutant subunits. This may explain the broadening of peaks in the histograms of mutant speckle lifetimes and distances traveled (Supplemental Figures S2, S4). The effect of having two ATP hydrolysis mutations, one on Arp2 and the other on Arp3, was additive. WT Arp2 and Arp3 speckles have average lifetimes of 20.6 seconds (Table 2, Supplemental Figure S2A, S2B). Double mutant cells had greater speckle lifetimes (38.7

sec.), than cells in which a single subunit, either Arp2 or Arp3, was replaced with an ATP hydrolysis mutant (31 sec.) (Supplemental Figures S2E, S2F, Table 2).

Arp2/3 ATP hydrolysis mutants are more resistant to cofilin-mediated disassembly, *in vitro*

Our *in vivo* S2 cell observations led us to believe that ATP hydrolysis on both the Arp2 and Arp3 subunits of the complex aids in disassembly of the dendritic Arp2/3-actin network. We tested this hypothesis in a reconstituted *in vitro* motility system containing a limited number of purified components, as used by Akin et al. (2008). We used polystyrene beads with the VCA domain of the Arp2/3 activator, ActA, covalently linked to the bead surface. In the absence of "recycling" components, cofilin and profilin, a shell composed of actin, Arp2/3, and capping protein grew at the surface of the ActA-VCA-coated beads. Following symmetry breaking of the shell, we observed sustained growth of an actin tail from the bead surface (Figure 6A, 6B). At 50 nM Arp2/3 concentrations, wild type and ATP hydrolysis defective Arp2/3 complexes supported growth of actin tails with similar lengths (Figure 6C), comparable tail intensities (Figure 6D), and similar shell intensities (Figure 6E).

The addition of "recycling" components, profilin and cofilin, to the bead motility assay allowed us to observe differences between the behaviors of wild type and ATP hydrolysis mutant Arp2/3 complexes during disassembly. Cofilin, which severs actin filaments, and profilin, which promotes nucleotide exchange by actin monomers, together promote turnover and recycling of actin monomers in the *in vitro* motility

reaction. Inclusion of profilin and cofilin in the actin motility reaction leads to shell detachment from growing actin tails (Figure 7A, B). We measured shell length at time of detachment (Figure 7C), as well as shell intensity (Figure 7D). Despite having an actin nucleation rate comparable to wild type Arp2/3 complex (Figure 1A) and building a shell and tail of similar intensity, double ATP hydrolysis mutant Arp2/3 complex had a distinctly longer shell at its time of detachment and we observed a clear delay in time of shell detachment from the actin tail (Figure 7E). Based on these observations, we conclude that ATP hydrolysis by the Arp2 and Arp3 subunits contributes to Arp2/3 debranching and to actin network disassembly.

Discussion

Arp2 and Arp3 are members of the actin super-family, a group of proteins defined by a common fold that forms a nucleotide binding pocket with a preference for ATP (Bork et al., 1992). The pocket consists of two globular domains separated by a flexible hinge region (Kabsch et al., 1990). Contacts between the globular domains and the bound ATP hold the pocket closed and hydrolysis of bound ATP weakens the contacts between the globular domains, opening the pocket. This simple conformational change has been adapted to many biochemical activities, including: phosphorylation of sugar molecules (hexokinase), catalysis of protein folding (Hsp70), and destabilization of cytoskeletal filaments (Actin and ParM).

A chemical mechanism of ATP hydrolysis by actin family proteins was suggested by high resolution atomic structures (Vorobiev et al., 2003). In this model, one critical residue in the nucleotide binding pocket (Q137) positions a catalytic water molecule

near the gamma phosphate of the bound ATP while another residue (H161) acts as a base catalyst to activate the water molecule, promoting hydrolysis of the γ-phosphate of ATP. This model was first tested experimentally in the bacterial actin-like protein ParM. The proposed catalytic residues of actin, Q137 and H161, were mapped onto the structure of ParM and mutated to alanines (Garner et al., 2004). ParM containing a mutation homologous to Q137A in Actin lacked ATPase activity, but polymerized with essentially wild type kinetics, while mutations spatially equivalent to H161A altered the ATP critical concentration and inhibited polymerization. These results verified the involvement of Q137 in ATP hydrolysis, but suggested that mutation of H161 produces additional defects unrelated to ATP hydrolysis.

Arp2 mutations equivalent to H161A and Q137A produced different growth phenotypes in budding yeast (Martin et al., 2006). Both mutations abolished ATP hydrolysis; H161A produced a growth defect while Q137A did not. The authors focused on analysis of the H161A phenotype and, based on their analysis of actin patch dynamics in Arp2H161A cells, proposed that ATP hydrolysis on the Arp2 subunit promotes dissociation of the complex from actin and is required for disassembly of Arp2/3-generated networks (Martin et al., 2006).

Building on this work, we examined the dynamics of wild type and ATPase mutant Arp2 and Arp3 in the context of a lamellipodial actin network. We focused primarily on mutations equivalent to Q137A because they completely abolish ATP hydrolysis, with minimal additional effects on protein structure and function. We used Drosophila S2 cells because they construct well-defined lamellipodial actin networks at

the cell periphery, are flat and well-suited to light microscopy, and are highly amenable to protein depletion by RNAi (Rogers et al., 2003; Iwasa and Mullins, 2007).

At the leading-edge, the lamellipodial actin network enables cells to move, change shape, adhere to surfaces, and endocytose nutrients. This network is defined by the rapid assembly and retrograde flow of actin filaments (Salmon et al., 2002), as well as the presence of a characteristic set of actin regulatory proteins including the Arp2/3 complex, capping protein, and cofilin (Iwasa and Mullins, 2007). Filaments in the lamellipodial network are nucleated in a three-dimensional, dendritic array by the Arp2/3 complex; their rapid growth is terminated by capping protein, and they are disassembled by cofilin. Loss of either capping protein or the Arp2/3 complex abolishes the lamellipodial network entirely, while loss of cofilin leads to dramatic expansion of the lamellipod (Iwasa and Mullins, 2007). Additional factors, such as tropomyosin, also control the size of the lamellipod, probably by blocking access of the Arp2/3 complex to actin filaments. Similar to loss of cofilin, loss of tropomyosin causes dramatic expansion of the lamellipod (Gupton et al., 2005; Iwasa and Mullins, 2007).

If, as suggested by Martin et al. (2006), Arp2/3 complex dissociation from the actin network depends on its ability to hydrolyze ATP, we would expect non-hydrolyzing Arp2 mutants to mimic the loss of cofilin and to significantly expand the size of the lamellipodial network. We do, in fact, find that non-hydrolyzing Arp2 and Arp3 mutants widen the lamellipodial network, as judged from tracking both actin and Arp2/3 speckles. The effect, however, is mild compared to the loss of either cofilin or tropomyosin. The same effect is also produced by non-hydrolyzing Arp3 mutants. These results suggest

that ATP hydrolysis occurs on both the Arp2 and Arp3 subunits and accelerates dissociation of the Arp2/3 complex, but is not strictly required for lamellipodial network disassembly.

In cells expressing both fluorophore-labeled WT and ATP hydrolysis mutant Arp2 or Arp3, we observed a clear disparity in the movements of ATPase mutant and WT Arp2 or Arp3 (Figure 4). These observations concur with the *in vitro* experiments of Kawska et al.. Our work similarly suggests that, Arp2/3, along with other network components, builds up many entangled sub-networks, from which lamellipodial network properties emerge.

Previous studies of ATP hydrolysis by the Arp2/3 complex focused on the Arp2 subunit. Yet, it is not entirely surprising that ATP hydrolysis on the Arp3 subunit also plays a role in the activity cycle of the complex. Previously, it was reported that almost 100% of ATP bound to the Arp2 subunit of *Acanthamoeba* Arp2/3 complex is hydrolyzed during or soon after nucleation and that approximately 15% of ATP bound to the Arp3 subunit is also hydrolyzed during the same time interval (Dayel et al., 2006). Likely, the covalent cross-linking of radiolabeled ATP into the active site of Arp3 inhibits efficient hydrolysis. Recent biochemical work (Padrick et al., 2011) has shown that the Arp2/3 complex binds two VCA domains, which deliver two actin monomers to the complex, one to each of the Arp subunits. In addition, high resolution structural analysis of the complex suggests that actin nucleation by the complex requires closure of the ATP binding pocket of the Arp3 subunit (Xu et al., 2011). Our work concurs with the idea that ATP hydrolysis is important on both Arp subunits.

In S2 cells, Arp2 and Arp3 ATP hydrolysis mutants slow down, but do not completely inhibit, disassembly of the lamellipodial actin network. Our *in vitro* motility assay experiments show that Arp2/3 ATP hydrolysis mutants build actin tails very similar in structure to those built by WT Arp2/3. Cofilin's known preference for ADP-actin (Blanchoin and Pollard, 1999) seemingly extends to the actin-related subunits of the Arp2/3 complex. Actin tails constructed with Arp2/3 ATP hydrolysis mutants have delayed network disassembly and delayed cofilin-mediated shell detachment from actin tails, supporting the hypothesis that ATP hydrolysis and/or phosphate release by Arp2 and Arp3 promotes more rapid disassembly, but is not absolutely required for network disassembly.

Similar to Akin and Mullins (2008) and Reymann et al. (2011), we found that cofilin preferentially targets regions of ADP-actin for disassembly. Our observation that dendritic actin networks constructed with ATP-hydrolysis deficient Arp2/3 complex are more resistant to cofilin-mediated disassembly echoes the idea of Reymann et al. that cofilin participate in a macroscopic network disassembly process, rather than in individual filament depolymerization. These results are consistent with the idea of "array treadmilling" proposed by Svitkina and Borisy (1999).

Recent work has shown that other proteins are involved in disassembly of the dendritic actin network. Cofilin destabilizes Arp2/3 branchpoints (Chan et al., 2009) and a related protein, GMF, which lacks actin severing and depolymerizing activity, has been shown to inhibit Arp2/3 nucleation activity (Gandhi et al., 2010). In addition, Coronin may serve to remodel Arp2/3-containing actin branchpoints (Cai et al., 2008).

We propose that ATP hydrolysis on the Arp2 and Arp3 subunits of the complex contributes to the activities of other factors to induce actin network disassembly.

Acknowledgements

We are grateful to David Drubin for generously sharing yeast strains and plasmids and to Matthew Welch for generously sharing Arp2/3 baculovirus constructs. We thank Eugene Ingerman for advice and assistance with MATLAB. We thank Peter Bieling for sharing his hCofilin1 and hProfilin1 plasmids. We are grateful to Lawrence LeClaire, Orkun Akin, and Margot Quinlan for sharing reagents and for much helpful advice. We especially thank Christopher Rivera for his unflagging enthusiasm, countless thoughtful discussions regarding experimental design and data presentation, and for carefully proofreading and editing the manuscript. We thank Lauren Goins and other members of the Mullins Lab for their insights and comments. We are grateful to Eric Griffis and Michael D'Ambrosio for advice on S2 cell culture and to other members of the Vale Lab for useful discussions and for use of the Actin-GFP plasmid. We would like to thank Jon Schaefer and other members of the Morgan Lab for their helpful advice about yeast. We are very grateful to Kurt Thorn and the UCSF Nikon Imaging Center, where all live cell imaging was performed.

This work was supported, in part, by NIH grant 2R01GM061010 to RDM and an NIH post-doctoral fellowship to EI.

EI would like to dedicate this paper to teachers of Lowell High School: Ms. A. Puretz, Ms. O. Tilton, Mr. R. Shapiro, Mr. P. Luk, Mr. S. Granucci, and Dr. T. Briggs. JYH would like to dedicate this work to her coach and lifelong mentor, Joanna Santarsiere.

Abbreviations

ARP Actin-related protein

ATP Adenosine-triphosphate

dsRNA Double-stranded ribonucleic acid

NPF Nucleation promoting factor

RNAi Ribonucleic acid interference

UTR Untranslated region

VCA Verprollin-homology\ central\ acidic domain

WH2 WASP-homology 2 domain

References

Akin O., R.D. Mullins. 2008. Capping protein increases the rate of actin-based motility by promoting filament nucleation by the Arp2/3 complex. *Cell*. 133:841-851.

Blanchoin L., K.J. Amann, H.N. Higgs, J.B. Marchand, D.A. Kaiser, and T.D. Pollard. 2000.
Direct observation of dendritic actin filament networks nucleated by Arp2/3 complex and WASP/Scar proteins. *Nature*. 404:1007-10011.

Blanchoin, L. and T.D. Pollard. 1999. Mechanism of interaction of Acanthamoeba actophorin (ADF/Cofilin) with actin filaments. *J. Biol. Chem*. 274:15538-15546.

Blanchoin, L. and T.D. Pollard. 2002. Hydrolysis of ATP by polymerized actin depends on the bound divalent cation but not profilin. *Biochemistry*. 41:597-602.

Bork, P., C. Sander, and A. Valencia. 1992. An ATPase domain common to prokaryotic cell cycle proteins, sugar kinases, actin, and hsp70 heat shock proteins. *Proc. Natl. Acad. Sci. U. S. A.* 89:7290-7294.

Cai, L., A.M. Makhov, D.A. Schafer, and J.E. Bear. 2008. Coronin 1B antagonizes cortactin and remodels Arp2/3-containing actin branches in lamellipodia. *Cell*. 134:828-842.

Campellone, K.G., N.J. Webb, E.A. Znameroski, and M.D. Welch. 2008. WHAMM is an Arp2/3 complex activator that binds microtubules and functions in ER to Golgi transport. *Cell*. 134:148-161.

Campellone, K.G. and M.D. Welch. 2010. A nucleator arms race: cellular control of actin assembly. *Nat. Rev. Mol. Cell Biol*. 11:237-251.

Carlier, M.F., V. Laurent, J. Santolini, R. Melki, D. Didry, G.X. Xia, Y. Hong, N.H. Chua, D. Pantaloni. 1997. Actin depolymerizing factor (ADF/cofilin) enhances the rate of filament turnover: implication in actin-based motility. *J. Cell Biol*. 136:1307-1322.

Chan, C., C.C. Beltzner, and T.D. Pollard. 2009. Cofilin dissociates Arp2/3 complex and branches from actin filaments. *Curr. Biol*. 19:537-545.

Cooper, J.A., S.B. Walker, and T.D. Pollard. 1983. Pyrene actin: documentation of the validity of a sensitive assay for actin polymerization. *J. Muscle Res. Cell Motil.* 4:253-262.

Cramer, L.P. 1999. Role of actin-filament disassembly in lamellipodium protrusion in motile cells revealed using the drug jasplakinolide. *Curr. Biol*. 9:1095-1105.

Dayel, M.J. and R.D. Mullins. 2004. Activation of Arp2/3 complex: addition of the first subunit of the new filament by a WASP protein triggers rapid ATP hydrolysis on Arp2. *PLoS Biol.* 2:E91.

Dayel, M.J., E.A. Holleran, and R.D. Mullins. 2001. Arp2/3 complex requires hydrolyzable ATP for nucleation of new actin filaments. *Proc. Natl. Acad. Sci. U. S. A*. 98:14871-14876.

Duleh, S.N. and M.D. Welch. 2010. WASH and the Arp2/3 complex regulate endosome shape and trafficking. *Cytoskeleton*. 67:193-206.

Gandhi, M., B.A. Smith, M. Bovellan, V. Paavilainen, K. Daugherty-Clarke, J. Gelles, P. Lappalainen, and B.L. Goode. 2010. GMF is a cofilin homolog that binds Arp2/3 complex to stimulate filament debranching and inhibit actin nucleation. *Curr. Biol*. 20:861-867.

Garner, E.C., C.S. Campbell, and R.D. Mullins. 2004. Dynamic instability in a DNA-segregating prokaryotic actin homolog. *Science*. 306:1021-1025.

Gordon, D.J., E. Eisenberg, and E.D. Korn. 1976. Characterization of cytoplasmic actin isolated from *Acanthamoeba castellanii* by a new method. *J. Biol. Chem.* 251:4778-4786.

Goshima, G., R. Wollman, S.S. Goodwin, N. Zhang, J.M. Scholey, R.D. Vale, and N. Stuurman. 2007. Genes required for mitotic spindle assembly in Drosophila S2 cells. *Science*. 316:417-421.

Gournier, H., E.D. Goley, H. Niederstrasser, T. Trinh, and M.D. Welch. 2001. Reconstitution of Human Arp2/3 Complex Reveals Critical Roles of Individual Subunits in Complex Structure and Activity. *Molecular Cell*. 8: 1041-1052.

Gupton, S.L., K.L. Anderson, T.P. Kole, R.S. Fischer, A. Ponti, S.E. Hitchcock-DeGregori, G. Danuser, V.M. Fowler, D. Wirtz, D. Hanein, and C.M. Waterman-Storer. 2005. Cell migration without a lamellipodium: translation of actin dynamics into cell movement mediated by tropomyosin. *J. Cell Biol*. 168:619-631.

Higgs, H.N., L. Blanchoin, and T.D. Pollard. 1999. Influence of the C terminus of Wiskott-Aldrich syndrome protein (WASp) and the Arp2/3 complex on actin polymerization. *Biochemistry*. 38:15212-15222.

Ito, H., Y. Fukuda, K. Murata, and A. Kimura. 1983. Transformation of intact yeast cells treated with alkali cations. *J. Bacteriol*. 153:163-168.

Iwasa, J.H. and R.D. Mullins. 2007. Spatial and temporal relationships between actin-filament nucleation, capping, and disassembly. Curr. Biol. 17:395-406.

Kabsch, W., H.G. Mannherz, D. Suck, E.F. Pai, and K.C. Holmes. 1990. Atomic structure of the actin:DNase I complex. *Nature*. 347:37-44.

Kawska, A., K. Carvalho, J. Manzi, R. Boujemaa-Paterski, L. Blanchoin, J.L. Martiel, and C. Sykes. How actin network dynamics control the onset of actin-based motility. 2012. *Proc. Natl. Acad. Sci. U. S. A*. 109:14440-14445.

Kelly, A.E., H. Kranitz, V. Dötsch, and R.D. Mullins. 2006. Actin binding to the central domain of WASP/Scar proteins plays a critical role in the activation of the Arp2/3 complex. *J. Biol. Chem*. 281:10589-10597.

Machesky, L.M., R.D. Mullins, H.N. Higgs, D.A. Kaiser, L. Blanchoin, R.C. May, M.E. Hall, and T.D. Pollard. 1999. Scar, a WASp-related protein, activates nucleation of actin filaments by the Arp2/3 complex. *Proc. Natl. Acad. Sci. U. S. A*. 96:3739-3744.

Marchand, J.B., D.A. Kaiser, T.D. Pollard, and H.N. Higgs. 2001. Interaction of WASP/Scar proteins with actin and vertebrate Arp2/3 complex. *Nat. Cell Biol*. 3:76-82.

Martin, A.C., X.P. Xu, I. Rouiller, M. Kaksonen, Y. Sun, L. Belmont, N. Volkmann, D. Hanein, M. Welch, and D.G. Drubin. 2005. Effects of Arp2 and Arp3 nucleotide-binding pocket mutations on Arp2/3 complex function. *J. Cell Biol*. 168:315-328.

Martin, A.C., M.D. Welch, and D.G. Drubin. 2006. Arp2/3 ATP hydrolysis-catalysed branch dissociation is critical for endocytic force generation. *Nat. Cell Biol.* 8:826-833.

Mullins, R.D., W.F. Stafford, and T.D. Pollard. 1997. Structure, subunit topology, and actin-binding activity of the Arp2/3 complex from Acanthamoeba. *J. Cell Biol*. 136:331-343.

Mullins, R.D., J.A. Heuser, and T.D. Pollard. 1998. The interaction of Arp2/3 complex with actin: nucleation, high affinity pointed end capping, and formation of branching networks of filaments. *Proc. Natl. Acad. Sci. U. S. A*. 95:6181-6186.

Padrick, S.B., L.K. Doolittle, C.A. Brautigam, D.S. King, and M.K. Rosen. 2011. Arp2/3 complex is bound and activated by two WASP proteins. *Proc. Natl. Acad. Sci. U. S. A*. 108:E472-E479.

Palmgren, S., P.J. Ojala, M.A. Wear, J.A. Cooper, and P. Lappalainen. 2001. Interactions with PIP2, ADP-actin monomers, and capping protein regulate the activity and localization of yeast twinfilin. *J. Cell Biol*. 155: 251-260.

Reichstein, E., and E.D. Kom. 1979. Acanthamoeba profilin-protein of low-molecular weight from *Acanthamoeba-castellanii* that inhibits actin nucleation. *J Biol. Chem*. 254:6174-6179.

Reymann, A.C., C. Suarez, C. Guérin, J.L. Martiel, C.J. Staiger, L. Blanchoin, and R. Boujemaa-Paterski. 2011. Turnover of branched actin filament networks by stochastic fragmentation with ADF/cofilin. *Mol. Biol. Cell*. 22: 2541-2550.

Rogers, S.L., U. Wiedemann, N. Stuurman, and R.D. Vale. 2003. Molecular requirements for actin-based lamella formation in Drosophila S2 cells. *J. Cell Biol.* 162: 1079-1088.

Rohatgi, R., L. Ma, H. Miki, M. Lopez, T. Kirchhausen, T. Takenawa, and M.W. Kirschner. 1999. The interaction between N-WASP and the Arp2/3 complex links Cdc42-dependent signals to actin assembly. *Cell*. 97:221-231.

Salmon, W.C., M.C. Adams, and C.M. Waterman-Storer. 2002. Dual-wavelength fluorescent speckle microscopy reveals coupling of microtubule and actin movements in migrating cells. *J. Cell Biol.* 158:31-37.

Sherman, F., G.R. Fink, and J.B. Hicks, 1986. *Methods in Yeast Genetics.* Cold Spring Harbor Laboratory, Cold Spring Harbor, NY.

Svitkina, T.M. and G.G. Borisy. 1999. Arp2/3 complex and actin depolymerizing factor/cofilin in dendritic organization and treadmilling of actin filament array in lamellipodia. *J. Cell Biol*. 145:1009-1026.

Vorobiev, S., B. Strokopytov, D.G. Drubin, C. Frieden, S. Ono, J. Condeelis, P.A. Rubenstein, and S.C. Almo. 2003. The structure of nonvertebrate actin: implications for the ATP hydrolytic mechanism. *Proc. Natl. Acad. Sci. U. S. A*. 100:5760-5765.

Welch, M.D. and R.D. Mullins. 2002. Cellular control of actin nucleation. *Annu. Rev. Cell Dev. Biol*. 18:247-288.

Xu X.P., I. Rouiller, B.D. Slaughter, C. Egile, E. Kim, J.R. Unruh, X. Fan, T.D. Pollard, R. Li, D. Hanein, and N. Volkmann. 2011. Three-dimensional reconstructions of Arp2/3 complex with bound nucleation promoting factors. *EMBO J*. 31: 236-247.

Zuchero, J.B., A.S. Coutts, M.E. Quinlan, N.B.Thangue, and R.D. Mullins. 2009. p53-cofactor JMY is a multifunctional actin nucleation factor. *Nat. Cell Biol*. 11:451-459.

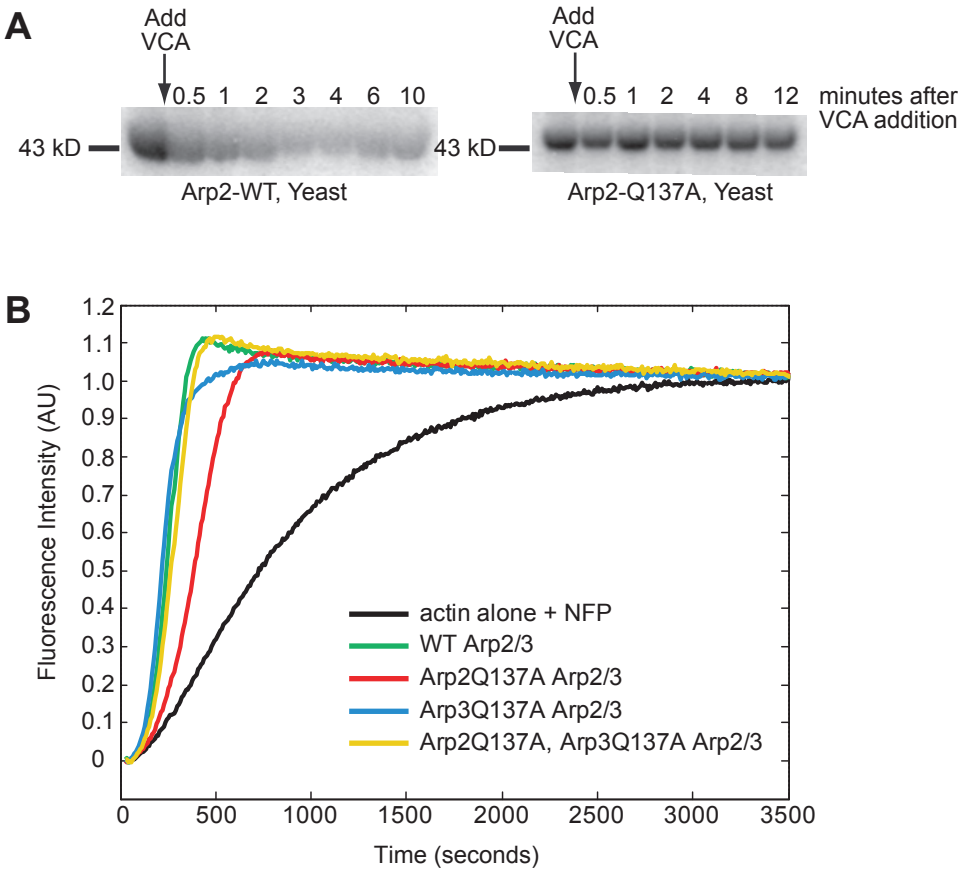

Figure 1. Arp2/3 ATP hydrolysis mutants nucleate actin at levels near that of wild type Arp2/3 complex. (A) Arp2Q137A does not hydrolyze ATP, in contrast to wild-type Arp2. We cross-linked Azido-γ32P-ATP to WT and Arp2Q137A yeast Arp2/3. The VCA domain of the yeast NPF, Las17, was added to stimulate ATP hydrolysis by Arp2/3. Samples were removed from the reaction tubes at the indicated times, methanol precipitated, resuspended in sample buffer, and resolved by SDS-PAGE. Wild-type yeast Arp2/3 shows an appreciable loss of 32P signal over time, signifying hydrolysis and subsequent dissociation of the γ32-phosphate of cross-linked nucleotide from the ATP-binding pocket. (B) Fluorimetry of pyrene-labeled actin demonstrating Arp2/3-accelerated actin polymerization with WT and ATP hydrolysis mutant Human Arp2/3 variants. Reactions were performed in 1X KMEI (50 mM KCl, 1 mM MgCl2, 1 mM EGTA, 10 mM imidazole, pH 7.0), with 4 μM Actin (5% pyrene labeled), 41 nM Human Arp2/3, 100 nM nWASP WWCA. Each pyrene reaction was performed two times. The data shown are from a single representative experiment.

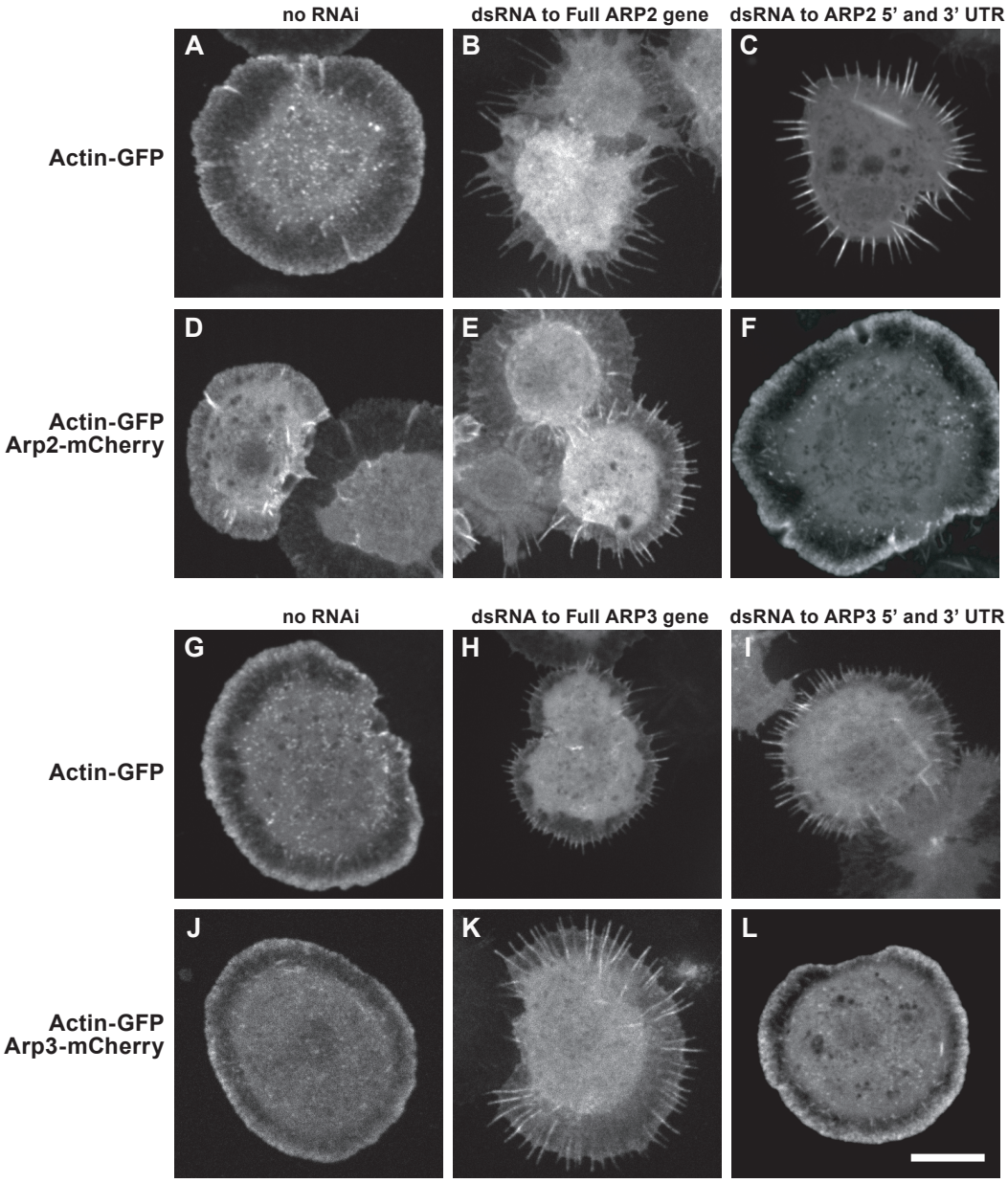

Figure 2. Double-stranded RNA (dsRNA) directed against the 5' and 3' untranslated regions (UTRs) of ARP2 or ARP3 depletes the targeted endogenous protein, producing the serrated phenotype. Arp2-GFP and Arp3-GFP each rescues cells depleted of endogenous Arp2 and Arp3, respectively. We created stable S2 cells lines that express Actin-GFP, either alone or with Arp2-mCherry (or Arp3-mCherry). DsRNA targeting the coding sequence of ARP2 (or ARP3) depletes the corresponding protein, resulting in the serrated phenotype (B, E, H, K). In contrast, cells transfected with dsRNA targeting the 5' and 3' UTRs of ARP2 or ARP3 are selectively depleted of endogenous Arp2 or Arp3 (C) and (I), and are rescued by exogenously-expressed Arp2-mCherry (F) and Arp3-mCherry (L). Scale bar = 10 μm.

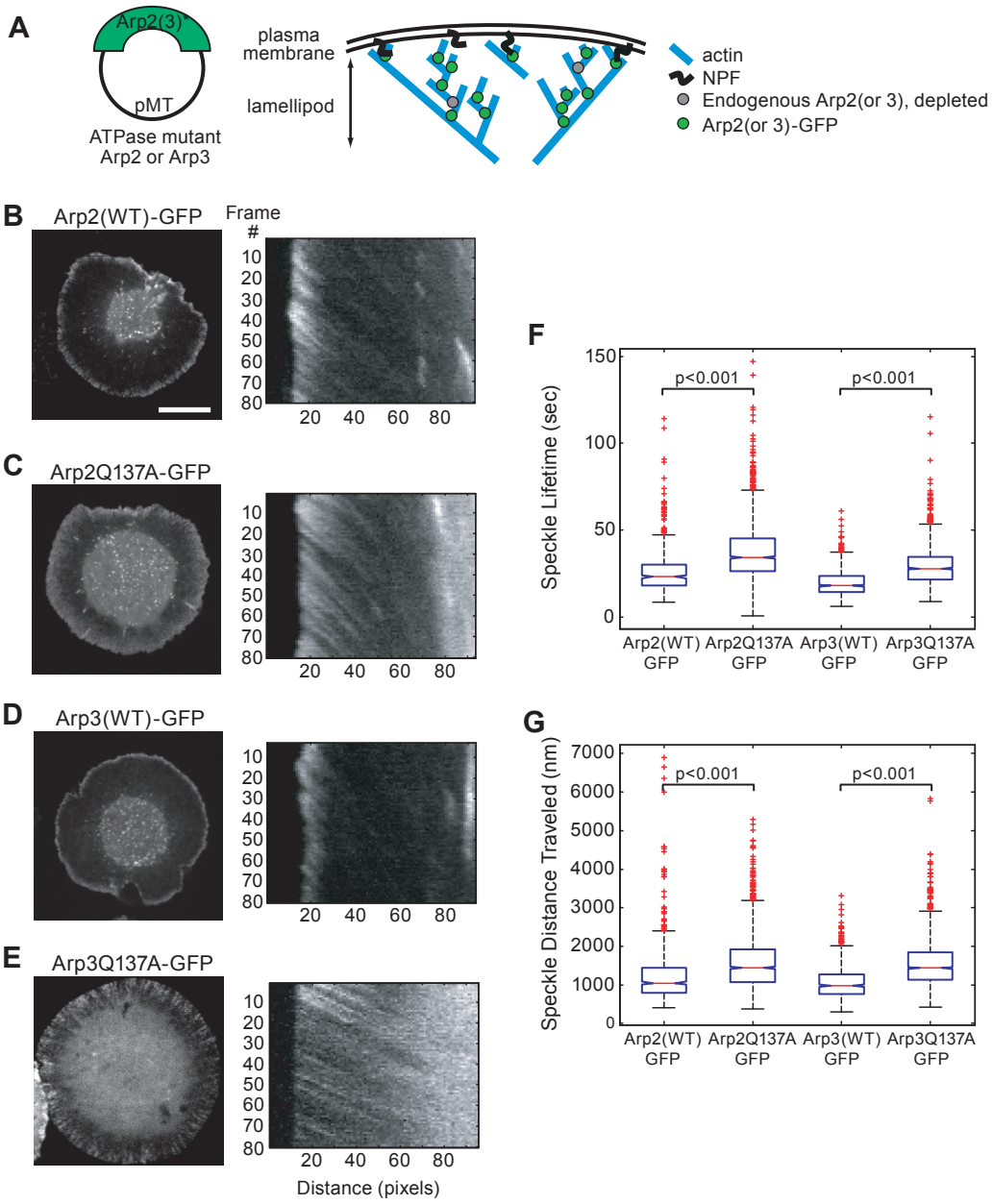
A
Arp2(3)
pMT
ATPase mutant
Arp2 or Arp3
plasma
membrane
lamellipod
actin
NPF
Endogenous Arp2(or 3), depleted
Arp2(or 3)-GFP
B
Arp2(WT)-GFP
Frame
#
C
Arp2Q137A-GFP
D
Arp3(WT)-GFP
E
Arp3Q137A-GFP
10
20
30
40
50
60
70
80
20
40
60
80
Distance (pixels)
F
Speckle Lifetime (sec)
150
100
50
0
p<0.001
p<0.001
Arp2(WT) GFP
Arp2Q137A GFP
Arp3(WT) GFP
Arp3Q137A GFP
G
Speckle Distance Traveled (nm)
7000
6000
5000
4000
3000
2000
1000
0
p<0.001
p<0.001
Arp2(WT) GFP
Arp2Q137A GFP
Arp3(WT) GFP
Arp3Q137A GFP

Figure 3. ATP hydrolysis mutant Arp2/3 complex produces dendritic actin network disassembly defects. This is demonstrated by the longer lifetimes and greater distances traveled of Arp2/3 speckles, as compared to WT Arp2/3. (A) We created the following Drosophila S2 stable cell lines: Arp2(WT)-GFP (3); Arp2Q137A-GFP (4); Arp3(WT)-GFP (6); and Arp3Q137A-GFP (7) (See Table 1 for complete list of cell lines.) We imaged these stable cell lines and created kymographs from the movies (B-E, second column). We quantified the speckle distances traveled and speckle lifetimes. Endogenous Arp2 (B, C) and Arp3 (D, E) were depleted by dsRNA directed against the 5' and 3' UTRs, leaving Arp2-GFP (B, C) and Arp3-GFP (D, E) as the sole copy of Arp2 (B, C) and Arp3 (D, E) in the cell. Scale bar = 10 μm. (F) We re-plotted our speckle lifetime and distance traveled measurements using box and whiskers plot. We used the non-parametric Kolmogorov-Smirnov test to compare ATP hydrolysis mutant data against WT data. We calculated p-values to be less than 0.001. The central mark in the box represents the median value; the edges of the box represent the 25th and 75th percentiles. Whiskers extend to the most extreme data points not considered outliers, and outliers are plotted individually, in red.

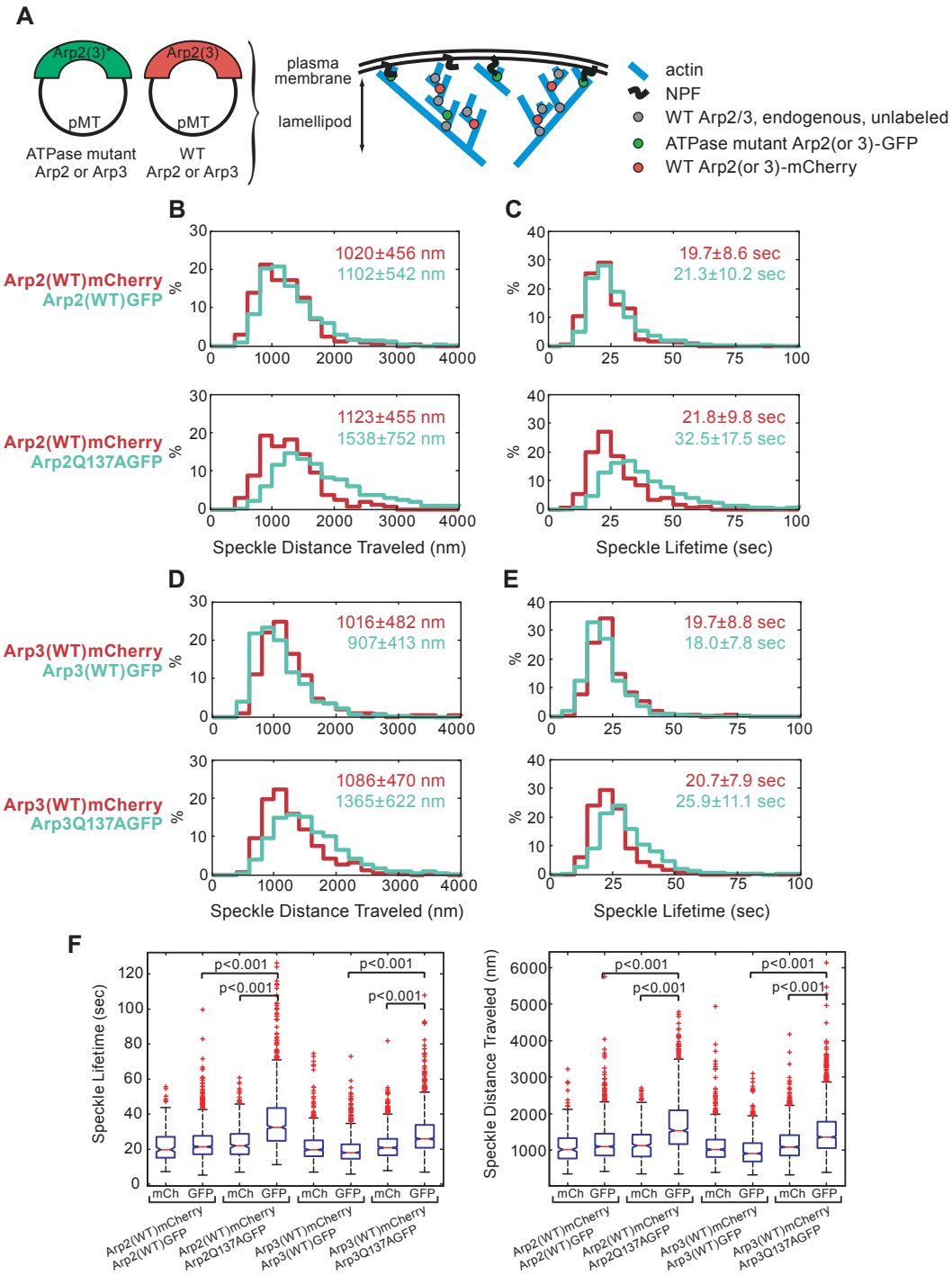
A
Arp2(3)*
pMT
ATPase mutant
Arp2 or Arp3
Arp2(3)
pMT
WT
Arp2 or Arp3
plasma
membrane
lamellipod
actin
NPF
WT Arp2/3, endogenous, unlabeled
ATPase mutant Arp2(or 3)-GFP
WT Arp2(or 3)-mCherry
B
C
Arp2(WT)mCherry
Arp2(WT)GFP
1020±456 nm
1102±542 nm
19.7±8.6 sec
21.3±10.2 sec
Arp2(WT)mCherry
Arp2Q137AGFP
1123±455 nm
1538±752 nm
21.8±9.8 sec
32.5±17.5 sec
Speckle Distance Traveled (nm)
Speckle Lifetime (sec)
D
E
Arp3(WT)mCherry
Arp3(WT)GFP
1016±482 nm
907±413 nm
19.7±8.8 sec
18.0±7.8 sec
Arp3(WT)mCherry
Arp3Q137AGFP
1086±470 nm
1365±622 nm
20.7±7.9 sec
25.9±11.1 sec
Speckle Distance Traveled (nm)
Speckle Lifetime (sec)
F
Speckle Lifetime (sec)
Speckle Distance Traveled (nm)
p<0.001
mCh
GFP
Arp2(WT)mCherry
Arp2(WT)GFP
Arp2(WT)mCherry
Arp2Q137AGFP
Arp3(WT)mCherry
Arp3(WT)GFP
Arp3(WT)mCherry
Arp3Q137AGFP

Figure 4. ATP hydrolysis is necessary for timely detachment of Arp2/3 from the lamellipodial actin network, as seen from the ATP hydrolysis mutant's longer lifetime and longer distance traveled. Arp2/3 containing a single ATP hydrolysis mutant subunit behaves differently than wild-type Arp2/3 within the same cell. (A) We expressed wild-type mCherry-tagged Arp2 (or Arp3) along with ATP hydrolysis mutant GFP-tagged Arp2 (or Arp3) in the same cells. (B) and (C) Imaging of stable S2 cell lines (1-3): Arp2(WT)-GFP, Arp2(WT)-mCherry (30 cells, 907 GFP speckles, 244 mCherry speckles); (1-4): Arp2Q137A-GFP, Arp2(WT)-mCherry (34 cells, 972 GFP speckles, 321 mCherry speckles). (D) and (E) Imaging of stable S2 cell lines (2-6): Arp3(WT)-GFP, Arp3(WT)-mCherry (41 cells, 915 GFP speckles, 692 mCherry speckles.); (2-7): Arp3Q137A-GFP, Arp3(WT)-mCherry (45 cells, 1673 GFP speckles, 952 mCherry speckles). We created kymographs showing speckle trajectories, which we used to determine speckle distances traveled and speckle lifetimes. Median values for speckle distances traveled, (B) and (D) or speckle lifetimes, (C) and (E) are noted. Each imaging experiment was repeated on three separate occasions and speckle data were combined. (F) As in Figures 3F and 3G, we re-plotted our data in a box and whiskers plot and used the non-parametric Kolmogorov-Smirnov test to compare ATP hydrolysis mutant data against WT data. We calculated p-values to be less than 0.001.

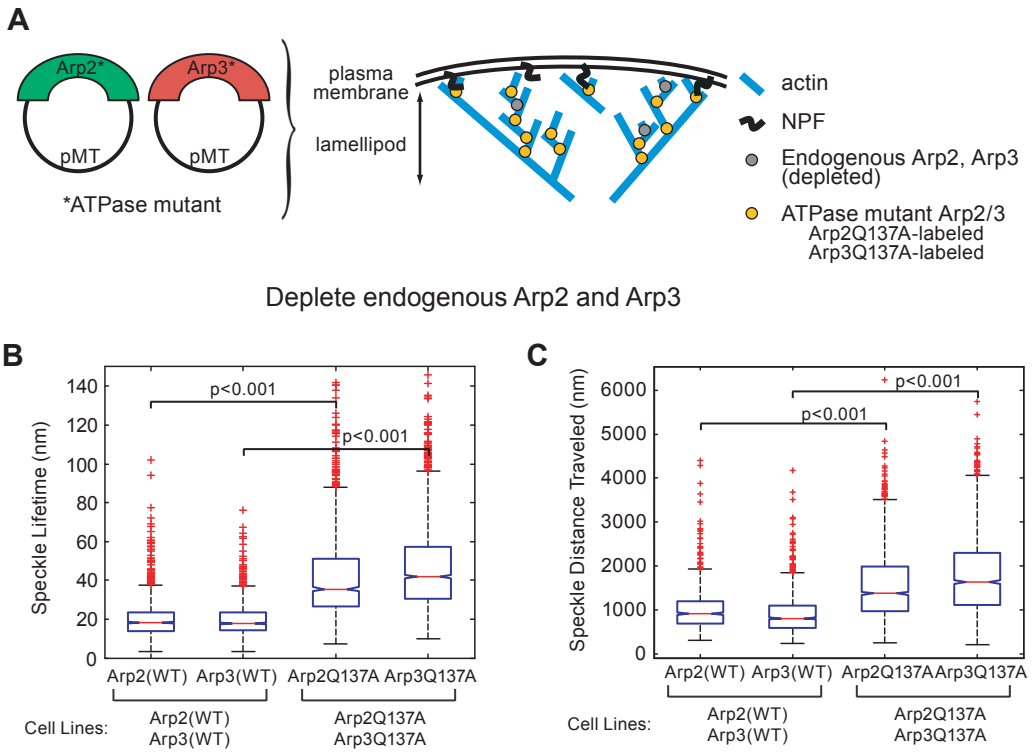

Figure 5. Replacing both the Arp2 and the Arp3 subunits of the Arp2/3 complex with ATP hydrolysis mutant variants produces a more severe disassembly phenotype than replacing a single subunit. (A) We created stable cell lines that express mCherry-tagged Arp2 ATP hydrolysis mutant and GFP-tagged Arp3 ATP hydrolysis mutant. We also created stable cell lines in which we switched the fluorescent tags on Arp2 and Arp3; thus, cells express GFP-tagged Arp2 ATP hydrolysis mutant and mCherry-tagged Arp3 ATP hydrolysis mutant. In all cases, we combined speckle measurements from cells expressing Arp2-GFP and Arp3-mCherry with measurements from cells expressing Arp2-mCherry and Arp3-GFP. We plotted our speckle lifetimes (B) and speckle distances traveled (C) in a box and whiskers plot and used the non-parametric Kolmogorov-Smirnov test to compare ATP hydrolysis mutant data against WT data. We calculated p-values to be less than 0.001.

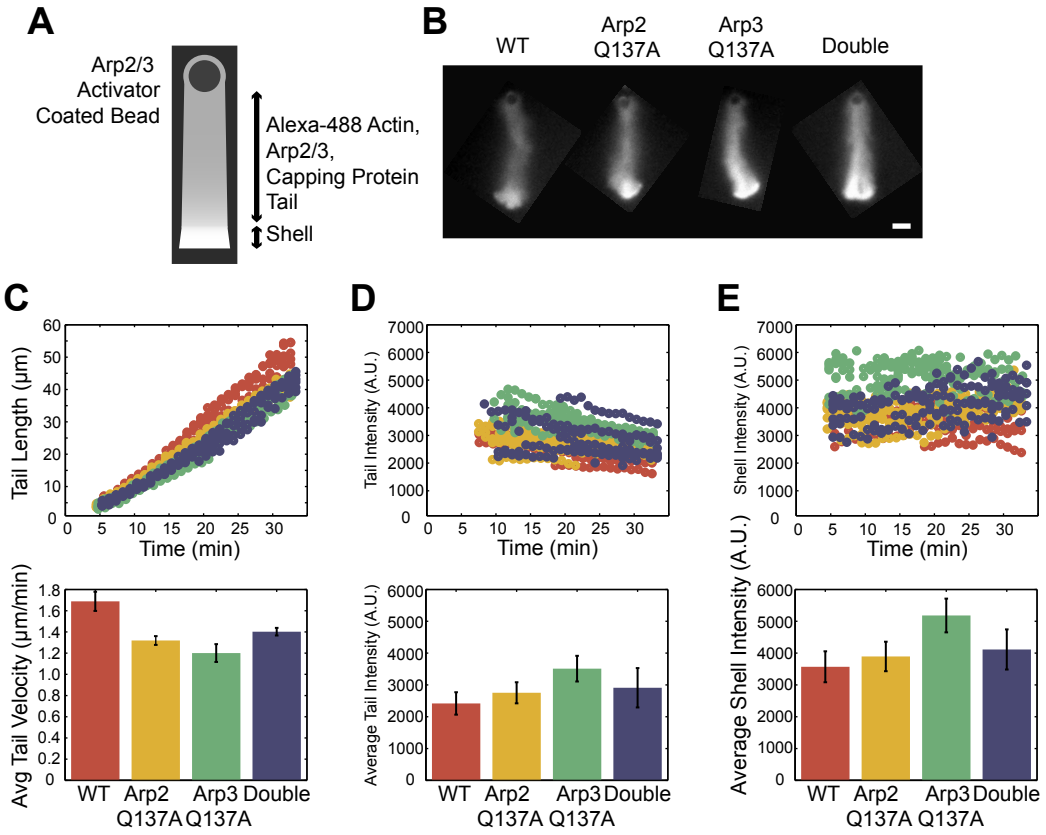

Figure 6. Wild type and ATP hydrolysis mutant variants of Arp2/3 complex build actin networks in a reconstituted actin-based motility system. (A) The VCA domain of ActA, an Arp2/3-activating protein from the pathogen, Listeria monocytogenes, is covalently attached to polystyrene beads. In the presence of 3% Alexa488 labeled cytoplasmic actin, Arp2/3 complex, and capping protein, a dendritic actin network grows in a spherical array from the bead surface, creating a shell of actin. After the actin shell breaks symmetry, a sustained tail of actin continues to grow from the bead surface. At 50 nM, wild type Arp2/3, Arp2Q137A Arp2/3, Arp3Q137A Arp2/3, and Arp2Q137A/Arp3Q137A Arp2/3 all build (B) similar actin networks (C) with comparable actin tail lengths, and similar actin intensities in (C) the tail, and (D) shell regions. Scale bar = 10 μm.

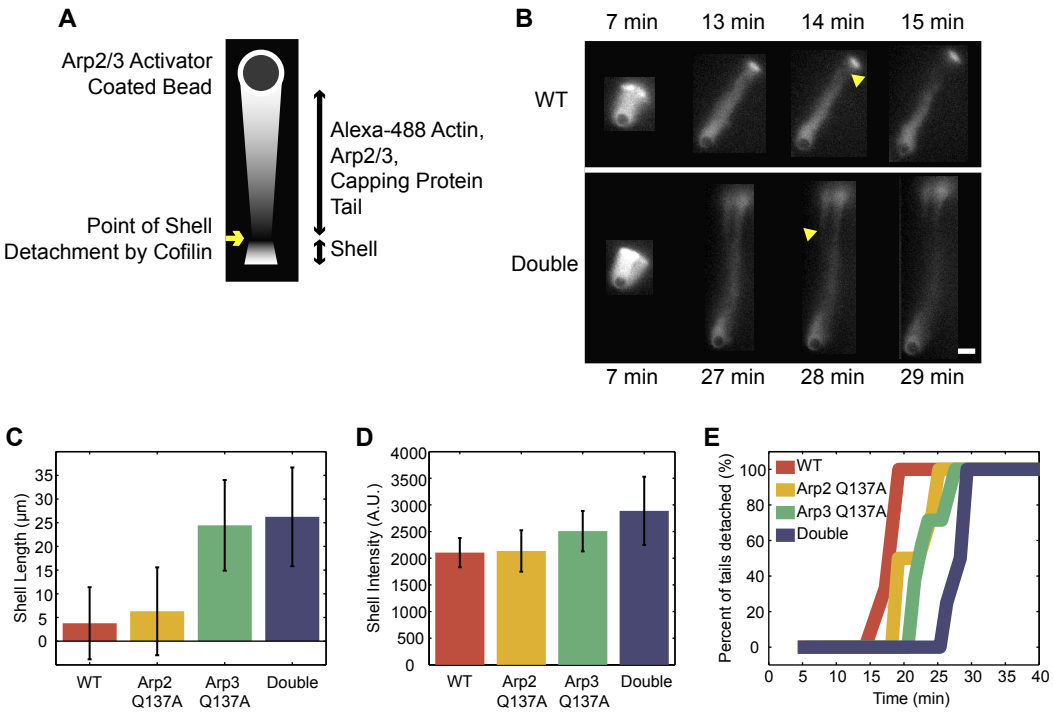

Figure 7. Differences in actin disassembly between networks constructed with wild type versus ATP hydrolysis mutant Arp2/3 complex become apparent under recycling conditions. (A) The addition of cofilin and profilin to the in vitro actin-based motility system causes turnover and recycling of actin monomers by promoting disassembly of actin filaments. Cofilin severs the actin shell, detaching it from the tail. (B) and (E) Severing of shells from growing tails occurs 14 minutes earlier in networks built with wild type Arp2/3 complex (upper panel) than in networks built with double ATP hydrolysis mutant Arp2/3 complex (lower panel). (C) Shells built with ATP hydrolysis mutant Arp2/3 grow to longer lengths than shells built with wild type Arp2/3 complex. (D) Actin intensities of shells constructed with wild type Arp2/3 are comparable or slightly lower than intensities of shells constructed with ATP hydrolysis mutant Arp2/3. (E) Quantification of the timing of tail severing for wild type (13 tails), Arp2Q137A (9 tails), Arp3Q137A (9 tails), and double ATP hydrolysis mutant (8 tails). Arp2Q137A, Arp3Q137A, and double mutant tails result in shells severed later than wild type tails by 3.5 min, 4.5 min, and 12 min, respectively. Scale bar = 10 μm.

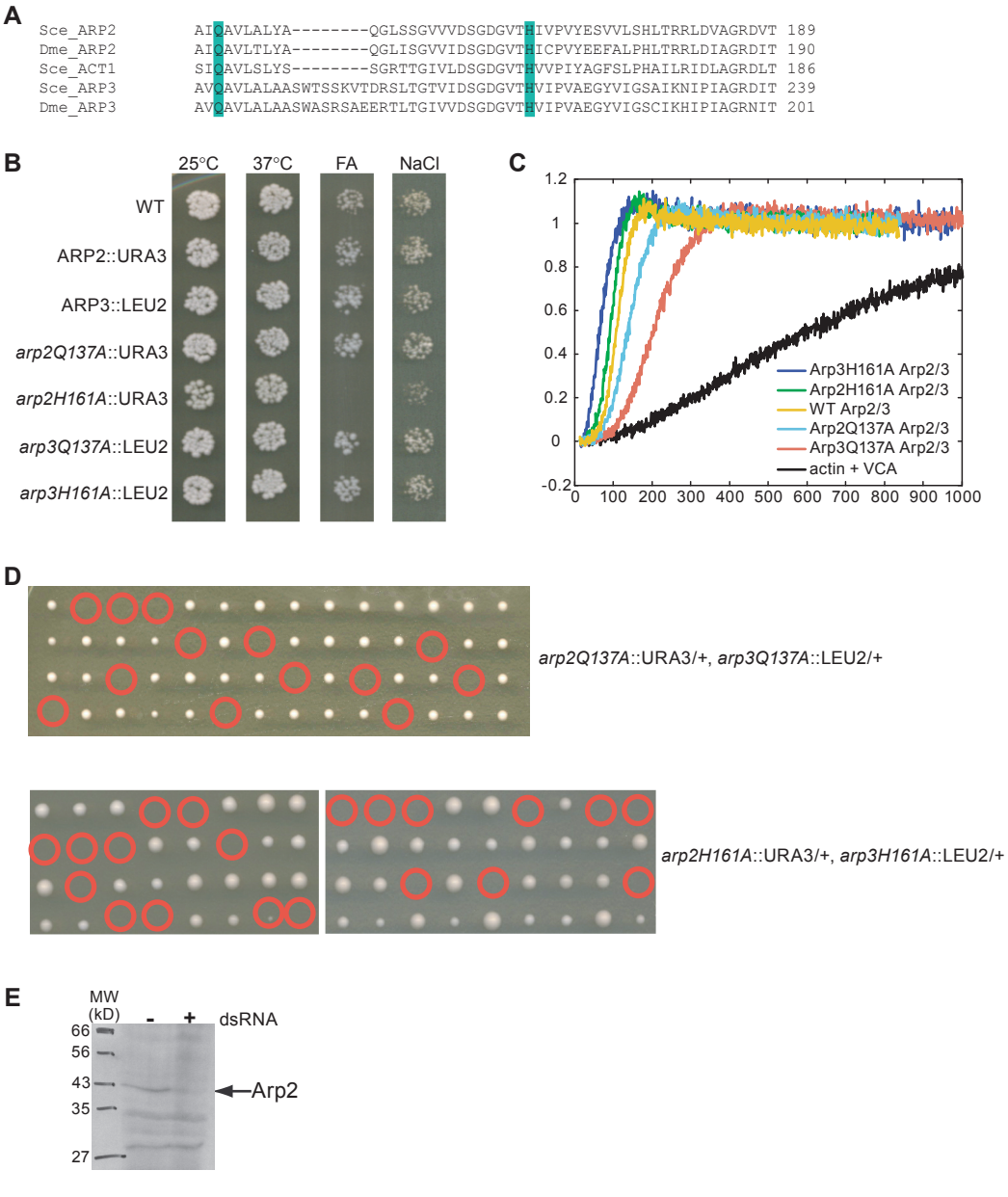
A
Sce_ARP2 AIQAVLALYA--------QGLSSGVVVDSGDGVTHIVPVYESVVLSHLTRRLDVAGRDVT 189
Dme_ARP2 AIQAVLTLYA--------QGLISGVVIDSGDGVTHICPVYEEFALPHLTRRLDIAGRDIT 190
Sce_ACT1 SIQAVLSLYS--------SGRTTGIVLDSGDGVTHVVPIYAGFSLPHAILRIDLAGRDLT 186
Sce_ARP3 AVQAVLALAASWTSSKVTDRSLTGTVIDSGDGVTHVIPVAEGYVIGSAIKNIPIAGRDIT 239
Dme_ARP3 AVQAVLALAASWASRSAEERTLTGIVVDSGDGVTHVIPVAEGYVIGSCIKHIPIAGRNIT 201
B
25°C
37°C
FA
NaCl
WT
ARP2::URA3
ARP3::LEU2
arp2Q137A::URA3
arp2H161A::URA3
arp3Q137A::LEU2
arp3H161A::LEU2
C
1.2
1
0.8
0.6
0.4
0.2
0
-0.2
0 100 200 300 400 500 600 700 800 900 1000
Arp3H161A Arp2/3
Arp2H161A Arp2/3
WT Arp2/3
Arp2Q137A Arp2/3
Arp3Q137A Arp2/3
actin + VCA
D
arp2Q137A::URA3/+, arp3Q137A::LEU2/+
arp2H161A::URA3/+, arp3H161A::LEU2/+
E
MW (kD)
-
+
dsRNA
66
56
43
35
27
Arp2

Supplemental Figure S1. (A) Clustal-W alignment of Saccharomyces ACT1, ARP2, ARP3 and Drosophila ARP2 and ARP3. In ARP2 and ARP3 of yeast and Drosophila, we mutated residues analogous to Q137 and H161 of yeast actin to create our ATP hydrolysis mutants. (B) The ATP hydrolysis mutant allele H161A compromises yeast growth. Arp2 ATPase mutant arp2H161A::URA3 confers a growth defect upon yeast under high stress conditions. FA denotes 3% formamide. NaCl denotes 0.9M NaCl. (C) The allele arp2-Q137A::URA3 is synthetically lethal with arp3-Q137A::LEU2. The allele arp2-H161A::URA3 is synthetically lethal with arp3-H161A::LEU2. Red circles denote double mutants. (D) Double stranded RNA directed against the 5' and 3' untranslated regions of ARP2 deplete Arp2 protein. Whole cell lysates from S2 cells treated with dsRNA were resolved by SDS PAGE, transferred to PVDF membrane, and Western blotted with Arp2 antibodies.

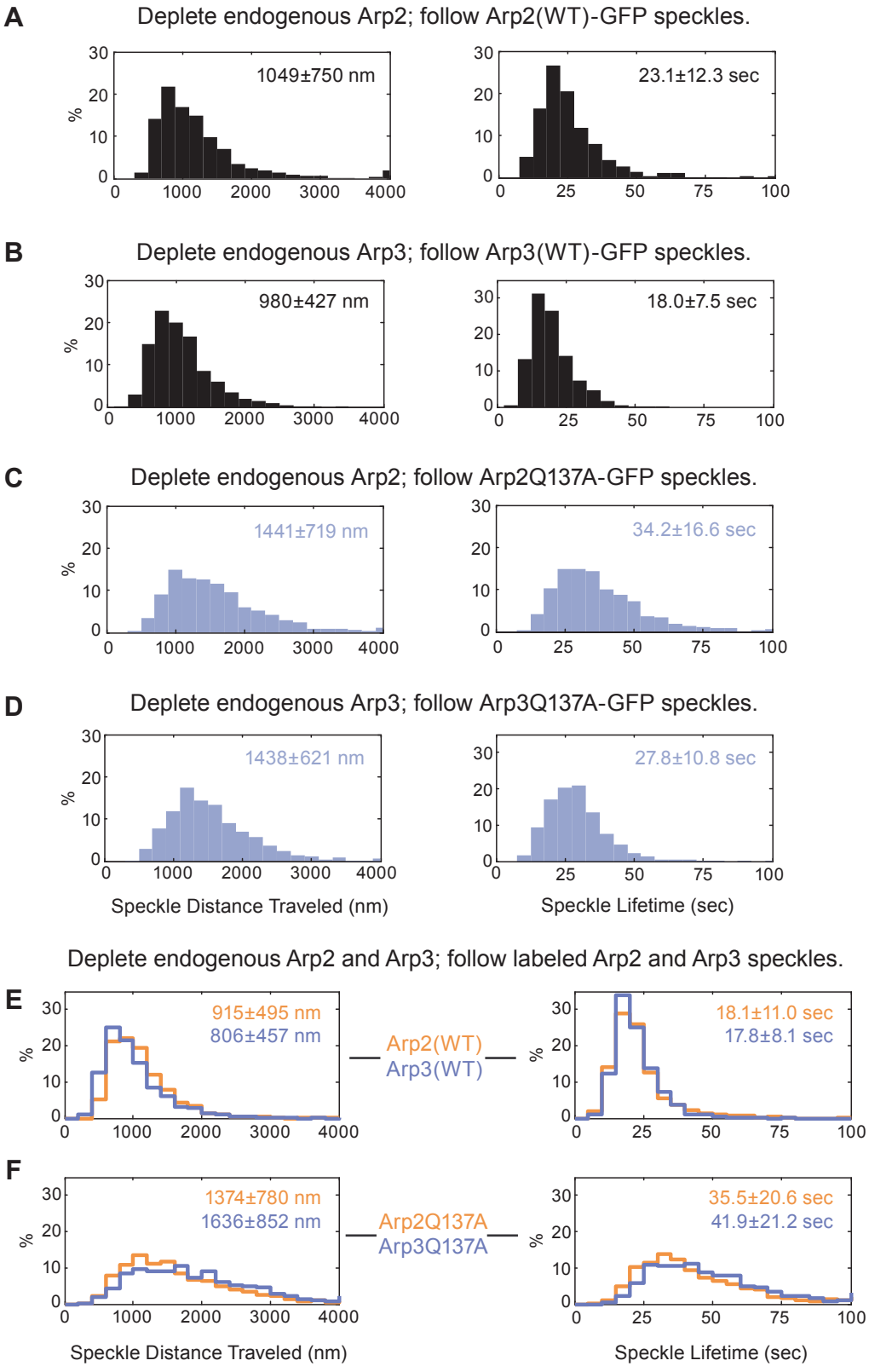
A
Deplete endogenous Arp2; follow Arp2(WT)-GFP speckles.
1049±750 nm
23.1±12.3 sec
B
Deplete endogenous Arp3; follow Arp3(WT)-GFP speckles.
980±427 nm
18.0±7.5 sec
C
Deplete endogenous Arp2; follow Arp2Q137A-GFP speckles.
1441±719 nm
34.2±16.6 sec
D
Deplete endogenous Arp3; follow Arp3Q137A-GFP speckles.
1438±621 nm
27.8±10.8 sec
Speckle Distance Traveled (nm)
Speckle Lifetime (sec)
Deplete endogenous Arp2 and Arp3; follow labeled Arp2 and Arp3 speckles.
E
915±495 nm
806±457 nm
Arp2(WT)
Arp3(WT)
18.1±11.0 sec
17.8±8.1 sec
F
1374±780 nm
1636±852 nm
Arp2Q137A
Arp3Q137A
35.5±20.6 sec
41.9±21.2 sec
Speckle Distance Traveled (nm)
Speckle Lifetime (sec)
%

Supplemental Figure S2. (A) to (D) Histograms corresponding to data from Figure 3. (A) Arp2(WT) GFP speckles (25 cells, 676 speckles). (B) Arp3(WT) GFP speckles (70 cells, 853 speckles). (C) Arp2Q137A-GFP speckles (41 cells, 1398 speckles). (D) Arp3Q137A-GFP speckles (77 cells, 1600 speckles). (E), (F) Histograms corresponding to box and whiskers plots from Figure 5. Median values are noted on each histogram. Left column: speckle distance traveled; Right column: speckle lifetime. (E) (67 cells, 788 Arp2 speckles, 1236 Arp3 speckles). (F) (80 cells, 1515 Arp2 speckles, 1904 Arp3 speckles).

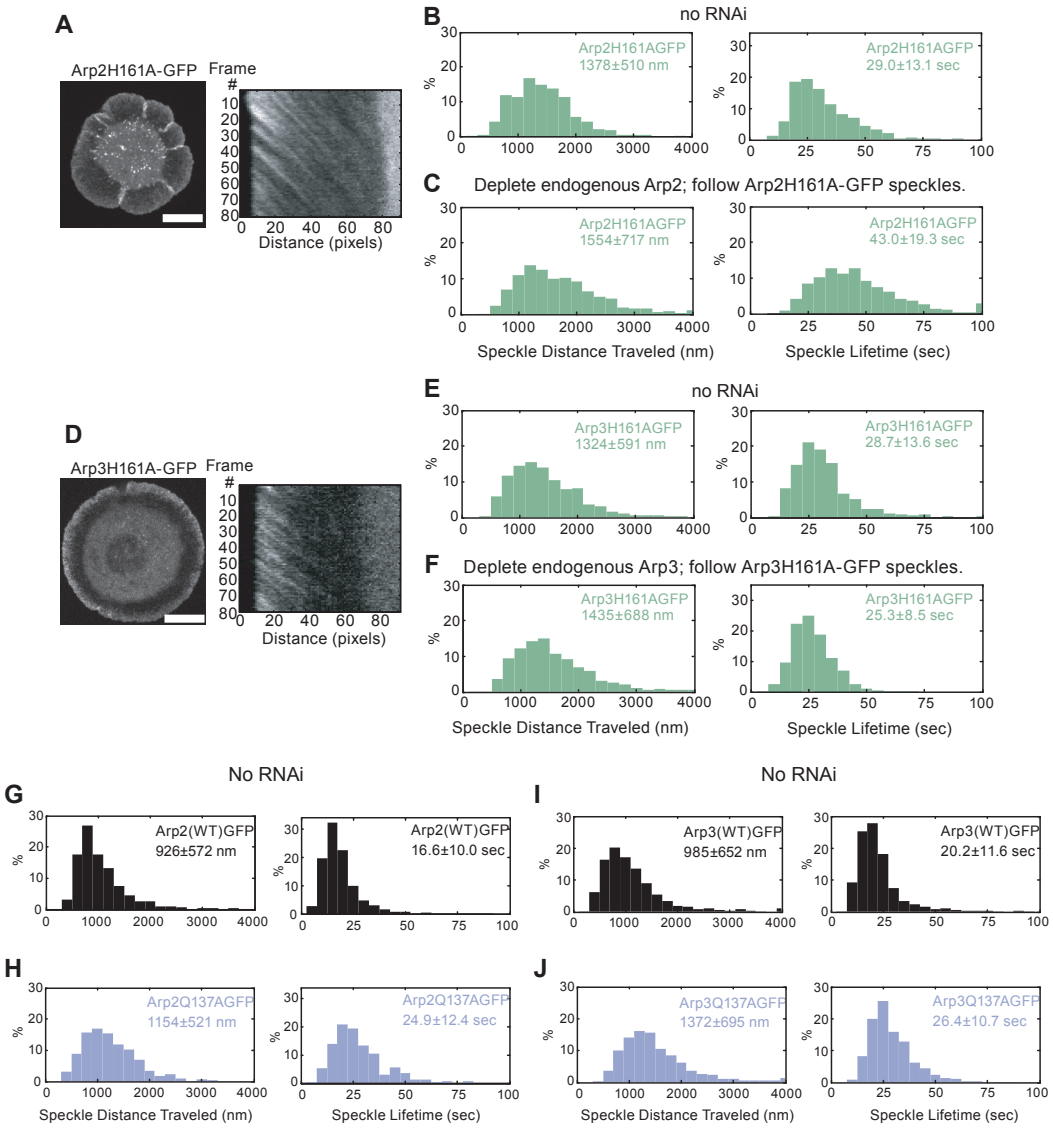

Supplemental Figure S3. Another Arp2/3 ATP hydrolysis mutant, H161A, exhibits network disassembly defects. As in Figure 3, we created Drosophila S2 cell lines stably expressing Arp2H161A-GFP (5) and Arp3H161A-GFP (8) (See Table 1.) We imaged stable cell lines in time lapse, created kymographs, and quantified the speckle distances traveled and speckle lifetimes. Endogenous Arp2 (C) and Arp3 (F) were depleted by dsRNA directed against the 5' and 3' UTRs, leaving Arp2H161A-GFP (C) and Arp3Arp2H161A-GFP (F) as the sole copy of Arp2 or Arp3, respectively, in the cell. We plotted distributions of the speckle distances traveled and speckle lifetimes. (G-J) These experiments are analogous to those shown in Figure 3 and in Supplemental Figure S2 A-D, but with no depletion of endogenous Arp2 or Arp3. We created Drosophila S2 cell lines stably expressing Arp2(WT)-GFP, Arp2Q137A-GFP, Arp3(WT)-GFP, and Arp3Q137A-GFP (Also, see Table 1.) We imaged these stable cell lines, created kymographs from the movies, and quantified the distances traveled and speckle lifetimes. Median values for speckle distances traveled or speckle lifetimes are noted. Scale bar = 10 μm. (B) 9 cells, 562 speckles. (C) 32 cells, 1138 speckles. (E) 26 cells, 723 speckles. (F) 64 cells, 1470 speckles. (G) 21 cells, 1329 speckles. (H) 17 cells, 661 speckles. (I) 21 cells, 878 speckles. (J) 29 cells, 1195 speckles.

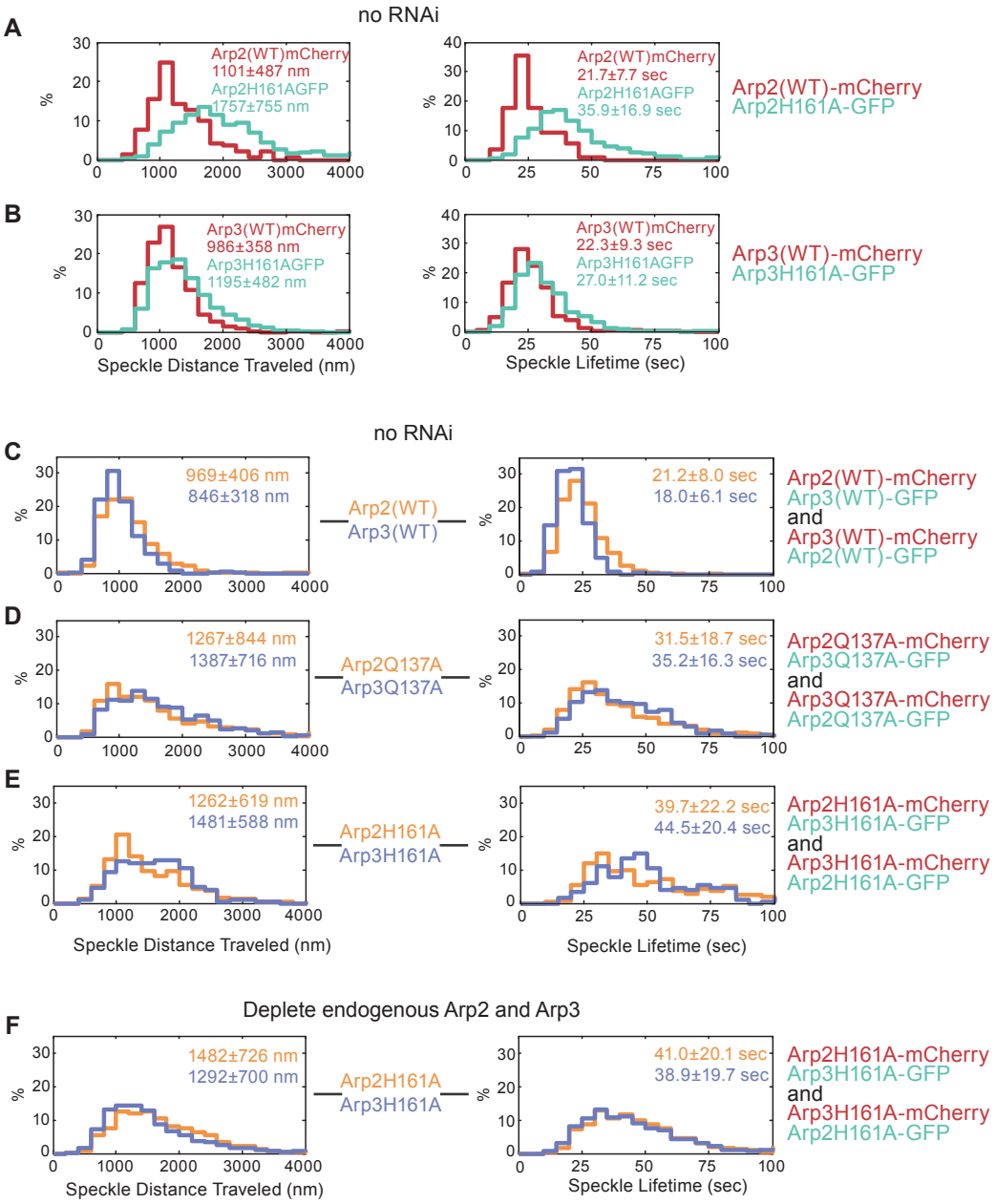
no RNAi
A
Arp2(WT)mCherry
1101±487 nm
Arp2H161AGFP
1757±755 nm
Arp2(WT)mCherry
21.7±7.7 sec
Arp2H161AGFP
35.9±16.9 sec
Arp2(WT)-mCherry
Arp2H161A-GFP
B
Arp3(WT)mCherry
986±358 nm
Arp3H161AGFP
1195±482 nm
Arp3(WT)mCherry
22.3±9.3 sec
Arp3H161AGFP
27.0±11.2 sec
Arp3(WT)-mCherry
Arp3H161A-GFP
Speckle Distance Traveled (nm)
Speckle Lifetime (sec)
%
no RNAi
C
969±406 nm
846±318 nm
Arp2(WT)
Arp3(WT)
21.2±8.0 sec
18.0±6.1 sec
Arp2(WT)-mCherry
Arp3(WT)-GFP
and
Arp3(WT)-mCherry
Arp2(WT)-GFP
D
1267±844 nm
1387±716 nm
Arp2Q137A
Arp3Q137A
31.5±18.7 sec
35.2±16.3 sec
Arp2Q137A-mCherry
Arp3Q137A-GFP
and
Arp3Q137A-mCherry
Arp2Q137A-GFP
E
1262±619 nm
1481±588 nm
Arp2H161A
Arp3H161A
39.7±22.2 sec
44.5±20.4 sec
Arp2H161A-mCherry
Arp3H161A-GFP
and
Arp3H161A-mCherry
Arp2H161A-GFP
Speckle Distance Traveled (nm)
Speckle Lifetime (sec)
%
Deplete endogenous Arp2 and Arp3
F
1482±726 nm
1292±700 nm
Arp2H161A
Arp3H161A
41.0±20.1 sec
38.9±19.7 sec
Arp2H161A-mCherry
Arp3H161A-GFP
and
Arp3H161A-mCherry
Arp2H161A-GFP
Speckle Distance Traveled (nm)
Speckle Lifetime (sec)
%

Supplemental Figure S4. (A, B) Another ATP hydrolysis mutant, H161, produces results similar to those of mutant Q137A. We expressed wild-type mCherry-tagged Arp2 (or Arp3) along with ATP hydrolysis mutant GFP-tagged Arp2 (or Arp3) in the same cells. We imaged stable S2 cell lines (1-5): Arp2H161A-GFP, Arp2(WT)-mCherry and (2-8): Arp3H161A-GFP, Arp3(WT)-mCherry. As in Figure 4, we created kymographs showing speckle trajectories, which we used to determine speckle distances traveled and speckle lifetimes. Median values are noted for speckle distance traveled, (left column) or speckle lifetime, (right column). (C, D, E) Analogous experiments to those shown in Figure 5, but with endogenous Arp2 and Arp3 remaining present in the cell. (F) Similar experiment as in Figure 5, but using ATPase mutant H161A to replace WT Arp2 and Arp3. As seen for Q137A mutants, we observed an increase in speckle lifetimes and distances traveled. (A) 41 cells, 589 GFP speckles, 141 mCherry speckles. (B) 48 cells, 1723 GFP speckles, 943 mCherry speckles. (C) 18 cells, 1025 Arp2 speckles, 474 Arp3 speckles. (D) 23 cells, 670 Arp2 speckles, 370 Arp3 speckles. (E) 17 cells, 251 Arp2 speckles, 202 Arp3 speckles. (F) 37 cells, 1297 Arp2 speckles, 1867 Arp3 speckles.

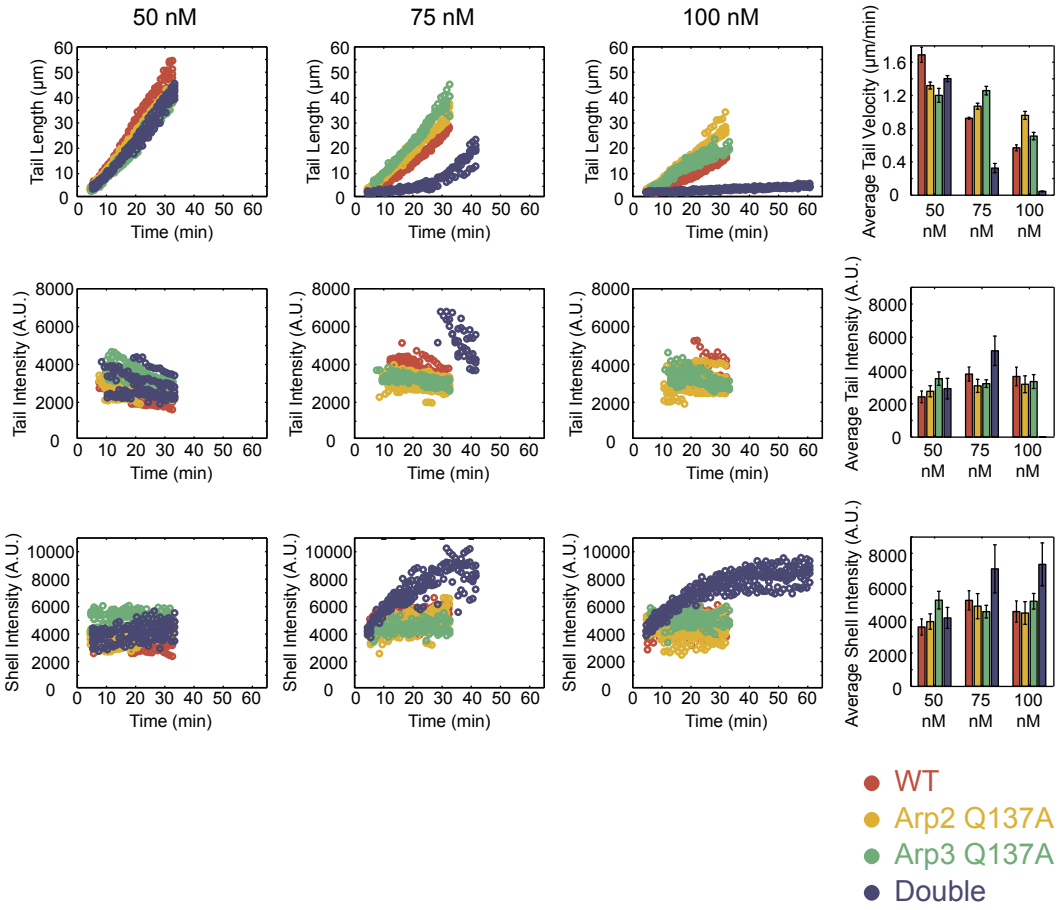

Supplemental Figure S5. In vitro actin-based bead motility reactions, under non-recycling conditions. As in Figure 6, we also performed the experiments at 75 nM and 100 nM Arp2/3 concentrations. At 75 nM Arp2/3 concentration, actin tails formed more slowly. At 100 nM Arp2/3, shells failed to break symmetry, producing actin tails too short to be measured accurately. Data from a single experiment is presented for each Arp2/3 variant and concentration. Wild type Arp2/3 (6-9 tails per concentration); Double ATP hydrolysis mutant Arp2/3 (7-8 tails per concentration); Arp2Q137A Arp2/3 (9-13 tails per concentration); Arp3Q137A Arp2/3 (9-10 tails per concentration).

Chapter 6

Paper In Review

Multiple mechanisms determine the timing of APC/C substrate degradation in mitosis.

Lu D., Hsiao J.Y., Davey N., Foster S., Tang C., Morgan D.O. Multiple mechanisms determine the timing of APC/C substrate degradation in mitosis. Manuscript in review.

Personal Note about my Collaboration with Dan Lu

Dan Lu, another dear friend and graduate student in the Morgan/Tang labs, needed help analyzing her 3D live cell images of dividing budding yeast. Her work was focused on the degradation timing of different APC/Cdc20 substrates during mitosis. As two different internal time references, she used the duplication and separation of the spindle pole bodies. These spindle pole bodies needed to be tracked from one image to the next in 3D. To help, I wrote a complete MATLAB script to locate and track over time the duplication and separation of these punctate structures. Later on, I also wrote MATLAB scripts to identify the minimum, 50%, and maximum levels of protein during a degradation cycle, as well as the timing of these events. Below is her paper.

Summary

The ubiquitin-protein ligase APC/C controls mitosis by promoting ordered degradation of securin, cyclins, and other proteins. The mechanisms underlying the timing of APC/C substrate degradation are poorly understood. We explored these mechanisms using quantitative fluorescence microscopy of GFP-tagged APC/C^{Cdc20} substrates in living budding yeast cells. Degradation of the S cyclin, Clb5, begins early in mitosis, followed 6 minutes later by the degradation of securin and Dbf4. Anaphase begins when less than half of securin is degraded. The spindle-assembly checkpoint

delays the onset of Clb5 degradation but does not influence securin degradation. Early Clb5 degradation depends on its interaction with the Cdk1-Cks1 complex and the presence of a Cdc20-binding 'A motif' in its N-terminal region. The degradation of securin and Dbf4 is delayed by Cdk1-dependent phosphorylation near their Cdc20-binding sites. Thus, a remarkably diverse array of mechanisms generates robust ordering of APC/C^{Cdc20} substrate destruction.

Introduction

Cell division is a fundamental biological process governed by a complex network of regulatory molecules, and the key to its success lies in having the right molecules become active (or inactive) at the right time. The regulatory network controlling cell division is hierarchical: a few master regulators, primarily the cyclin-dependent kinases (Cdks) and the anaphase-promoting complex or cyclosome (APC/C), orchestrate the activities of hundreds of downstream proteins and processes (Morgan, 2007). As the activities of the master regulators rise and fall, they also drive changes in the activities of downstream players. One interesting feature of this regulatory system is that downstream components, even when regulated by the same master regulator, can become active or inactive in an ordered fashion, rather than simultaneously (Pines, 2006; Sullivan and Morgan, 2007). To decipher how the master regulators discriminate between their substrates and achieve this ordering is crucial to our understanding of the orchestration of the cell cycle and other complex processes.

The APC/C is a ubiquitin-protein ligase or E3 that governs mitotic events by promoting timely degradation of key mitotic proteins (Barford, 2011; Peters, 2006;

Pines, 2011; Primorac and Musacchio, 2013). Together with its early mitotic activator subunit Cdc20, APC/C promotes the degradation of securin, an inhibitor of separase. Separase then cleaves the cohesins that link the sister-chromatid pairs, triggering sister-chromatid separation (Figure 1A) (Nasmyth and Haering, 2009). APC/C^{Cdc20} also promotes the degradation of S and M cyclins, which lowers Cdk activity. In budding yeast, APC/C^{Cdc20}-dependent separase activation also leads to the activation of Cdc14, a phosphatase that dephosphorylates a large number of Cdk substrates (Queralt et al., 2006; Queralt and Uhlmann, 2008; Stegmeier and Amon, 2004). Among these Cdk substrates is the alternative APC/C activator Cdh1, which together with APC/C promotes the degradation of late-mitotic substrates and drives the completion of mitosis, cytokinesis and entry into G1 (Figure 1A) (Sullivan and Morgan, 2007).

APC/C^{Cdc20} and APC/C^{Cdh1} each have multiple substrates, which are degraded at distinct times in the cell cycle (Pines, 2006; Sullivan and Morgan, 2007). In the case of mammalian APC/C^{Cdc20}, the substrates Nek2A and cyclin A are degraded in prometaphase, immediately following nuclear envelope breakdown, while securin and cyclin B are degraded in metaphase (den Elzen and Pines, 2001; Geley et al., 2001; Hagting et al., 2002; Hames et al., 2001). Ordered degradation is equally prevalent among APC/C^{Cdh1} substrates in anaphase and G1 (Pines, 2006; Sullivan and Morgan, 2007). It is not clear how the same APC/C complex robustly distinguishes among its substrates and promotes their degradation at different times in the cell cycle.

The timing of APC/C^{Cdc20} substrate degradation in vertebrate cells is influenced by the spindle assembly checkpoint (SAC), which is activated by unattached

kinetochores and inhibits APC/C^{Cdc20} activity toward different substrates to varying degrees. Upon SAC activation, kinetochore-localized SAC components stimulate the formation of soluble Mad2-Cdc20 complexes, leading to the formation of the mitotic checkpoint complex (MCC) consisting of Cdc20, Mad2, Mad3 (in yeast) or BubR1 (in vertebrates), and Bub3 (Lara-Gonzalez et al., 2012; Musacchio and Salmon, 2007). The MCC is the major effector of the SAC. It binds to APC/C and strongly inhibits its activity towards securin and cyclin B, while cyclin A and Nek2A can still be degraded in an active checkpoint due to less efficient inhibition by the MCC (Collin et al., 2013; den Elzen and Pines, 2001; Dick and Gerlich, 2013; Geley et al., 2001; Hagting et al., 2002; Hames et al., 2001). When all kinetochores are properly attached to the spindle, the SAC is turned off and the MCC is disassembled to allow APC/C^{Cdc20}-dependent degradation of securin and anaphase onset. The protein components and mechanisms of the SAC are highly conserved across species. However, even though the SAC plays an essential role in mammalian cell division (Meraldi et al., 2004; Michel et al., 2004; Michel et al., 2001), disabling the SAC in yeast has very little impact on the cell cycle under normal conditions, and the SAC becomes essential only in the presence of spindle defects (Hoyt et al., 1991; Li and Murray, 1991).

The APC/C recognizes its targets through short sequence motifs called the D box or KEN box, which are often found in unstructured N-terminal regions of APC/C substrates (Glotzer et al., 1991; Pfleger and Kirschner, 2000). However, both Nek2A and cyclin A are thought to possess extra binding sites for the APC/C, allowing them to bypass or overcome inhibition by SAC proteins. Nek2A employs a C-terminal motif that

resembles Cdc20 and Cdh1 C-termini to bind to the APC/C core directly without the need of an activator (Hames et al., 2001; Hayes et al., 2006; Sedgwick et al., 2013). Cyclin A gains additional affinity for the APC/C^{Cdc20} by forming a complex with Cdk and the accessory subunit Cks1 (Wolthuis et al., 2008). Cks1 binds to Cdk and contributes to recognition of Cdk substrates carrying specific phosphothreonines (Brizuela et al., 1987; Hadwiger et al., 1989; Koivomagi et al., 2013; McGrath et al., 2013; Richardson et al., 1990; Tang and Reed, 1993). There is also evidence that Cks1 binds APC/C directly to promote its phosphorylation by Cdk (Patra and Dunphy, 1998; Rudner and Murray, 2000; Shteinberg and Hershko, 1999). Thus, cyclin A interacts directly with APC/C^{Cdc20} through its D box and also indirectly through Cdk-Cks1.

Modifications of APC/C substrates also influence their ubiquitination by the APC/C. Budding yeast securin has two Cdk1 sites near its D box and KEN box, and phosphorylation of these sites inhibits its ubiquitination *in vitro* (Holt et al., 2008; Holt et al., 2009). Cdc14 dephosphorylates these sites *in vitro*. Given that securin degradation leads to Cdc14 activation indirectly through separase, these results suggested the existence of positive feedback in securin degradation. Although this phosphoregulation of securin by Cdk1 improves the fidelity of sister-chromatid segregation (Holt et al., 2008), it remains unclear how this regulation influences securin degradation rate and timing. Cdk1 sites are also found inside or near the D box of other budding yeast APC/C substrates (Holt et al., 2009), including Dbf4, the activating subunit for Cdc7 (also known as the Dbf4-dependent kinase or DDK). DDK collaborates with S cyclin-Cdk1 to initiate DNA replication (Bell and Dutta, 2002). Dbf4 is an APC/C^{Cdc20} substrate (Ferreira

et al., 2000; Oshiro et al., 1999; Sullivan et al., 2008), but it is not clear whether Cdk phosphorylation contributes to its degradation timing or dynamics.

Here we explore how the interplay among the SAC, Cdk1, APC/C^{Cdc20}, and its substrates lays out the path toward the metaphase-anaphase transition in budding yeast, and we dissect the mechanisms responsible for ordered APC/C^{Cdc20} substrate degradation. We used single-cell analyses of fluorescently-tagged proteins to show that APC/C substrates are degraded in a specific order, with early degradation of the S cyclin Clb5 followed by degradation of securin, Dbf4, and then finally the M cyclin Clb2. We also show that the SAC is largely turned off before the degradation of Clb5 and thus does not contribute to the degradation timing of later substrates. Instead, we find that Cdk-dependent phosphorylation of securin and Dbf4 delays their degradation, and we present evidence that Cks1 and a previously undiscovered sequence motif in Clb5 promote early Clb5 degradation. Together our results provide a temporal and mechanistic view of the key regulatory steps leading to the metaphase-anaphase transition.

Results

APC/C Substrates are Degraded in a Defined Order

To analyze the timing and dynamics of APC/C substrate degradation in living yeast cells, we used an assay based on fluorescence microscopy and *in silico* synchronization (Hagting et al., 2002). We constructed a series of yeast strains in which a single APC/C substrate (Clb5, securin/Pds1, Dbf4, or Clb2) was tagged at its endogenous locus with a C-terminal GFP. In these strains, the spindle-pole body (SPB)

component Spc42 was also tagged at its endogenous locus with C-terminal mCherry. Following their duplication in early S phase, SPBs display two distinctive behaviors that serve as useful indices of mitotic timing: first, at the beginning of mitosis, the two SPBs separate from each other and form a short spindle; and second, at anaphase onset, the two SPBs move quickly away from each other as the spindle begins to elongate, which coincides with separase activation and the onset of sister-chromatid separation (Figure 1B) (Pearson et al., 2001; Straight et al., 1997; Yaakov et al., 2012).

Using spinning-disk confocal microscopy with 30-sec time resolution, we analyzed these fluorescent markers in individual cells in unperturbed, asynchronously proliferating cultures (Figure 1B). We first measured the time from SPB separation to spindle elongation in single cells as an estimate of the time from mitotic entry to anaphase onset. This time was highly variable from cell to cell, ranging from 15 to 45 min, with a median of 21 min. Thus, following SPB separation, cells display remarkable variability in the timing of APC/C^{Cdc20} activation and anaphase onset. This timing and variability did not change significantly in any of the strains carrying GFP-tagged APC/C substrates (Figure 2A, one-way ANOVA *p*-value = 0.47), consistent with the fact that GFP tagging had no effect on the doubling times of all strains (data not shown). We also confirmed that fluorescence imaging had little impact on mitotic duration (Figure S1A; see Experimental Procedures for optimization of imaging conditions).

Next, in each single cell progressing through mitosis, we monitored the degradation of the GFP-labeled substrate relative to the two SPB events (Figures 1B, 2B). With this information, we could compare different cells by referencing to the same

SPB event, allowing us to compare cells with different GFP-tagged substrates, as well as cells from the same GFP-tagged strain (Figure 2C, D).

Our results revealed sequential degradation of APC/C substrates during mitosis. At 30°C, Clb5 degradation began an average of 10 min after SPB separation and was almost complete when the spindle started to elongate. Degradation of securin and Dbf4 began about 16 min after SPB separation and was less than half complete when the spindle started to elongate. A small fraction of Clb2 was degraded at the time of anaphase onset, but the majority was degraded later in anaphase (Figure 1B, 2B, C, D). The substrate ordering we observed is consistent with previous results from population measurements (Ferreira et al., 2000; Lianga et al., 2013). The two phases of Clb2 degradation we observed also support previous evidence that Clb2 degradation is initiated by APC/C^{Cdc20} and later completed by APC/C^{Cdh1} (Baumer et al., 2000; Wäsch and Cross, 2002; Yeong et al., 2000).

With single cell measurements, we were also able to observe variations in the population. When cells were synchronized *in silico* with SPB separation, degradation timing of the same substrate was highly variable in different cells, similar to the variability in mitotic timing (Figure 2C, top panel; see also Figure 3A, left panel). This accounts for the fact that the first phase of Clb2 degradation was obscured when we averaged the GFP traces over the population (Figure 2C as compared to Figure 2D, bottom panels). Thus, the timing of APC/C activation, and thus its substrate degradation, is not closely correlated to the timing of mitotic onset (SPB separation).

On the other hand, when cells were aligned with spindle elongation, substrate degradation timing was much less variable (Figure 2D, top panel; see also Figure 3A, right panel), consistent with the causal relationship between APC/C^{Cdc20} activation and anaphase onset. Compared to Clb5, the timing of securin degradation had a particularly strong correlation with spindle elongation, in agreement with the fact that securin degradation directly leads to sister-chromatid separation and spindle elongation. Interestingly, Dbf4 was not only degraded at the same time as securin, but its degradation timing also strongly correlated with spindle elongation (Figure 2D, top panel; see also Figure S3C), suggesting some link between the regulation of their degradation. The first phase of Clb2 degradation also occurred immediately before spindle elongation, similar to the timing of securin and Dbf4 degradation, consistent with it being APC/C^{Cdc20}-dependent (Figure 2D).

The Spindle Assembly Checkpoint Determines the Degradation Timing of Clb5 but not that of Securin

We next pursued the mechanisms underlying the sequential degradation of APC/C^{Cdc20} substrates. To quantify and compare the timing of substrate degradation in each cell, we determined the time point when 50% of the substrate was degraded, and calculated its timing relative to the reference SPB events (Figure S1B, C; Figure 3A, bottom panels; see also Experimental Procedures). Note that substrate degradation dynamics depend on two factors: the timing of degradation onset and the rate of degradation. Our quantification of the time of 50% degradation provides a combinatorial indication of both factors, and is also more robust than measuring the timing of

degradation onset given the noise in our GFP signals (Figure S1C, unsmoothed traces). In most cases, we also calculated the rate constant of degradation by fitting each single-cell GFP trace to a single exponential decay, and we present them here in terms of protein half-life (Figure 3A, insert; Figure S1D; see also Experimental Procedures).

In mammalian cells, the SAC is known to influence the timing of APC/C^{Cdc20} substrate degradation. To assess the contribution of the SAC in our system, we disabled the SAC by deleting *MAD2* (Figure 3A) or *MAD1* (Figure S2A), either of which is sufficient to abolish SAC activity (Li and Murray, 1991). To our surprise, disabling the SAC caused Clb5 degradation to occur several minutes earlier than in wild-type cells (Student's *t*-test, *p*-value < 0.001) but left securin degradation timing largely unchanged (Figure 3A and Figure S2A). These data suggest that the SAC normally inhibits Clb5 degradation, and that the timing of Clb5 degradation onset in the absence of the SAC likely indicates the time when APC/C^{Cdc20} becomes active, possibly as a result of APC/C phosphorylation by Cdk1 (Kraft et al., 2003; Rudner and Murray, 2000). In addition, the rate of Clb5 degradation in wild-type cells was very similar to that in *mad2Δ* cells, if not slightly faster (Figure 3A, insert). This suggests that in wild-type cells the SAC is removed abruptly and APC/C^{Cdc20} is fully activated before Clb5 degradation begins.

The yeast SAC is known to be dispensable for growth in normal conditions but becomes essential under spindle stress. One possibility is that the SAC is activated only in cells that need it, and therefore in normal growth conditions the SAC is activated only in a small subset of cells that experiences kinetochore attachment defects. If this were the case, then there would be a subpopulation of cells with delayed Clb5 degradation

due to SAC activation. Disabling the SAC would eliminate this subpopulation and reduce the variability in the timing of Clb5 degradation in the whole population. However, our observations were inconsistent with this possibility. Disabling the SAC led to earlier Clb5 degradation in the entire population without a decrease in variability (Figure 3A and Figure S2A), supporting the idea that in yeast cells, as in mammalian cells, the SAC operates in most cells as an integral feature of cell cycle control.

Securin degradation was largely unaffected by deletion of SAC components (Figure 3A), and the timing of anaphase onset was also unchanged (Figure S2B). These results are consistent with our evidence from Clb5 timing that the SAC is likely shut off and APC/C^{Cdc20} is activated several minutes before the onset of securin degradation.

Clb5 can be Degraded During an Active Spindle Assembly Checkpoint Arrest

Given that transient SAC activation in a normal cell cycle delays Clb5 degradation, we wondered whether a prolonged SAC activation would fully stabilize it. We thus plated cells on media containing the microtubule poison nocodazole, which prevents spindle formation and thereby produces a sustained SAC signal. We observed collapsed spindles immediately after nocodazole treatment, indicating an active SAC. Interestingly, we also observed that after 1-2 hours in the arrest, cells began to assemble a spindle and progress into anaphase, perhaps because nocodazole was inactivated under our experimental conditions. We thus used spindle reformation as a single-cell timing marker, before which the cells should have an active SAC and after which cells are recovering from the SAC arrest.

Consistent with previous observations made on a population level, an active SAC inhibited Clb5 degradation but did not fully stabilize the protein (Keyes et al., 2008). Clb5 was degraded slowly in a nearly linear fashion (Figure 3B, before spindle reformation), even though securin was fully stabilized and cells arrested without a spindle (Figure 3C, before spindle reformation). Disabling the SAC by deletion of *MAD2* allowed degradation of Clb5 and securin in nocodazole at a normal rate in the absence of a spindle (Figure 3D). When we shut off *CDC20* expression from a galactose-inducible promoter (Mumberg et al., 1994), Clb5 was fully stabilized in the presence or absence of nocodazole (Figure 3E) (Keyes et al., 2008), indicating that the slow degradation in nocodazole depended on APC/C^{Cdc20}. We suspect that this slow degradation of Clb5 also occurs in a normal cell cycle, during the brief time window after APC/C^{Cdc20} becomes active towards Clb5 and before the SAC is turned off. However, because this time window is so short, and Clb5 degradation during an active SAC is so slow, this partial Clb5 degradation is not noticeable in wild-type cells.

All nocodazole-treated cells eventually assembled a spindle and entered anaphase after 1-2 hours on the nocodazole plate, presumably because nocodazole was inactivated under our experimental conditions. The reassembly of spindles in these cells suggested that escape from the arrest was due to proper biorientation of sister chromatids, and thus inactivation of the SAC, rather than checkpoint adaptation (Vernieri et al., 2013). This fortuitous escape from the checkpoint allowed us to make interesting additional observations. Soon after reformation of the spindle, both Clb5 and securin underwent rapid degradation with a rate very similar to that in an unperturbed

cell cycle (Figure 3B, C, after spindle reformation), indicating abrupt activation of APC/C^{Cdc20} upon SAC inactivation, as observed in unperturbed wild-type cells.

Phosphorylation by Cdk1 Delays Securin and Dbf4 Degradation

To further address the mechanisms that determine the differences in the timing of Clb5 and securin degradation, we studied the influence of Cdk1-dependent phosphorylation on securin degradation. Phosphorylation near its KEN and D boxes (Thr27 and Ser71) was shown previously to inhibit securin ubiquitination by APC/C^{Cdc20} *in vitro*, but it was unclear how this phosphorylation influences the rate or timing of securin degradation *in vivo* (Holt et al., 2008). To determine the effects of this phosphorylation, we replaced the endogenous copy of the securin gene with a mutant encoding securin-2A (T27A, S71A). The securin-2A mutant was degraded 2 min earlier than the wild-type protein (Figure 4A, p-value < 0.001), revealing that phosphorylation normally delays securin degradation. Interestingly, a larger fraction of securin-2A was degraded at the onset of spindle elongation compared to wild-type securin (Figure 4B, p-value < 0.001). This delay between securin-2A degradation and spindle elongation compensated for the earlier degradation of securin-2A to result in only a small but reproducible decrease in the time between SPB separation and spindle elongation (Figure S3A). In addition, securin-2A was degraded at a slightly greater rate than the wild-type protein (Figure 4A, insert).

Similar results were obtained with Dbf4. We found that Cdk1 inhibited Dbf4 ubiquitination by the APC/C *in vitro*, and the effects of Cdk1 were reversed by the phosphatase Cdc14 (Figure 4C). Dbf4 has two putative D boxes starting at Arg10 and

Arg62. It was previously shown that mutating Arg62 and Leu65 to alanines stabilized Dbf4 *in vivo* (Ferreira et al., 2000), but we found that mutating Arg10 and Leu13 had a more dramatic inhibitory effect on the ubiquitination of the Dbf4 N-terminal fragment by the APC/C *in vitro* (Figure S3B). Furthermore, Dbf4 is phosphorylated by Cdk1 at Ser11 *in vivo* (Holt et al., 2009), prompting us to make a Dbf4-A mutant in which Ser11 is mutated to alanine. Like securin-2A, Dbf4-A was degraded slightly earlier than the wild-type protein (Figure 4D). Although the difference was small, it was consistent whether we synchronized cells to SPB separation (Figure 4D, p-value = 0.035) or to spindle elongation (Figure S3C, p-value < 0.001). Thus, Dbf4 and securin are governed by similar Cdk1-dependent regulatory mechanisms, perhaps explaining why they are degraded simultaneously and why Dbf4 degradation is strongly correlated with spindle elongation.

DNA damage is also thought to inhibit securin degradation through Chk1-dependent phosphorylation of securin (Agarwal et al., 2003; Wang et al., 2001). We deleted *CHK1* in the securin-2A strain and did not observe any further change in the timing of securin-2A degradation (Figure S3D), suggesting that this branch of the DNA damage response does not have a significant impact on mitotic timing in an unperturbed cell cycle.

Cks1 Binding Promotes Early Degradation of Clb5

Our results indicate that securin phosphorylation accounts for only a part of the difference in the timing of Clb5 and securin degradation. We therefore considered the possibility that there is some feature of Clb5 that promotes its early degradation,

perhaps by making it a better APC/C^{Cdc20} substrate. First, we replaced the N-terminal 95 residues of Clb5 with the N-terminal 110 residues of securin-2A. These N-terminal regions contain all of the known APC/C^{Cdc20} binding motifs. This Clb5 chimera was degraded only slightly later than wild-type Clb5 (Figure S4A). We therefore hypothesized that early Clb5 degradation depends primarily on features within the C-terminal region of Clb5, starting from residue 96.

The Clb5 C-terminal region contains the globular domain that binds and activates Cdk1 (Jeffrey et al., 1995). Interestingly, the early SAC-resistant degradation of mammalian cyclin A depends in part on its binding to the Cdk1-Cks1 complex (Wolthuis et al., 2008). Yeast APC/C^{Cdc20} can bind directly to Cks1, and this interaction promotes APC/C^{Cdc20} phosphorylation by Cdk1 (Rudner and Murray, 2000). These results motivated us to test the contribution of Cdk1 and Cks1 to Clb5 degradation. Given their essential functions in cell-cycle progression, we reasoned that any perturbation in Cdk1 or Cks1 would be likely to have ubiquitous effects on multiple cell-cycle processes, in which case it would be difficult to pinpoint the direct role of these proteins in Clb5 degradation. Instead, we analyzed the degradation of a Clb5 mutant that cannot bind Cdk1. Based on structural homology and conservation in the cyclin family (see Experimental Procedures and Figure S4B), we identified four hydrophobic residues (Ile166, Phe169, Phe254, Phe291) at the predicted Clb5-Cdk1 interface (Figure S4C) and mutated a combination of them to aspartate or arginine. We then assessed their interaction with Cdk1 *in vivo*. Ectopic expression of a stabilized Clb5 protein lacking its N-terminal region (Clb5-ΔN, with residues 2-95 deleted) under control of the *CLB5*

promoter is known to be lethal due to excess Clb5-Cdk1 activity (Sullivan et al., 2008). If our mutations disrupted Clb5-Cdk1 binding, then introduction of these mutants into Clb5-ΔN should prevent its dominant lethal effects. Indeed, when these mutants were expressed under the control of the *CLB5* promoter (582 bp upstream of the *CLB5* ORF) in an integration plasmid, we observed improved growth as we increased the number of mutations in Clb5-ΔN (Figure S4D), even though all mutants had a similar expression level in the cell (Figure S4E). When we combined three mutations (F169D, F254D, F291D; henceforth the Clb5-3D mutant), the cells grew with a doubling time (85.4+/-0.2 min) very similar to that of wild-type cells (84.1+/-0.5 min); adding a fourth mutation (I166D, F169A, F254D, F291D) did not further improve growth (85.6+/-0.1 min). We therefore used the mutant Clb5-3D for the following experiments.

We expressed either full-length Clb5-GFP or full-length Clb5-3D-GFP under the control of the *CLB5* promoter, using an integration plasmid. Both strains retained the endogenous copy of *CLB5* to maintain a normal cell cycle. We found that Clb5-3D displayed two phases of degradation: a slow phase and a fast phase (Figure 5A). The slow phase displayed a nearly linear rate and was not dependent on Cdc20 (Figure 5B), and so it likely reflected non-specific degradation of Clb5-3D due to destabilizing effects of the mutations. The fast phase, however, disappeared if we shut off Cdc20 expression and thus reflected APC/C^{Cdc20}-dependent degradation (Figure 5B). This fast phase of Clb5-3D degradation was significantly delayed relative to the degradation of wild-type Clb5 (Figure 5A, *p*-value < 0.001), suggesting that Cdk1 binding contributes to early Clb5 degradation.

These results are consistent with a role for Cdk1 binding in Clb5 degradation, and this is most likely mediated through Cks1, which binds to both Cdk1 and APC/C (Patra and Dunphy, 1998; Rudner and Murray, 2000; Shteinberg and Hershko, 1999; Wolthuis et al., 2008). To directly test the role of Cks1, we fused Cks1-GFP to the C-terminus of securin-2A and compared degradation of the fusion protein with that of securin-2A-GFP. In both cases, the endogenous copy of securin was replaced to ensure that the cells have only one securin variant, the degradation of which would drive sister-chromatid separation. Securin-2A-Cks1 was degraded significantly earlier than securin-2A (Figure 5C, p-value < 0.001) and at a slightly faster rate. Interestingly, as in our earlier observations with securin-2A, more securin-2A-Cks1 was degraded than securin-2A when spindle elongation occurred (Figure 5C, D, p-value < 0.001), suggesting that securin degradation is not the sole determinant of anaphase onset.

However, Cdk1-Cks1 binding did not fully explain early Clb5 degradation relative to securin-2A: Clb5-3D was still degraded earlier than securin-2A (Figure 5A, p-value < 0.005), and securin-2A-Cks1 was degraded later than Clb5 (Figure 5C, p-value < 0.001). We suspected that additional mechanisms exist to promote early degradation of Clb5.

The Cdc20-binding 'A Motif' Contributes to Clb5 Degradation in the Presence or Absence of an Activated SAC

Recent studies suggest that a short sequence motif exists in cyclin A that facilitates its degradation in the presence of the SAC (Di Fiore, Davey, and Pines, manuscript in preparation). This motif resembles the 'A motif' that was first identified in

the yeast protein Acm1 and interacts with an interblade groove in the WD40 domain of Cdh1 (Burton et al., 2011; Enquist-Newman et al., 2008; He et al., 2013). We tested the possibility that a similar motif also exists in Clb5 and might help promote early Clb5 degradation. We performed a motif search in Clb5 homologs from closely-related yeast species of the *Saccharomyces* clan (Davey et al., 2012), and we were able to identify a putative A motif at residues 99-105 in Clb5, within a highly conserved region (Figure 6A).

To test the function of the putative A motif in Clb5, we replaced the key residues Ile102 and Tyr103 with alanines to generate the Clb5-2A mutant. Clb5-2A was degraded significantly later than Clb5 (Figure 6B, p-value < 0.001), but at a very similar rate (Figure 6B insert). We also analyzed a Clb5 mutant (Clb5-2A3D) in which both Cdk1 binding and the A motif were disrupted. The rapid phase of degradation of this mutant now occurred slightly later than the degradation of securin-2A (Figure 6C).

The A motifs in Clb5 homologs differ from the A motifs in Acm1 and cyclin A by having conserved basic residues upstream of the core Ile102 and Tyr103 (Figure 6A). We wondered whether this was accompanied by differences in the A motif binding site on Cdc20. Based on homology modeling of the Acm1-Cdh1 structure (He et al., 2013), we identified residues on Cdc20 that potentially interact with the A motif, and we compared them to those on Cdh1. One striking difference was a cluster of acidic residues (Asp311, Asp312, Asp313) in Cdc20 that are absent in Cdh1 (Figure 6D). If these residues are important for binding to the basic residues in the Clb5 A motif, then replacing the endogenous *CDC20* with a *CDC20-GAG* (D311G, D312A, D313G) mutant

should delay wild-type Clb5 degradation but have little impact on Clb5-2A degradation. Indeed, this is what we observed (Figure 6D, p-value < 0.001 and p-value = 0.8775, respectively). We therefore conclude that the early degradation of Clb5 arises mostly, if not entirely, through binding to Cdk1-Cks1 and through the A motif, both of which provide additional binding sites for APC/C^{Cdc20}.

We also tested the effect of A motif disruption on Clb5 degradation in nocodazole. Compared to wild-type Clb5, the Clb5-2A mutant was still degraded in a linear fashion but at a significantly slower rate (Figure 6E). Thus, the A motif also contributes to Clb5 degradation in an active SAC.

Discussion

Our results, together with those from previous single-cell studies, provide a detailed temporal picture of how yeast cells progress towards the metaphase-anaphase transition (Figure 7). The process begins with inactivation of the SAC, which inhibits APC/C^{Cdc20} activity until all sister-chromatids are properly attached to the spindle. Activated APC/C^{Cdc20} first degrades the S cyclin Clb5 with an average half-life of 3.4 min. About 6 min later, securin is degraded with an average half-life of 4.7 min. Soon after securin degradation begins, separase is abruptly activated, and only 1 min is required for separase to cleave enough cohesin to promote sister-chromatid separation (Yaakov et al., 2012). By the time of sister-chromatid separation, Clb5 is fully degraded but more than half of securin remains.

The SAC is not essential for the viability of yeast cells under normal growth conditions (Hoyt et al., 1991; Li and Murray, 1991), and thus it has not been clear what

role, if any, the SAC plays in the normal timing of yeast mitotic regulatory events. Our experiments now reveal that the SAC is activated in most yeast cells as an integral part of progression through mitosis. Compared to the SAC in mammalian cells, however, the yeast checkpoint appears to be inactivated relatively early in mitosis and determines the timing of S cyclin degradation and not that of securin. Our results are consistent with the observation that, in yeast, bi-orientation of sister-chromatids on the spindle begins immediately after spindle assembly and is possibly complete many minutes before anaphase onset (Goshima and Yanagida, 2000; He et al., 2000; Pearson et al., 2001; Tanaka et al., 2000). Thus, the nonessential nature of the SAC may be due, at least in part, to the waiting period between the proper attachment of sister-chromatids (and SAC inactivation) and their separation. Even without the surveillance provided by the SAC, the sister-chromatid pairs would normally achieve proper attachment to the spindle minutes before securin degradation triggers their separation.

With the SAC turned off or disabled, we found that the ordered degradation of Clb5, securin, and Dbf4 is established primarily through differences in their interaction with APC/C^{Cdc20}. Cdk1-dependent phosphorylation near KEN and D boxes in securin and Dbf4 can delay their degradation, and this similarity in regulation results in almost simultaneous degradation of these substrates. We also found that the early degradation of Clb5 depends on two factors that provide additional binding sites for APC/C^{Cdc20}: the interaction of Clb5 with the Cdk1-Cks1 complex and the presence of the A motif in the Clb5 N-terminal region. These post-translational modifications and multiple binding sites are likely to have a significant impact on binding affinity for APC/C^{Cdc20}, and might also

contribute to the proper positioning of substrates for efficient ubiquitin transfer. Our studies illustrate how APC/C^{Cdc20} can discriminate among its substrates and achieve robust ordering of their degradation.

A major difference between mammalian and yeast cells is that cyclin A is thought to be degraded in the presence of an active SAC and needs to compete with SAC proteins for APC/C^{Cdc20} binding (den Elzen and Pines, 2001; Geley et al., 2001), whereas Clb5 degradation appears to occur just after the SAC is normally turned off. Interestingly, despite these very different circumstances, the same two mechanisms—Cks1 and the A motif—allow cyclin A and Clb5 to be degraded earlier than other substrates (Wolthuis et al., 2008) (Di Fiore, Davey, and Pines, manuscript in preparation). It was shown recently that the degradation of cyclin A and securin or cyclin B seems to remain sequential in mammalian cells without a functional SAC (Collin et al., 2013). We suspect that in this scenario, the same mechanisms promote cyclin A degradation earlier than that of other substrates.

We found that Clb5, like cyclin A, is degraded in cells with an active SAC, but the rate of degradation was much slower than that in the absence of the SAC (Keyes et al., 2008). This slow degradation depends on Cdc20 and on the A motif, suggesting that this motif is capable of driving some interaction with APC^{Cdc20} even in the presence of an active SAC. We also suspect that Clb5 degradation in the presence of the SAC depends on Cdk1-Cks1 binding, but we could not test this possibility due to the intrinsic instability of our Clb5-3D mutant.

Securin degradation leads to sister-chromatid separation, but the timing of sister separation also seems to depend on other factors. Among the different variants of securin we tested, including the wild-type protein, securin-2A and securin-2A-Cks1, earlier degradation correlated with an increase in the amount of securin that was degraded before anaphase onset. This suggests another branch of regulation in the timing of sister-chromatid separation. Indeed, the cohesin subunit Scc1 is phosphorylated by Polo kinase, which increases the rate of cleavage by separase by several fold (Alexandru et al., 2001; Yaakov et al., 2012). One can imagine that when securin is degraded early, and separase is released early, Scc1 is not yet fully phosphorylated and cohesin cleavage will take longer to complete. Consistent with this idea, Scc1 is indeed cleaved more slowly in securin-2A cells than in wild-type cells (Yaakov et al., 2012).

Our results suggest that there is a 9 min delay between the completion of sister-chromatid biorientation (SAC satisfaction) and the initiation of sister-chromatid separation via securin degradation. Does this time delay serve a purpose? One possibility is that the delay allows time for complete Clb5 degradation before anaphase begins. Clb5-Cdk1 phosphorylates numerous specific substrates that have functions in anaphase (Loog and Morgan, 2005), and these functions are inhibited by Cdk1-dependent phosphorylation. These substrates includes the spindle stabilizer Fin1 (Woodbury and Morgan, 2007), the spindle midzone organizer Ase1 (Juang et al., 1997; Khmelinskii et al., 2009), the SPB component Spc110 (Kilmartin et al., 1993; Liang et al., 2013), the late mitotic APC/C activator Cdh1 (Jaspersen et al., 1999; Visintin et al.,

1997), and the kinetochore component Cnn1 (Bock et al., 2012; Schleiffer et al., 2012). Several of these proteins are dephosphorylated by Cdc14 (Jaspersen et al., 1999; Khmelinskii et al., 2009; Woodbury and Morgan, 2007). The early degradation of Clb5, which is completed by the onset of anaphase and coincides with activation of Cdc14, may allow earlier and more abrupt activation of these Clb5 substrates and lead to a more efficient and coherent anaphase. Indeed, removing securin phosphorylation, which disturbs the coordination between Clb5 degradation and anaphase onset, was shown to impede spindle elongation and increase chromosome loss (Holt et al., 2008). Stabilized Clb5 has also been shown to slow down spindle elongation (Liang et al., 2013) and delay rDNA segregation (Sullivan et al., 2008). There is also recent evidence in mammalian cells that cyclin A destruction before anaphase is important for the stabilization of kinetochore-microtubule attachments (Kabeche and Compton, 2013). Thus, differences in the relative timing of cyclin and securin degradation are likely to make important contributions to the overall orchestration of mitosis.

References

Agarwal, R., Tang, Z., Yu, H., and Cohen-Fix, O. (2003). Two distinct pathways for inhibiting pds1 ubiquitination in response to DNA damage. J Biol Chem *278*, 45027-45033.

Alexandru, G., Uhlmann, F., Mechtler, K., Poupart, M.A., and Nasmyth, K. (2001). Phosphorylation of the cohesin subunit Scc1 by Polo/Cdc5 kinase regulates sister chromatid separation in yeast. Cell *105*, 459-472.

Barford, D. (2011). Structure, function and mechanism of the anaphase promoting complex (APC/C). Quarterly reviews of biophysics *44*, 153-190.

Baudin, A., Ozier-Kalogeropoulos, O., Denouel, A., Lacroute, F., and Cullin, C. (1993). A simple and efficient method for direct gene deletion in Saccharomyces cerevisiae. Nucleic Acids Res *21*, 3329-3330.

Baumer, M., Braus, G.H., and Irniger, S. (2000). Two different modes of cyclin clb2 proteolysis during mitosis in Saccharomyces cerevisiae. FEBS letters *468*, 142-148.

Bell, S.P., and Dutta, A. (2002). DNA replication in eukaryotic cells. Annu Rev Biochem *71*, 333-374.

Bock, L.J., Pagliuca, C., Kobayashi, N., Grove, R.A., Oku, Y., Shrestha, K., Alfieri, C., Golfieri, C., Oldani, A., Dal Maschio, M.*, et al.* (2012). Cnn1 inhibits the interactions between the KMN complexes of the yeast kinetochore. Nat Cell Biol *14*, 614-624.

Brizuela, L., Draetta, G., and Beach, D. (1987). $p13^{suc1}$ acts in the fission yeast cell division cycle as a component of the $p34^{cdc2}$ protein kinase. EMBO J. *6*, 3507-3514.

Brown, N.R., Lowe, E.D., Petri, E., Skamnaki, V., Antrobus, R., and Johnson, L.N. (2007). Cyclin B and cyclin A confer different substrate recognition properties on CDK2. Cell Cycle *6*, 1350-1359.

Burton, J.L., Xiong, Y., and Solomon, M.J. (2011). Mechanisms of pseudosubstrate inhibition of the anaphase promoting complex by Acm1. EMBO J *30*, 1818-1829.

Collin, P., Nashchekina, O., Walker, R., and Pines, J. (2013). The spindle assembly checkpoint works like a rheostat rather than a toggle switch. Nat Cell Biol *15*, 1378-1385.

Davey, N.E., Cowan, J.L., Shields, D.C., Gibson, T.J., Coldwell, M.J., and Edwards, R.J. (2012). SLiMPrints: conservation-based discovery of functional motif fingerprints in intrinsically disordered protein regions. Nucleic Acids Res *40*, 10628-10641.

den Elzen, N., and Pines, J. (2001). Cyclin A is destroyed in prometaphase and can delay chromosome alignment and anaphase. J Cell Biol *153*, 121-136.

Dick, A.E., and Gerlich, D.W. (2013). Kinetic framework of spindle assembly checkpoint signalling. Nat Cell Biol *15*, 1370-1377.

Enquist-Newman, M., Sullivan, M., and Morgan, D.O. (2008). Modulation of the mitotic regulatory network by APC-dependent destruction of the Cdh1 inhibitor Acm1. Mol Cell *30*, 437-446.

Ferreira, M.F., Santocanale, C., Drury, L.S., and Diffley, J.F. (2000). Dbf4p, an essential S phase-promoting factor, is targeted for degradation by the anaphase-promoting complex. Mol Cell Biol *20*, 242-248.

Foster, S.A., and Morgan, D.O. (2012). The APC/C subunit Mnd2/Apc15 promotes Cdc20 autoubiquitination and spindle assembly checkpoint inactivation. Mol Cell *47*, 921-932.

Fukuhara, N., and Kawabata, T. (2008). HOMCOS: a server to predict interacting protein pairs and interacting sites by homology modeling of complex structures. Nucleic Acids Res *36*, W185-189.

Geley, S., Kramer, E., Gieffers, C., Gannon, J., Peters, J.M., and Hunt, T. (2001). Anaphase-promoting complex/cyclosome-dependent proteolysis of human cyclin A starts at the beginning of mitosis and is not subject to the spindle assembly checkpoint. J Cell Biol *153*, 137-148.

Glotzer, M., Murray, A.W., and Kirschner, M.W. (1991). Cyclin is degraded by the ubiquitin pathway. Nature *349*, 132-138.

Goldstein, A.L., and McCusker, J.H. (1999). Three new dominant drug resistance cassettes for gene disruption in Saccharomyces cerevisiae. Yeast *15*, 1541-1553.

Goshima, G., and Yanagida, M. (2000). Establishing biorientation occurs with precocious separation of the sister kinetochores, but not the arms, in the early spindle of budding yeast. Cell *100*, 619-633.

Hadwiger, J.A., Wittenberg, C., Mendenhall, M.D., and Reed, S.I. (1989). The Saccharomyces cerevisiae CKS1 gene, a homolog of the Schizosaccharomyces pombe suc1+ gene, encodes a subunit of the Cdc28 protein kinase complex. Mol Cell Biol *9*, 2034-2041.

Hagting, A., Den Elzen, N., Vodermaier, H.C., Waizenegger, I.C., Peters, J.M., and Pines, J. (2002). Human securin proteolysis is controlled by the spindle checkpoint and reveals when the APC/C switches from activation by Cdc20 to Cdh1. J Cell Biol *157*, 1125-1137.

Hames, R.S., Wattam, S.L., Yamano, H., Bacchieri, R., and Fry, A.M. (2001). APC/C-mediated destruction of the centrosomal kinase Nek2A occurs in early mitosis and depends upon a cyclin A-type D-box. EMBO J *20*, 7117-7127.

Hayes, M.J., Kimata, Y., Wattam, S.L., Lindon, C., Mao, G., Yamano, H., and Fry, A.M. (2006). Early mitotic degradation of Nek2A depends on Cdc20-independent interaction with the APC/C. Nat Cell Biol *8*, 607-614.

He, J., Chao, W.C.H., Zhang, Z., Yang, J., Cronin, N., and Barford, D. (2013). Insights into degron recognition by APC/C coactivators from the structure of an Acm1-Cdh1 complex. Mol. Cell *50*, 649-660.

He, X., Asthana, S., and Sorger, P.K. (2000). Transient sister chromatid separation and elastic deformation of chromosomes during mitosis in budding yeast. Cell *101*, 763-775.

Holt, L.J., Krutchinsky, A.N., and Morgan, D.O. (2008). Positive feedback sharpens the anaphase switch. Nature *454*, 353-357.

Holt, L.J., Tuch, B.B., Villen, J., Johnson, A.D., Gygi, S.P., and Morgan, D.O. (2009). Global analysis of Cdk1 substrate phosphorylation sites provides insights into evolution. Science *325*, 1682-1686.

Honda, R., Lowe, E.D., Dubinina, E., Skamnaki, V., Cook, A., Brown, N.R., and Johnson, L.N. (2005). The structure of cyclin E1/CDK2: implications for CDK2 activation and CDK2-independent roles. EMBO J *24*, 452-463.

Hoyt, M.A., Totis, L., and Roberts, B.T. (1991). S. cerevisiae genes required for cell cycle arrest in response to microtubule function. Cell *66*, 507-517.

Hunter, J.D. (2007). Matplotlib: A 2D graphics environment. Comput Sci Eng *9*, 90-95.

Jansen, G., Wu, C., Schade, B., Thomas, D.Y., and Whiteway, M. (2005). Drag&Drop cloning in yeast. Gene *344*, 43-51.

Jaspersen, S.L., Charles, J.F., and Morgan, D.O. (1999). Inhibitory phosphorylation of the APC regulator Hct1 is controlled by the kinase Cdc28 and the phosphatase Cdc14. Curr. Biol. *9*, 227-236.

Jeffrey, P.D., Russo, A.A., Polyak, K., Gibbs, E., Hurwitz, J., Massague, J., and Pavletich, N.P. (1995). Mechanism of CDK activation revealed by the structure of a cyclin A-CDK2 complex. Nature *376*, 313-320.

Juang, Y.-L., Huang, J., Peters, J.-M., McLaughlin, M.E., Tai, C.-Y., and Pellman, D. (1997). APC-mediated proteolysis of Ase1 and the morphogenesis of the mitotic spindle. Science *275*, 1311-1314.

Kabeche, L., and Compton, D.A. (2013). Cyclin A regulates kinetochore microtubules to promote faithful chromosome segregation. Nature *502*, 110-113.

Keyes, B.E., Yellman, C.M., and Burke, D.J. (2008). Differential regulation of anaphase promoting complex/cyclosome substrates by the spindle assembly checkpoint in Saccharomyces cerevisiae. Genetics *178*, 589-591.

Khmelinskii, A., Roostalu, J., Roque, H., Antony, C., and Schiebel, E. (2009). Phosphorylation-dependent protein interactions at the spindle midzone mediate cell cycle regulation of spindle elongation. Dev Cell *17*, 244-256.

Kilmartin, J.V., Dyos, S.L., Kershaw, D., and Finch, J.T. (1993). A spacer protein in the Saccharomyces cerevisiae spindle poly body whose transcript is cell cycle-regulated. J Cell Biol *123*, 1175-1184.

Koivomagi, M., Ord, M., Iofik, A., Valk, E., Venta, R., Faustova, I., Kivi, R., Balog, E.R., Rubin, S.M., and Loog, M. (2013). Multisite phosphorylation networks as signal processors for Cdk1. Nat Struct Mol Biol.

Kraft, C., Herzog, F., Gieffers, C., Mechtler, K., Hagting, A., Pines, J., and Peters, J.M. (2003). Mitotic regulation of the human anaphase-promoting complex by phosphorylation. EMBO J *22*, 6598-6609.

Lara-Gonzalez, P., Westhorpe, F.G., and Taylor, S.S. (2012). The spindle assembly checkpoint. Curr Biol *22*, R966-980.

Li, R., and Murray, A.W. (1991). Feedback control of mitosis in budding yeast. Cell *66*, 519-531.

Liang, F., Richmond, D., and Wang, Y. (2013). Coordination of chromatid separation and spindle elongation by antagonistic activities of mitotic and S-phase CDKs. PLoS Genet *9*, e1003319.

Lianga, N., Williams, E.C., Kennedy, E.K., Dore, C., Pilon, S., Girard, S.L., Deneault, J.S., and Rudner, A.D. (2013). A Wee1 checkpoint inhibits anaphase onset. J Cell Biol *201*, 843-862.

Longtine, M.S., McKenzie, A., Demarini, D.J., Shah, N.G., Wach, A., Brachat, A., Philippsen, P., and Pringle, J.R. (1998). Additional modules for versatile and economical PCR-based gene deletion and modification in *Saccharomyces cerevisiae*. Yeast *14*, 953-961.

Loog, M., and Morgan, D.O. (2005). Cyclin specificity in the phosphorylation of cyclin-dependent kinase substrates. Nature *434*, 104-108.

McGrath, D.A., Balog, E.R., Koivomagi, M., Lucena, R., Mai, M.V., Hirschi, A., Kellogg, D.R., Loog, M., and Rubin, S.M. (2013). Cks confers specificity to phosphorylation-dependent CDK signaling pathways. Nat Struct Mol Biol.

Meraldi, P., Draviam, V.M., and Sorger, P.K. (2004). Timing and checkpoints in the regulation of mitotic progression. Dev Cell *7*, 45-60.

Michel, L., Diaz-Rodriguez, E., Narayan, G., Hernando, E., Murty, V.V., and Benezra, R. (2004). Complete loss of the tumor suppressor MAD2 causes premature cyclin B degradation and mitotic failure in human somatic cells. Proc Natl Acad Sci U S A *101*, 4459-4464.

Michel, L.S., Liberal, V., Chatterjee, A., Kirchwegger, R., Pasche, B., Gerald, W., Dobles, M., Sorger, P.K., Murty, V.V., and Benezra, R. (2001). MAD2 haplo-insufficiency causes premature anaphase and chromosome instability in mammalian cells. Nature *409*, 355-359.

Morgan, D.O. (2007). The Cell Cycle: Principles of Control (London: New Science Press).

Mumberg, D., Muller, R., and Funk, M. (1994). Regulatable promoters of Saccharomyces cerevisiae: comparison of transcriptional activity and their use for heterologous expression. Nucleic Acids Res *22*, 5767-5768.

Musacchio, A., and Salmon, E.D. (2007). The spindle-assembly checkpoint in space and time. Nat Rev Mol Cell Biol *8*, 379-393.

Nasmyth, K., and Haering, C.H. (2009). Cohesin: its roles and mechanisms. Annu Rev Genet *43*, 525-558.

Oliphant, T.E. (2007). Python for scientific computing. Comput Sci Eng *9*, 10-20.

Oshiro, G., Owens, J.C., Shellman, Y., Sclafani, R.A., and Li, J.J. (1999). Cell cycle control of Cdc7p kinase activity through regulation of Dbf4p stability. Mol Cell Biol *19*, 4888-4896.

Patra, D., and Dunphy, W.G. (1998). Xe-p9, a Xenopus Suc1/Cks protein, is essential for the Cdc2-dependent phosphorylation of the anaphase-promoting complex at mitosis. Genes Dev. *12*, 2549-2559.

Pearson, C.G., Maddox, P.S., Salmon, E.D., and Bloom, K. (2001). Budding yeast chromosome structure and dynamics during mitosis. J Cell Biol *152*, 1255-1266.

Peters, J.M. (2006). The anaphase promoting complex/cyclosome: a machine designed to destroy. Nat Rev Mol Cell Biol *7*, 644-656.

Pfleger, C.M., and Kirschner, M.W. (2000). The KEN box: an APC recognition signal distinct from the D box targeted by Cdh1. Genes Dev *14*, 655-665.

Pines, J. (2006). Mitosis: a matter of getting rid of the right protein at the right time. Trends Cell Biol *16*, 55-63.

Pines, J. (2011). Cubism and the cell cycle: the many faces of the APC/C. Nat Rev Mol Cell Biol *12*, 427-438.

Primorac, I., and Musacchio, A. (2013). Panta rhei: The APC/C at steady state. J Cell Biol *201*, 177-189.

Queralt, E., Lehane, C., Novak, B., and Uhlmann, F. (2006). Downregulation of PP2A(Cdc55) phosphatase by separase initiates mitotic exit in budding yeast. Cell *125*, 719-732.

Queralt, E., and Uhlmann, F. (2008). Cdk-counteracting phosphatases unlock mitotic exit. Curr Opin Cell Biol *20*, 661-668.

Richardson, H.E., Stueland, C.S., Thomas, J., Russell, P., and Reed, S.I. (1990). Human cDNAs encoding homologs of the small $p34^{Cdc28/Cdc2}$-associated protein of Saccharomyces cerevisiae and Schizosaccharomyces pombe. Genes Dev. *4*, 1332-1344.

Rudner, A.D., and Murray, A.W. (2000). Phosphorylation by Cdc28 activates the Cdc20-dependent activity of the anaphase-promoting complex. J. Cell Biol. *149*, 1377-1390.

Russo, A.A., Jeffrey, P.D., and Pavletich, N.P. (1996). Structural basis of cyclin-dependent kinase activation by phosphorylation. Nature Struct. Biol. *3*, 696-700.

Schleiffer, A., Maier, M., Litos, G., Lampert, F., Hornung, P., Mechtler, K., and Westermann, S. (2012). CENP-T proteins are conserved centromere receptors of the Ndc80 complex. Nat Cell Biol *14*, 604-613.

Schneider, C.A., Rasband, W.S., and Eliceiri, K.W. (2012). NIH Image to ImageJ: 25 years of image analysis. Nat Methods *9*, 671-675.

Sedgwick, G.G., Hayward, D.G., Di Fiore, B., Pardo, M., Yu, L., Pines, J., and Nilsson, J. (2013). Mechanisms controlling the temporal degradation of Nek2A and Kif18A by the APC/C-Cdc20 complex. EMBO J *32*, 303-314.

Shteinberg, M., and Hershko, A. (1999). Role of Suc1 in the activation of the cyclosome by protein kinase Cdk1/cyclin B. Biochem Biophys Res Commun *257*, 12-18.

Sikorski, R.S., and Hieter, P. (1989). A system of shuttle vectors and yeast host strains designed for efficient manipulation of DNA in *Saccharomyces cerevisiae*. Genetics *122*, 19-27.

Stegmeier, F., and Amon, A. (2004). Closing mitosis: the functions of the Cdc14 phosphatase and its regulation. Annu Rev Genet *38*, 203-232.

Straight, A.F., Marshall, W.F., Sedat, J.W., and Murray, A.W. (1997). Mitosis in living budding yeast: anaphase A but no metaphase plate. Science *277*, 574-578.

Sullivan, M., Holt, L., and Morgan, D.O. (2008). Cyclin-specific control of ribosomal DNA segregation. Mol Cell Biol *28*, 5328-5336.

Sullivan, M., and Morgan, D.O. (2007). Finishing mitosis, one step at a time. Nat Rev Mol Cell Biol *8*, 894-903.

Tanaka, T., Fuchs, J., Loidl, J., and Nasmyth, K. (2000). Cohesin ensures bipolar attachment of microtubules to sister centromeres and resists their precocious separation. Nat Cell Biol *2*, 492-499.

Tang, Y., and Reed, S.I. (1993). The Cdk-associated protein Cks1 functions both in G_1 and G_2 in Saccharomyces cerevisiae. Genes Dev. *7*, 822-832.

Vernieri, C., Chiroli, E., Francia, V., Gross, F., and Ciliberto, A. (2013). Adaptation to the spindle checkpoint is regulated by the interplay between Cdc28/Clbs and PP2ACdc55. J Cell Biol *202*, 765-778.

Visintin, R., Prinz, S., and Amon, A. (1997). CDC20 and CDH1: a family of substrate-specific activators of APC-dependent proteolysis. Science *278*, 460-463.

Wang, H., Liu, D., Wang, Y., Qin, J., and Elledge, S.J. (2001). Pds1 phosphorylation in response to DNA damage is essential for its DNA damage checkpoint function. Genes Dev *15*, 1361-1372.

Wäsch, R., and Cross, F. (2002). APC-dependent proteolysis of the mitotic cyclin Clb2 is essential for mitotic exit. Nature *418*, 556-562.

Wolthuis, R., Clay-Farrace, L., van Zon, W., Yekezare, M., Koop, L., Ogink, J., Medema, R., and Pines, J. (2008). Cdc20 and Cks direct the spindle checkpoint-independent destruction of cyclin A. Mol Cell *30*, 290-302.

Woodbury, E.L., and Morgan, D.O. (2007). Cdk and APC activities limit the spindle-stabilizing function of Fin1 to anaphase. Nat Cell Biol *9*, 106-112.

Yaakov, G., Thorn, K., and Morgan, D.O. (2012). Separase biosensor reveals that cohesin cleavage timing depends on phosphatase PP2A(Cdc55) regulation. Dev Cell *23*, 124-136.

Yang, X., Lau, K.Y., Sevim, V., and Tang, C. (2013). Design principles of the yeast g1/s switch. PLoS Biol *11*, e1001673.

Yeong, F.M., Lim, H.H., Padmashree, C.G., and Surana, U. (2000). Exit from mitosis in budding yeast: biphasic inactivation of the Cdc28-Clb2 mitotic kinase and the role of Cdc20. Mol Cell *5*, 501-511.

Acknowledgements

We thank Hana El-Samad, Jaline Gerardin, Wendell A. Lim, Xili Liu, Geoff C. Rollins, Jacob Stewart-Ornstein, Orion D. Weiner, Xiaojing Yang, and members of Morgan and Tang labs for inspiring discussions and comments on the manuscript; Kurt Thorn, Alice Thwin and DeLaine Larsen at the UCSF Nikon Imaging Center for their critical help with microscopy; and Heather Eshleman, Matilde Galli, and Arda Mizrak for reagents. This work was supported by a fellowship (to D.L.) from the UC Cancer

Research Coordinating Committee (CRCC) and by funding from the National Institute of General Medical Sciences (R01-GM097115 to C.T. and R37-GM053270 to D.O.M.).

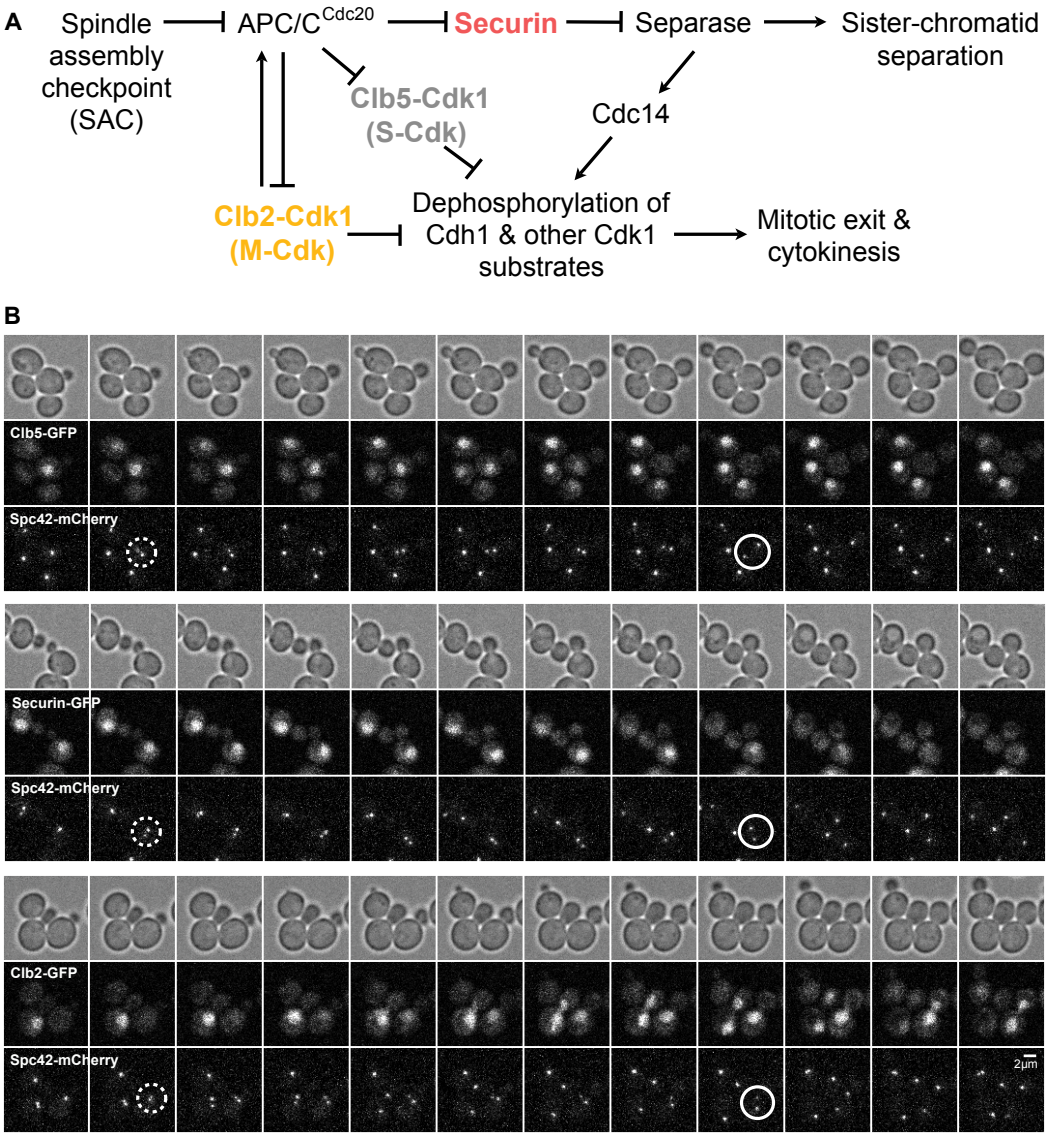

Figure 1. Metaphase-anaphase transition in cells carrying GFP-tagged APC/C substrates

(A) Network diagram of the metaphase-anaphase transition in budding yeast.

(B) GFP-tagged APC/CCdc20 substrates and mCherry-tagged SPBs in cycling cells, at 3-min intervals. Dashed circles indicate cells at the onset of SPB separation, and solid circles mark cells at the onset of spindle elongation.

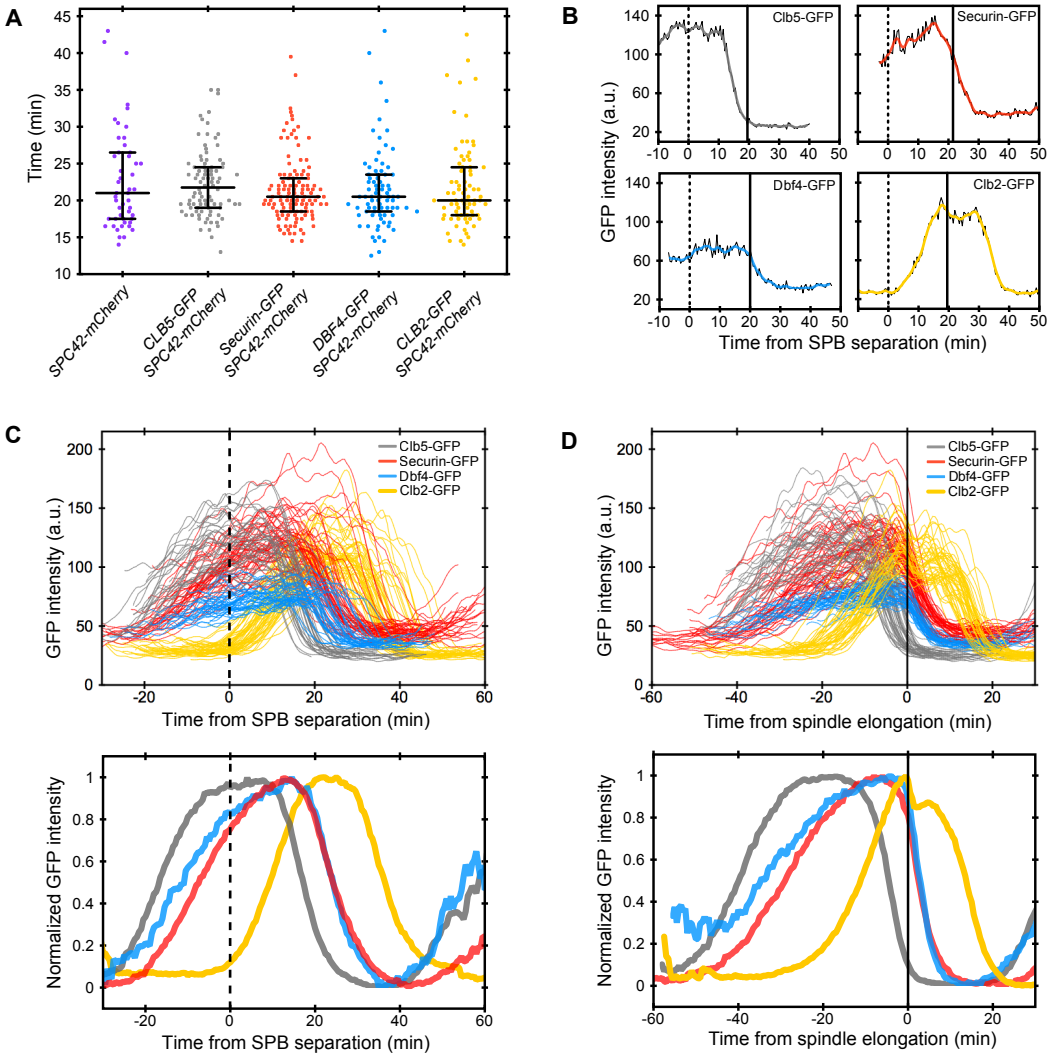

Figure 2. Timing and dynamics of APC/CCdc20 substrate degradation
(A) Time from SPB separation to spindle elongation in individual cells with GFP tags on APC/C substrates. Each dot represents a single cell. Starting from left, sample sizes are: n = 49, 90, 121, 82, 77 cells. For each strain, the middle bar indicates the median value and error bars indicate the 25th and 75th percentiles.
(B) GFP profiles of individual cells with tagged APC/CCdc20 substrates. Underlying black lines show the original data, and the colored lines are smoothed traces. The timing of SPB separation and spindle elongation are marked with dashed and solid lines, respectively.
(C, D) Comparison of different GFP-tagged substrates using SPB separation (C, dashed lines) or spindle elongation (D, solid lines) as the timing reference. In top panels, each line is a smoothed trace of a single cell. Bottom panels show the averaged traces, where unsmoothed traces were first aligned to the same time reference point, averaged at each time point and then normalized to maximum intensity.

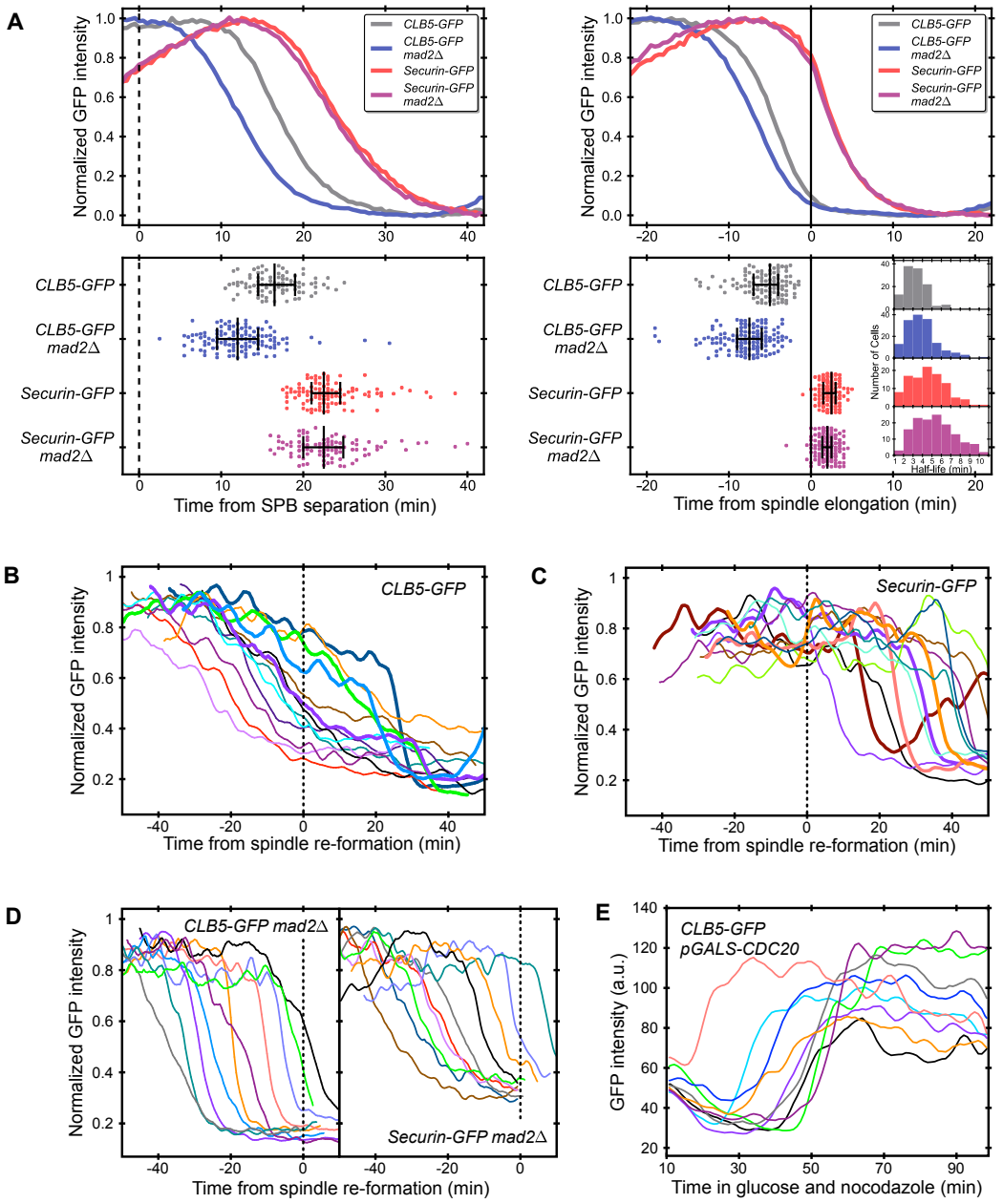
A
Normalized GFP intensity
CLB5-GFP
CLB5-GFP mad2Δ
Securin-GFP
Securin-GFP mad2Δ
Time from SPB separation (min)
Time from spindle elongation (min)
Number of Cells
Half-life (min)
B
CLB5-GFP
Time from spindle re-formation (min)
C
Securin-GFP
Time from spindle re-formation (min)
D
CLB5-GFP mad2Δ
Securin-GFP mad2Δ
Time from spindle re-formation (min)
E
CLB5-GFP
pGALS-CDC20
GFP intensity (a.u.)
Time in glucose and nocodazole (min)

Figure 3. Role of the SAC in APC/CCdc20 substrate degradation
(A) Clb5 and securin degradation profiles in wild-type and mad2Δ cells. Cells are aligned using either SPB separation (left panel, dashed line), or spindle elongation (right panel, solid line). Top panels show averaged and normalized traces as in Figure 2C, D. Bottom panels show the time of 50% substrate degradation in individual cells (Figure S1C). Each dot represents a single cell, and n > 90 cells per strain. For each strain, the middle bar indicates the median value, and error bars indicate the 25th and 75th percentiles. The insert in the lower right panel shows a histogram of rates of degradation in different strains, calculated from single cell traces; n > 100 cells per strain.
(B, C, D) Clb5 and securin degradation in nocodazole-treated cells. Asynchronous cells were plated on agarose pads with 15 mg/ml nocodazole 10 min before imaging began. Representative traces from individual cells are normalized and aligned to spindle reformation (dotted line). The traces shown here were selected on the basis of two criteria: minimum overlap among traces for clarity of viewing, and inclusion of only cells in mitosis judged by bud size. Wild-type (B, C) and mad2Δ cells (D) are shown. In (B, C), representative cells with fast substrate degradation after recovery from the SAC arrest are shown in bold lines.
(E) Clb5 degradation in nocodazole with CDC20 shut off. Asynchronous cells were grown in 2% galactose and plated on an agarose pad with 2% glucose and 15 mg /ml nocodazole 10 min prior to the start of imaging. Representative traces were selected to minimize overlap.

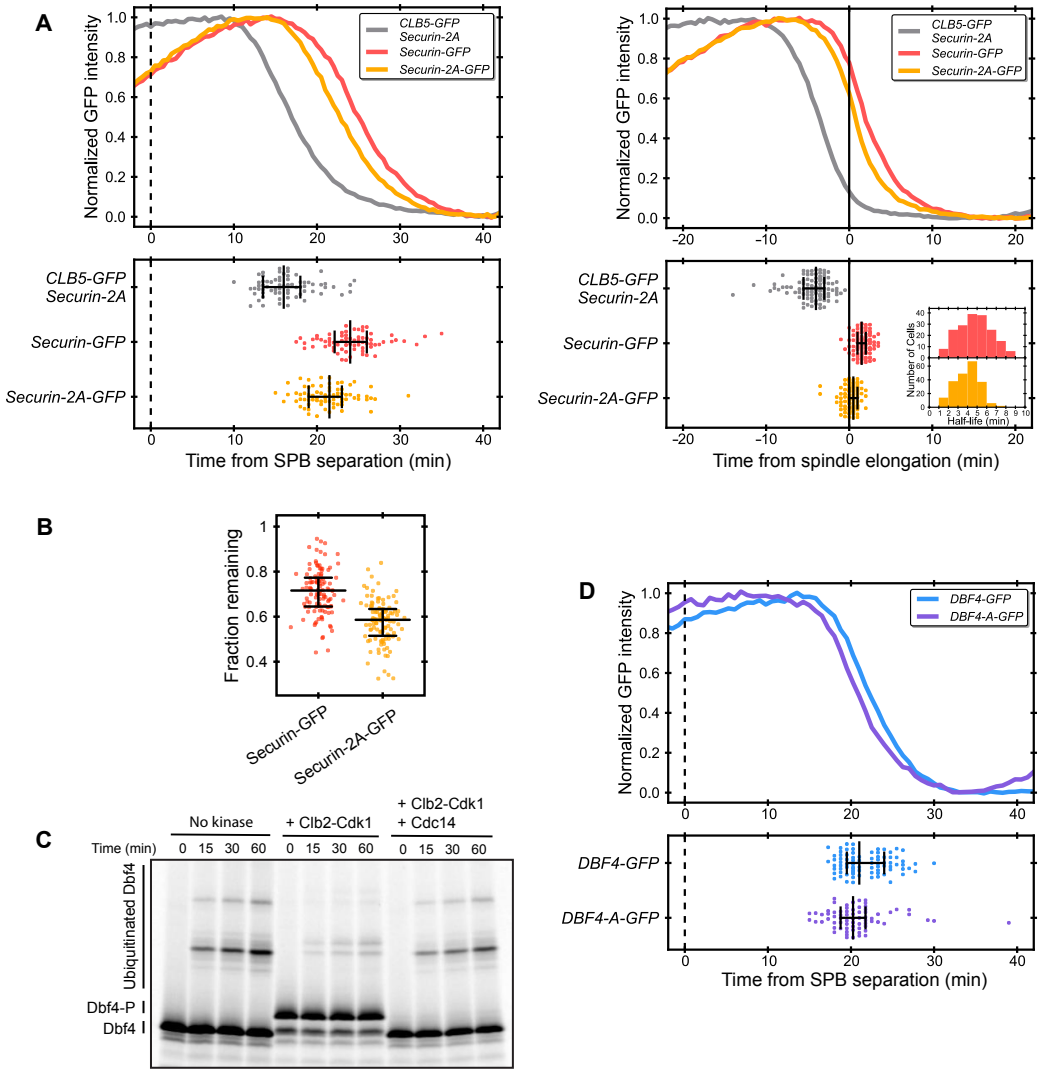

Figure 4. Role of phosphorylation by Cdk1 in APC/CCdc20 substrate degradation
(A) Degradation profiles of GFP-tagged securin-2A, wild-type securin and Clb5, as in Figure 3A; n > 70 cells per strain, and in the insert, n > 180 cells per strain.
(B) Fraction of securin or securin-2A remaining when spindle elongation occurs. Single-cell traces of GFP were smoothed, and the fraction remaining was calculated as the GFP intensity at spindle elongation divided by maximum GFP intensity. Each dot represents a single cell (n > 100 cells per strain). For each strain, the middle bar indicates the median value and error bars indicate the 25th and 75th percentiles.
(C) Dbf4 ubiquitination by APC/CCdc20 in vitro. Radiolabeled Dbf4 N-terminal fragment (residues 1-236) was produced by in vitro translation and incubated with buffer, purified Clb2-Cdk1, or both Clb2-Cdk1 and Cdc14, prior to the addition of purified APC/C, Cdc20, and other ubiquitination components for the indicated times. Reaction products were separated by SDS-PAGE and analyzed by autoradiography.
(D) Degradation profiles of Dbf4-A-GFP and wild-type Dbf4-GFP, as in Figure 3A; n > 70 cells per strain.

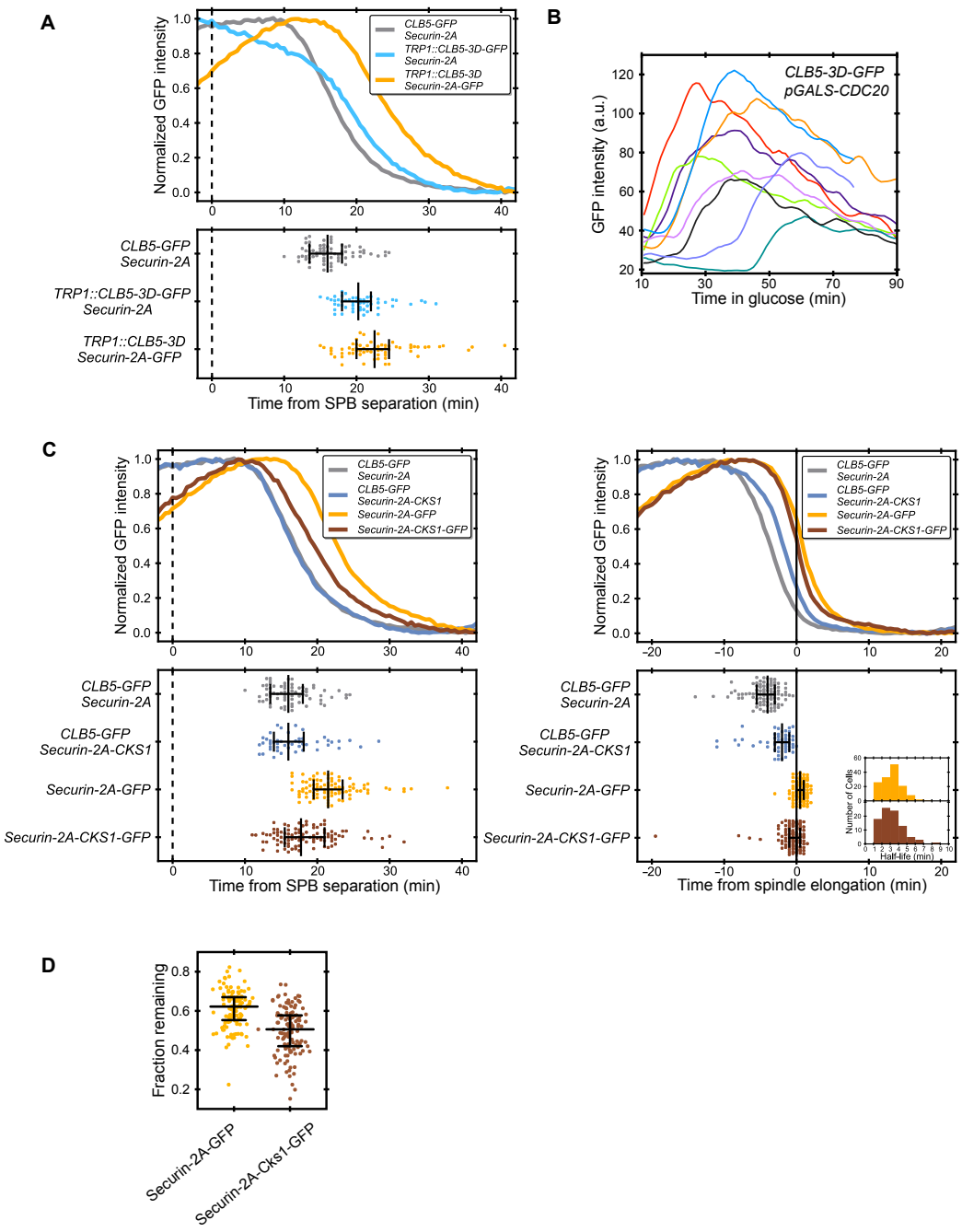

Figure 5. Contribution of Cdk1-Cks1 to Clb5 early degradation

(A) Degradation profiles of Clb5-3D-GFP, wild-type Clb5-GFP, and securin-2A-GFP, as in Figure 3A; n > 50 cells per strain.

(B) Clb5-3D-GFP degradation following CDC20 shutoff, as in Figure 3E. Representative traces were selected to minimize overlap.

(C) Degradation profiles of securin-2A-Cks1-GFP, securin-2A-GFP, and Clb5-GFP in the securin-2A-Cks1 or securin-2A background, as in Figure 3A; n > 50 cells in the Clb5-GFP strains and n > 90 cells in the securin-GFP strains. In the insert, n > 100 cells per strain.

(D) Fraction of securin-2A or securin-2A-Cks1 remaining when spindle elongation occurs, as in Figure 4B; n > 100 cells per strain.

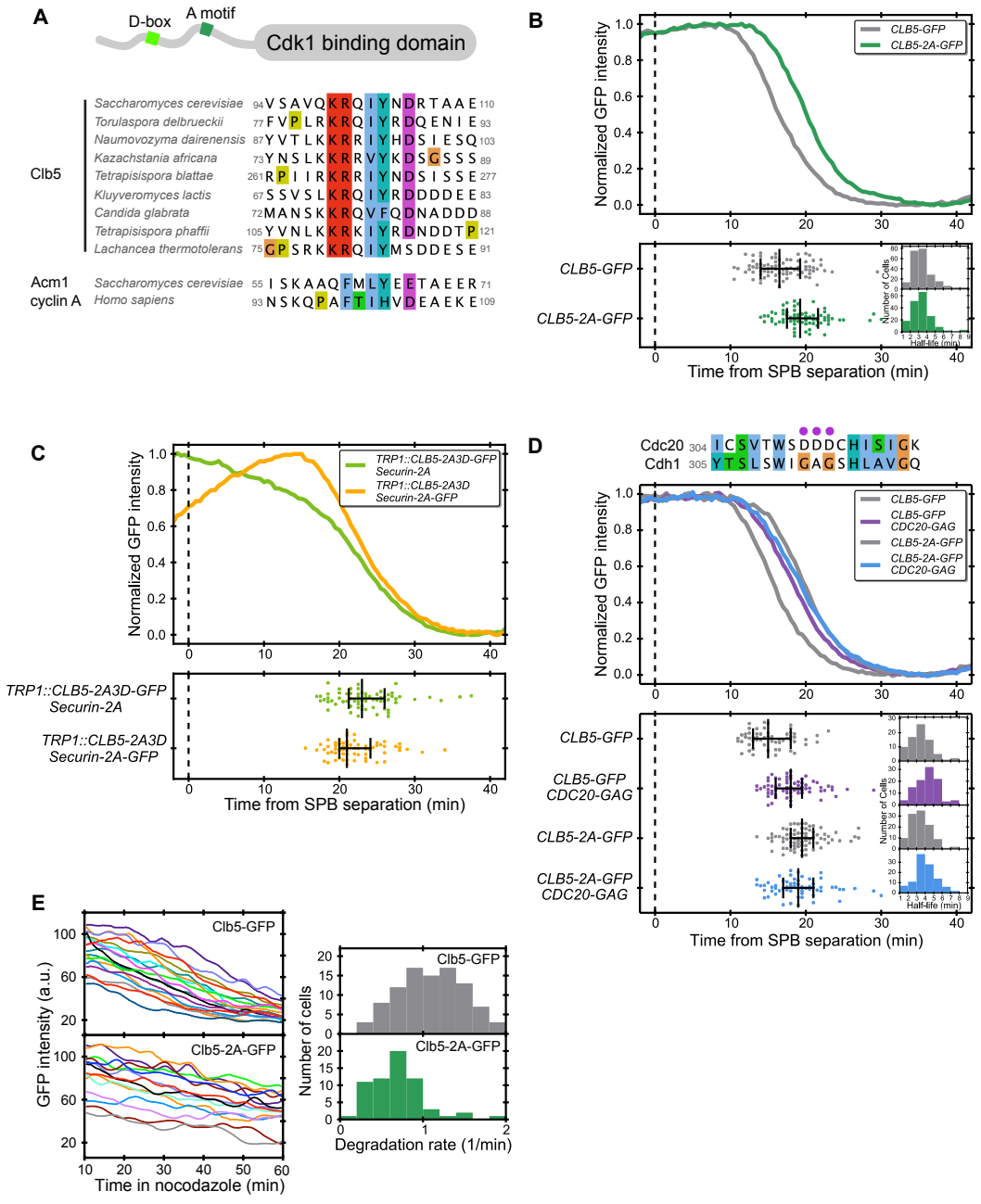
A
D-box
A motif
Cdk1 binding domain
Clb5
Saccharomyces cerevisiae 94 V S A V Q K R Q I Y N D R T A A E 110
Torulaspora delbrueckii 77 F V P L R K R Q I Y R D Q E N I E 93
Naumovozyma dairenensis 87 Y V T L K K R R I Y H D S I E S Q 103
Kazachstania africana 73 Y N S L K K R R V Y K D S G S S S 89
Tetrapisispora blattae 261 R P I I R K R R I Y N D S I S S E 277
Kluyveromyces lactis 67 S S V S L K R Q I Y R D D D D E E 83
Candida glabrata 72 M A N S K K R Q V F Q D N A D D D 88
Tetrapisispora phaffii 105 Y V N L K K R K I Y R D N D D T P 121
Lachancea thermotolerans 75 G P S R K K R Q I Y M S D D E S E 91
Acm1
cyclin A
Saccharomyces cerevisiae 55 I S K A A Q F M L Y E E T A E E R 71
Homo sapiens 93 N S K Q P A F T I H V D E A E K E 109
B
Normalized GFP intensity
CLB5-GFP
CLB5-2A-GFP
Number of Cells
Half-life (min)
Time from SPB separation (min)
C
Normalized GFP intensity
TRP1::CLB5-2A3D-GFP
Securin-2A
TRP1::CLB5-2A3D
Securin-2A-GFP
Time from SPB separation (min)
D
Cdc20 304 I C S V T W S D D D C H I S I G K
Cdh1 305 Y T S L S W I G A G S H L A V G Q
Normalized GFP intensity
CLB5-GFP
CLB5-GFP CDC20-GAG
CLB5-2A-GFP
CLB5-2A-GFP CDC20-GAG
Number of Cells
Half-life (min)
Time from SPB separation (min)
E
GFP intensity (a.u.)
Clb5-GFP
Clb5-2A-GFP
Time in nocodazole (min)
Number of cells
Degradation rate (1/min)

Figure 6. Contribution of the 'A motif' to Clb5 degradation
(A) Sequence alignment of Clb5 orthologs from members of the yeast Saccharomyces clan, showing the putative A motif in Clb5 in alignment with other known A motifs. Different colors represent chemical properties of the residues.
(B) Degradation profiles of Clb5-2A-GFP and wild-type Clb5-GFP, as in Figure 3A; n > 70 cells per strain. In the insert, n > 170 cells per strain.
(C) Degradation profiles of Clb5-2A3D-GFP and securin-2A-GFP, as in Figure 3A; n > 60 cells per strain.
(D) Sequence alignment of budding yeast Cdc20 and Cdh1; purple dots mark the potential A-motif interacting residues that are different between Cdc20 and Cdh1. Below is the degradation profile of Clb5-2A-GFP or wild-type Clb5-GFP in a CDC20-GAG background, compared to the wild-type CDC20 background; n > 57 cells per strain. In the insert, n > 75 cells per strain.
(E) Degradation of Clb5-GFP and Clb5-2A-GFP in nocodazole-treated cells. Asynchronous cells were plated on an agarose pad with 15 ?g/ml nocodazole 10 min prior to the start of imaging. Clb5-GFP dynamics before spindle reformation (SAC inactivation) were analyzed. Representative traces were selected to minimize overlap and omit cells that were not in mitosis. Right panel shows the rates of degradation calculated by fitting single-cell GFP traces to a linear decay; n > 55 cells per strain.

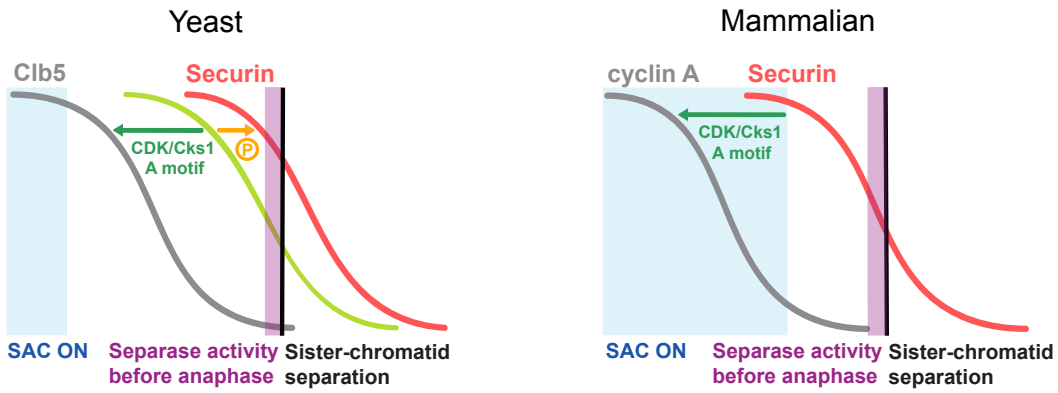

Figure 7. Metaphase-anaphase transition in yeast and mammalian cells

Summary of the regulatory events leading to the metaphase-anaphase transition in yeast and mammalian cells, and the mechanisms that determine the timing and order of APC/CCdc20 substrate degradation.

Figure S1

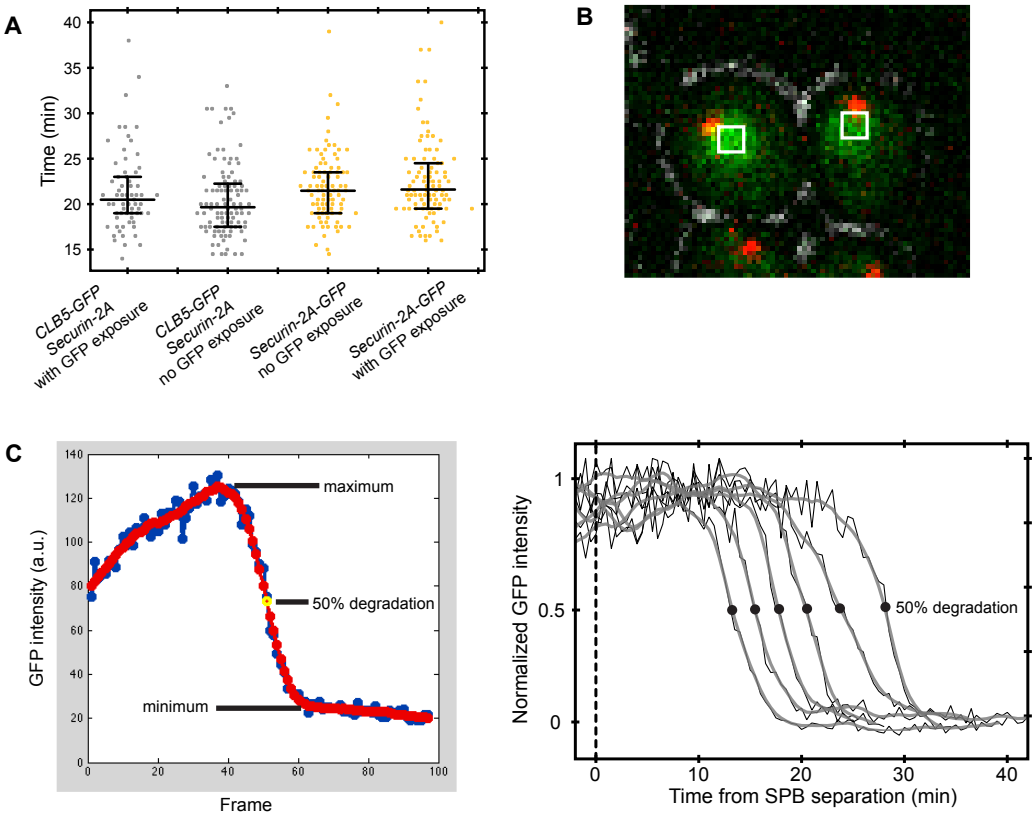
A
Time (min)
CLB5-GFP Securin-2A with GFP exposure
CLB5-GFP Securin-2A no GFP exposure
Securin-2A-GFP no GFP exposure
Securin-2A-GFP with GFP exposure
B
C
GFP intensity (a.u.)
maximum
50% degradation
minimum
Frame
Normalized GFP intensity
50% degradation
Time from SPB separation (min)
D
GFP intensity (a.u.)
Time (min)

Publishing Agreement

It is the policy of the University to encourage the distribution of all theses, dissertations, and manuscripts. Copies of all UCSF theses, dissertations, and manuscripts will be routed to the library via the Graduate Division. The library will make all theses, dissertations, and manuscripts accessible to the public and will preserve these to the best of their abilities, in perpetuity.

Please sign the following statement:

I hereby grant permission to the Graduate Division of the University of California, San Francisco to release copies of my thesis, dissertation, or manuscript to the Campus Library to provide access and preservation, in whole or in part, in perpetuity.

Author Signature

3/18/2014

Date